Autophagy

Volume 11 - Issue 11 - November 2015

Editor-in-Chief
Daniel J. Klionsky
University of Michigan

Taylor & Francis
Taylor & Francis Group

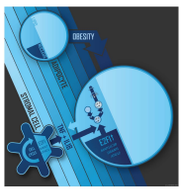

Autophagy

ISSN: 1554-8627 (Print) 1554-8635 (Online) Journal homepage: http://www.tandfonline.com/loi/kaup20

ZFYVE26/SPASTIZIN and SPG11/SPATACSIN mutations in hereditary spastic paraplegia types AR-SPG15 and AR-SPG11 have different effects on autophagy and endocytosis

Chiara Vantaggiato, Elena Panzeri, Marianna Castelli, Andrea Citterio, Alessia Arnoldi, Filippo Maria Santorelli, Rocco Liguori, Marina Scarlato, Olimpia Musumeci, Antonio Toscano, Emilio Clementi & Maria Teresa Bassi

To cite this article: Chiara Vantaggiato, Elena Panzeri, Marianna Castelli, Andrea Citterio, Alessia Arnoldi, Filippo Maria Santorelli, Rocco Liguori, Marina Scarlato, Olimpia Musumeci, Antonio Toscano, Emilio Clementi & Maria Teresa Bassi (2018): ZFYVE26/SPASTIZIN and SPG11/SPATACSIN mutations in hereditary spastic paraplegia types AR-SPG15 and AR-SPG11 have different effects on autophagy and endocytosis, Autophagy, DOI: 10.1080/15548627.2018.1507438

To link to this article: https://doi.org/10.1080/15548627.2018.1507438

ZFYVE26/SPASTIZIN and SPG11/SPATACSIN mutations in hereditary spastic paraplegia types AR-SPG15 and AR-SPG11 have different effects on autophagy and endocytosis

[1]Chiara Vantaggiato, [1]Elena Panzeri, [1]Marianna Castelli, [1]Andrea Citterio, [1]Alessia Arnoldi, [2]Filippo Maria Santorelli, [3]Rocco Liguori, [4]Marina Scarlato, [5]Olimpia Musumeci, [5]Antonio Toscano, [1,6]Emilio Clementi, [1]Maria Teresa Bassi.

[1]Scientific Institute, IRCCS E. Medea, Laboratory of Molecular Biology, Bosisio Parini, Lecco, Italy; [2]IRCCS Fondazione Stella Maris, Calambrone, Pisa, Italy; [3]Department of Biomedical and Neuromotor Sciences, University of Bologna; IRCCS Institute of Neurological Sciences, Bologna, Italy; [4]Dept. of Neurosciences and Institute of Experimental Neurology (INSpe), San Raffaele Scientific Institute, Milan, Italy; [5]Department of Clinical and Experimental Medicine, University of Messina, Messina, Italy; [6]Unit of Clinical Pharmacology, CNR Institute of Neuroscience, Department of Biomedical and Clinical Sciences, University Hospital "Luigi Sacco", Università di Milano, 20157 Milan, Italy.

Word count: 5803

Corresponding Author: Maria Teresa Bassi PhD, [1]Scientific Institute IRCCS E. Medea, Laboratory of Molecular Biology, Via D. L. Monza 20, 23842 Bosisio Parini, Lecco, Italy; phone 0039031877111, fax 0039031877499; email mariateresa.bassi@lanostrafamiglia.it.

Running title: Autophagy and endocytosis in AR-SPG15 and AR-SPG11

Key words: AR-SPG11, AR-SPG15, autophagosome-endosome fusion, autophagy, endocytosis, RAB5A, RAB11, SPG11, ZFYVE26.

Abstract

ZFYVE26/Spastizin and *SPG11/Spatacsin* encode 2 large proteins that are mutated in hereditary autosomal-recessive spastic paraplegia/paraparesis (HSP) type 15 (AR-SPG15) and type 11 (AR-SPG11), respectively. We previously have reported that AR-SPG15-related ZFYVE26 mutations lead to autophagy defects with accumulation of immature autophagosomes. ZFYVE26 and SPG11 were found to be part of a complex including the AP5 (adaptor related protein complex 5) and to have a critical role in autophagic lysosomal reformation with identification of autophagic and lysosomal defects in cells with both AR-SPG15- and AR-SPG11-related mutations. In spite of these similarities between the 2 proteins, here we report that ZFYVE26 and SPG11 are differently involved in autophagy and endocytosis. We found that both ZFYVE26 and SPG11 interact with RAB5A and RAB11, 2 proteins regulating endosome trafficking and maturation, but only ZFYVE26 mutations affected RAB protein interactions and activation. ZFYVE26 mutations lead to defects in the fusion between autophagosomes and endosomes, while SPG11 mutations do not affect this step and lead to a milder autophagy defect. We thus demonstrate that ZFYVE26 and SPG11 affect the same cellular physiological processes, albeit at different levels: both proteins have a role in autophagic lysosome reformation, but only ZFYVE26 acts at the intersection between endocytosis and autophagy, thus representing a key player in these 2 processes. Indeed expression of the constitutively active form of RAB5A in cells with AR-SPG15-related mutations partially rescues the autophagy defect. Finally the model we propose demonstrates that autophagy and the endolysosomal pathway are central processes in the pathogenesis of these complicated forms of hereditary spastic paraparesis.

Introduction

Hereditary spastic paraplegia/paraparesis (HSP) is a group of neurodegenerative disorders characterised by progressive spasticity and weakness at the lower limbs due to retrograde axonal degeneration of the corticospinal tracts. HSP can be classified either as pure or complicated, depending on the presence of neurological and non-neurological signs and symptoms in addition to spasticity [1,2]. This group of diseases currently has more than 80 published genes or loci that can be inherited in an autosomal-dominant (AD), autosomal-recessive (AR) or X-linked manner (XL) [3,4]. Spastic paraplegia (SPG) subtypes AR-SPG15 and AR-SPG11 are the 2 most prevalent autosomal recessive complicated HSP (AR-HSP) subtypes with thin corpus callosum (TCC) comprising about 70% of these forms. The AR-SPG15 and AR-SPG11 subtypes are clinically overlapping and are characterised by slowly progressive spastic paraparesis and mental deterioration with cerebellar ataxia, neuropathy and retinal abnormalities [5-7]. Onset is between the first and second decade of life. The MRI (magnetic resonance imaging) pattern includes thin corpus callosum and white matter changes as distinctive features [5-7]. The AR-SPG15 and AR-SPG11 subtypes are associated with mutations in the ZFYVE26 and SPG11 proteins respectively [8,9]. These are 2 large proteins of 270 to 280 kDa and both have predicted secondary structures containing α-solenoids related to those of clathrin heavy chain and COPI subunits [10]. SPG11 also has an N-terminal β-propeller–like domain [10], while ZFYVE26 contains a FYVE domain that confers binding affinity to the membrane-associated phosphatidylinositol-3-phosphate (PtdIns3P) [11], which is particularly enriched on endosomes. ZFYVE26 and SPG11 have a similar subcellular distribution, localizing on the endoplasmic reticulum, on vesicles, and in the endosomal and lysosomal compartment [10,12,13]. Moreover, ZFYVE26 has been detected on early endosomes, a localization that is lost in the presence of mutations either falling within the FYVE domain or inhibiting PtdIns3P synthesis [11,14,15]. ZFYVE26 and SPG11 form a complex with AP5 [10], whose mutations are associated with AR-SPG48, an autosomal-recessive HSP subtype clinically overlapping the AR-SPG15 and AR-SPG11 subtypes [16,17]. The AP5 complex is proposed to be

involved in cargo trafficking in the endolysosomal compartment, suggesting a role for the entire complex in this compartment. Indeed, knockdown of ZFYVE26, SPG11 or of any of the AP5 subunits results in alteration of endocytosis and delivery of M6PR/mannose 6-phosphate receptor to lysosomes [10].

We have reported that ZFYVE26 is required for generating mature autophagosomes and that autophagosome maturation is impaired when the protein is defective or absent [14,17]. ZFYVE26 interacts with BECN1 and with its interacting proteins PIK3C3, UVRAG and RUBCN, major regulators of autophagy and endocytosis. These interactions are lost in the presence of AR-SPG15-related ZFYVE26 mutations, and AR-SPG15-patient-derived cells showed accumulation of immature autophagosomes and defects in the autophagosome-to-lysosome fusion step [14]. Accumulation of enlarged lysosomes and increased autophagosomes number have also been observed in SPG11 mutated fibroblasts [18,19]. Additionally, a role for both ZFYVE26 and SPG11 has been demonstrated in autophagic lysosome reformation (ALR) [19,13], a process of lysosome biogenesis from autolysosomes after cargo degradation [20]. Loss of ZFYVE26 or SPG11 results in defects in lysosome biogenesis with depletion of free lysosomes and accumulation of autolysosomes in HeLa and primary human fibroblast cell lines [19]. Consistently, lysosomal depletion and impaired autophagy are found in *Spg11* knockout mice [13], while LAMP1-positive autofluorescent material and endolysosomal defects are reported in *Zfyve26* knockout mice [15].

Endocytosis and autophagy are strictly interconnected: autophagosome maturation requires the fusion of autophagosomes with early and late endosomes and depletion of proteins involved in endocytic trafficking and endosome fusion results in autophagosome accumulation [21-23].

The interaction between ZFYVE26 and SPG11 and the presence of autophagy defects in both AR-SPG15 and AR-SPG11 cells, suggest a close functional link between the 2 proteins, the nature of which, however, had not yet been investigated. Here we report on the role of ZFYVE26 and SPG11 in endocytosis and autophagy, their interactions with key proteins of these pathways and the pathogenic mechanisms of their action. Our observations account for the different cellular

phenotypes displayed by AR-SPG11 and AR-SPG15 mutated fibroblasts. We also discuss the clinical and genetic correlations of these findings.

Results

ZFYVE26 and SPG11 interact with the small GTP-binding proteins RAB5A and RAB11

Autophagosome maturation requires the fusion of autophagosomes with early or late endosomes such that depletion of proteins involved in endocytic trafficking and endosome fusion results in autophagosomes accumulation [21-23]. We decided to analyze the role of ZFYVE26 and SPG11 in the endocytic pathway. We first investigated if ZFYVE26 and SPG11 interact with RAB5 and RAB11, 2 small GTP-binding proteins that regulate endosome trafficking, fusion and maturation [24,25]. Total extracts from HeLa cells untreated and treated with EBSS to induce autophagy were immunoprecipitated with an anti-ZFYVE26 antibody (Ab) and immunodetected with antibodies to RAB5A, RAB7, RAB11, SPG11 or AP5Z1 (AP5) (Fig. 1A). We confirmed the interaction of ZFYVE26 with SPG11 and AP5 [10], demonstrating the formation of the ZFYVE26-SPG11-AP5 complex both in basal conditions and after autophagy induction (Fig. 1A and Fig. S1 for autophagy induction). Second, we demonstrated that ZFYVE26 interacts with RAB5A and RAB11, while no interactions were found with RAB7 (Fig. 1A). Interactions were confirmed by immunofluorescence (Fig. 1B and C), supporting the endosomal localization of ZFYVE26 on RAB5- and RAB11-positive structures [14,15,26], and suggesting a role for ZFYVE26 in the endosomal compartment. While RAB5 is a marker of early endosomes and its interaction with ZFYVE26 clearly suggests the localization of the protein on these structures, RAB11-positive structures represent different compartments: multivesicular bodies (MVBs), recycling endosomes and late endosomes [25]. To understand which structures ZFYVE26 and RAB11 interact with, we analyzed their colocalization with the MVB marker lysobisphosphatidic acid (LBPA) and the late endosomal marker RAB7 (Fig. 1C). To stain recycling endosomes, cells were incubated with Alexa Fluor 555-Transferrin (TF) for 1 h at 4°C followed by incubation at 37°C for 25 min [27]. We detected no colocalization between

ZFYVE26 and RAB11 on recycling and late endosomes; conversely ZFYVE26 and RAB11 partially colocalized on MVBs (Fig. 1C). LBPA is a marker of the internal membrane of MVBs, but it labels also lysosomes [28-29]. We have demonstrated the absence of localization of ZFYVE26 on lysosomes (LAMP1-positive) [14]; in our case we can exclude that colocalization of ZFYVE26 and RAB11 on LBPA-positive vesicles represents late endosomes and lysosomes, due to the absence of ZFYVE26 localization with the respective markers (RAB7 and LAMP1).

RAB proteins cycle between an inactive GDP-binding form and an active GTP-binding form. We therefore analyzed the interaction of ZFYVE26 with an active and an inactive form of RAB5A, to understand which form the protein does interact with. To this purpose we used 2 mutated forms of RAB5A: the constitutively active form GTP-bound mutant $RAB5A^{Q79L}$ (RAB5A[CA]) and the dominant-negative inactive GDP-bound mutant $RAB5A^{S34N}$ (RAB5A[DN]) [30]. HeLa cells were transfected with the vectors expressing RAB5A(CA) or RAB5A(DN), both with a GFP tag, and total extracts were immunoprecipitated with an anti-ZFYVE26 Ab and revealed with an anti-GFP Ab. As shown in the Fig. 1D, ZFYVE26 interacted only with the constitutively active form of RAB5A, as yet reported for BECN1 and EEA1 [31,32]. Interactions were confirmed also by immunofluorescence (Fig. 1D). The expression of RAB5A(CA) induced the formation of enlarged ring-shaped endosomes, as reported previously [30]. ZFYVE26 colocalized with RAB5A(CA), while no colocalization was detected with RAB5A(DN).

We have demonstrated that ZFYVE26 interacts with BECN1 and its interacting protein UVRAG and RUBCN, but not with ATG14, and it is therefore involved in autophagosome maturation [14]. We thus investigated if also the ZFYVE26-interacting proteins SPG11 and the AP5 complex interact with BECN1 complexes and RAB proteins. We found that both SPG11 and AP5, like ZFYVE26, interact with RAB5A, RAB11, BECN1, PIK3C3, PIK3R4, UVRAG and RUBCN, but not with RAB7 and ATG14 (Fig. 2A, Fig. S2 and S4), indicating that the entire ZFYVE26-SPG11-AP5 complex interacts with the BECN1 complexes containing UVRAG and RUBCN, involved in autophagosome maturation.

It has been demonstrated that RAB5 interacts with BECN1, PIK3R4 and PIK3C3 and these interactions are required for endocytic membrane trafficking, endosome fusion and endosome motility and recycling [31-33]. We confirmed the interactions of RAB5 in HeLa cells and we found that also RAB11 interacts with BECN1, PIK3R4, PIK3C3, UVRAG and RUBCN (Fig. 2B and 2C), suggesting that RAB11 functions require the interaction with the BECN1 complexes, as for RAB5. The interactions with ZFYVE26, SPG11 and the AP5 complex were also verified (Fig. 2B and 2C). All the interactions were proved using antibodies to RUBCN, UVRAG, BECN1, PIK3R4 and PIK3C3 (Fig. S5 and S6). Some interactions were also confirmed by immunofluorescence (Fig. S7 and S8).

ZFYVE26 mutations in AR-SPG15 cells affect RAB5 and RAB11 interactions and activation

In our previous work we demonstrate that the interactions of ZFYVE26 with BECN1, UVRAG and RUBCN are lost in the presence of ZFYVE26 mutations in AR-SPG15 mutated cells, even if BECN1 can still interact with its partners [14]. Therefore we decided to analyze if ZFYVE26 mutations affect the interaction of RAB proteins with the BECN1 complexes. To this purpose we used the patient-derived AR-SPG15 fibroblast cell lines we have previously characterized [14] (Table S1). These cells carry either the ZFYVE26^{L243P} point mutation or one of the 2 truncating ZFYVE26 mutations (S1312X or R1209fsX), both leading to the absence of the protein [14]. We found that in control cells both RAB5A and RAB11 interact with BECN1 and its interacting proteins UVRAG, RUBCN, PIK3R4 and PIK3C3 (Fig. 3A and S9), confirming previous data in HeLa cells (Fig. 2B and 2C). These interactions are lost in the absence of ZFYVE26 in the cells harboring the AR-SPG15 related truncating mutations (S1312X and R1209fsX) (Fig. 3A), indicating that ZFYVE26 mediates the interactions of RAB5A and RAB11 with the BECN1 complexes. Interactions were lost also in the AR-SPG15 cells carrying the ZFYVE26^{L243P} point mutation, consistently with previous immunoprecipitation data where the L243P mutation drastically reduced the interaction of ZFYVE26 with BECN1 and abolish the interaction with

RUBCN, UVRAG and PIK3C3 [14]. Immunoprecipitation data were confirmed in HeLa cells silenced with a specific *ZFYVE26* shRNA with high silencing efficiency used in our previous work (Fig. S10) [14].

RAB11 is present on multivesicular bodies (MVBs) and, besides its role in the endocytic pathway, it is involved also in autophagosome maturation [34]. Upon autophagy induction, RAB11 induces the fusion between RAB11-decorated MVBs and autophagosomes removing from mature late endosomes Hook, which is a negative regulator of endosome maturation [35]; we therefore analyzed the interaction between these 2 proteins in AR-SPG15 mutated cells. We found that ZFYVE26 mutations affect the interaction between RAB11 and HOOK1, a human ortholog of *Drosophila* Hook (Fig. 3A), suggesting a possible defect in MVB-autophagosome fusion.

Finally, we analyzed the effect of ZFYVE26 mutations on RAB5A and RAB11 activation state by using a RAB Activation Assay Kit specific for each protein. Since basal RAB protein activation levels were undetectable, we induced RAB activation by stimulating endocytosis through EGFR stimulation [36]. Control and AR-SPG15 mutated cells were starved for 2 h and treated with EGF 200 ng/ml for 15 min, as reported [36]. Total extracts were immunoprecipitated with anti-active RAB5A or RAB11 Abs that specifically recognize only the active GTP-bound form of the 2 proteins, which were then immunodetected with anti-RAB5A or -RAB11 Abs (Fig. 3B). We found that the activation state of both RAB5A and RAB11 is reduced in the presence of ZFYVE26 mutations.

ZFYVE26 mutations affect autophagosome-endosome fusion

One of the processes controlled by RAB5 is endosome fusion. Fusion between early endosomes requires PIK3C3 and RAB5 activity, necessary for the recruitment of the RAB5 effector EEA1 on the endosomal membrane [32]. Loss of interactions between RAB5 and BECN1 and PIK3C3 and the presence of a decreased RAB5 activity in AR-SPG15 mutated cells could thus induce defects in endosome fusion. We analyzed the effect of AR-SPG15-related ZFYVE26 mutations on endosome

fusion using a fluorescence assay in living cells as described [37]. AR-SPG15 mutated and control cells were incubated with Oregon Green 488-avidin to label late endosomes and with biotin-BSA to label early endosomes. Alexa Fluor 568 dextran was used as internal control to label endocytosed vesicles. The fusion between avidin- and biotin-labelled endosomes induces a significant increase in Oregon Green 488 fluorescence. Green fused endosomes were counted, normalized to the total number of endosome (dextran-positive vesicles) and reported as percentage (Fig. 4). AR-SPG15 mutated cells presented a reduction of 50 to 60% in the number of green vesicles compared with control cells, indicating a reduction in the endosome fusion rate [30].

Autophagy induction stimulates the fusion between RAB11-decorated MVBs and autophagosomes, with the translocation of RAB11; lack of RAB11 results in autophagosomes and late endosomes accumulation [35]. PIK3C3 regulates the biogenesis of MVB through the production of PtdIns3P and the generation of the internal vesicles [34]. We found that RAB11 activation and interaction with PIK3C3 are altered in AR-SPG15 mutated cells and that RAB11 is unable to interact with HOOK1. Loosening of these interactions could induce defect in the fusion between autophagosomes and MVBs. Therefore we decided to analyze the ability of autophagosomes to fuse with MVBs and form amphisomes in AR-SPG15 mutated cells (see Fig. 12 for a schematic representation), by checking the presence on autophagosomes of LBPA, a marker of the internal membrane of MVBs [28,29]. We analyzed also the presence of the early endosomal marker EEA1 to verify the fusion with early endosomes [22]. AR-SPG15 mutated and control cells were transfected with the pCMV6-RFP-MAP1LC3B vector to stain autophagosomes and then treated with EBSS for 30 min to induce autophagy and promote the interaction of MVBs with autophagosomes [34], and with bafilomycin A_1 (BafA), that blocks autophagosome-lysosome fusion. By this treatment we induced autophagosome accumulation also in control cells to assess whether AR-SPG15-related ZFYVE26 mutations affect the relative rate of autophagosome to amphisome formation with respect to control cells. Cells were immunostained with anti-EEA1 or LBPA Abs (Fig. 5A and 5B). RFP-LC3 and EEA1 or RFP-LC3 and LBPA double-positive

amphisomes were counted and expressed as percentage of the total number of RFP-LC3-positive vesicles (autophagosomes + amphisomes). In control cells under basal condition only a small number of early endosomes and MVBs colocalized with autophagosomes and autophagy induction resulted in increased colocalization, as reported [34]. Moreover, while in control cells, 35% and 25% of accumulated LC3-positive vesicles were amphisomes positive, respectively for EEA1 or LBPA, less than 5% of the vesicles accumulated in AR-SPG15 mutated cells presented EEA1 or LBPA markers, indicating defects in both autophagosome-early endosome and autophagosome-MVB fusion steps. The reduced colocalization of autophagosomes with endosomal population in AR-SPG15 cells were confirmed also by staining endogenous LC3 (Fig. S11). Moreover, to confirm the fusion defects between autophagosomes and MVBs, we took advantage of the mRFP-GFP tandem fluorescent tagged LC3B vector (ptfLC3B) (Fig. S12). The GFP signal is sensitive to acidic compartment and is quenched when autophagosomes fuse with lysosomes, but not with multivesicular bodies [23], thereby allowing us to discriminate between the 2 populations. Control and AR-SPG15 mutated cells were transfected with ptfLC3B vector, incubated with EBSS for 30 min to induce autophagy and stained with anti-LBPA antibody. Colocalization between autophagosomes and LBPA was analyzed. The results obtained confirmed that LC3 and LBPA double-positive vesicles were autophagosomes fused with MVBs; indeed vesicles presented both mRFP and GFP tags. Vesicle quantification also confirmed the reduced fusion between autophagosomes and MVBs in AR-SPG15 cells. Of note, quantification of red mRFP-LC3 ($mRFP^+$ GFP^-) vesicles evidenced the reduced acidification of LC3 vesicles in AR-SPG15 cells, indicating that most of the autophagosomes accumulated in these cells are not autolysosomes, as we reported in our previous work [14].

Constitutively active RAB5A partially rescues the autophagy defects in AR-SPG15 cells

We demonstrated that ZFYVE26 interacts with GTP-bound RAB5A and that in the presence of AR-SPG15 mutations RAB5A is unable to interact with BECN1 and its interacting proteins. The loss of

these interactions determines endosome fusion and autophagosome fusion defects with the accumulation of immature autophagosomes. We therefore decided to analyze the effect of the expression of a constitutively active form of RAB5A on autophagosome accumulation in AR-SPG15 cells (Fig. 6 and Fig. S13). Control and AR-SPG15 mutated cells were untransfected or transfected with the GTP-bound mutant RAB5A^{Q79L} (RAB5A[CA]) with a GFP tag and with the pCMV6-RFP-MAP1LC3B vector for the staining of autophagosomes. RFP-LC3-positive vesicles were counted and are shown in the graph (Fig. 6A and B). AR-SPG15 cells transfected with RAB5A(CA) presented a lower number of RFP-LC3-positive vesicles compared with untransfected AR-SPG15 cells, but still significantly increased compared with control cells. This indicates that the expression of a constitutively active form of RAB5A rescues the autophagy defect observed in AR-SPG15 cell, albeit in part. The partial rescue of the autophagy defect in AR-SPG15 cells was confirmed also staining endogenous LC3 (Fig. S13).

This experiment unmasked another important point. In control cells some autophagosomes colocalized with RAB5A(CA)-positive enlarged ring-shaped endosomes (Fig. 6A), confirming the fusion between early endosomes and autophagosomes (Fig. 5A). Moreover, the expression of RAB5A(CA) in AR-SPG15 cells rescued the reported fusion defect between endosomes and autophagosomes (Fig. 5A and Fig. S11), such that SPG15 and control cells presented the same percentage of LC3 and RAB5A(CA) double-positive autophagosomes (Fig. 6C and Fig. S13).

Moreover we analyzed endosome-endosome fusion in the presence of RAB5A(CA) whereby we found that the constitutively active form of RAB5A rescued endosome fusion in AR-SPG15 cells (Fig. S14). Control and AR-SPG15 mutated cells were either untransfected or transfected with mCherry-RAB5A(CA) and were incubated with Oregon Green 488-avidin to label late endosomes and with biotin-BSA to label early endosomes. Alexa Fluor 647 dextran was used as internal control to label endocytosed vesicles. Green fused endosomes were counted, normalized to dextran-positive vesicles and reported as percentage (Fig. S14). Control and RAB5A(CA)-transfected AR-SPG15 mutated cells presented a similar percentage of green vesicles.

The rescue of endosome fusion and early endosome-autophagosome fusion defects in SPG15 cells is likely responsible of the partial rescue of the autophagy defect.

SPG11 mutations do not alter RAB proteins interactions and autophagosome-endosome fusion

We showed above that, similarly to ZFYVE26, SPG11 interacts with RAB5 and RAB11 (Fig. 2A). We next investigated the effect of SPG11 mutations on RAB proteins interactions and activation. To this purpose we used fibroblast cell lines established from AR-SPG11 patients carrying 3 different SPG11 mutations (SPG11Δ1: c.4307_4308delAA, p.W221X; SPG11Δ2: [c.3121C>T/ p.R1041*]+[c.4636-3A>G] [38], SPG11Δ3: [c.1891+1G>T]+[c.7000G>C/p.A2334P] [39]) previously identified (Table S1), that lead to early protein truncation and to the resulting absence of the protein (Fig. 7A). Contrary to our observation with ZFYVE26, SPG11 mutations did not alter RAB proteins interactions: both RAB5A and RAB11 interact with ZFYVE26 and with BECN1 and its interactors (Fig. 7B and Fig. S15). Data were confirmed in HeLa cells transfected with a pool of *SPG11*-specific siRNA with high silencing efficiency (Fig. S16). Moreover SPG11 mutations had no effects on RAB5A and RAB11 activation state (Fig. 8A). In AR-SPG15 cells alteration of RAB5 and RAB11 activation and interactions are associated to defects in the fusion between autophagosomes and endosomes. In view of the different actions of SPG11 on RAB5 and RAB11, we analyzed in AR-SPG11 mutated cells the ability of autophagosomes to fuse with early endosomes and MVBs, by checking the presence of EEA1 and LBPA markers on autophagosomes. We did not detect any defect in the fusion between autophagosomes and endosomes in AR-SPG11 mutated cells. Indeed AR-SPG11 mutated and control cells shared the same percentage of LC3 and EEA1 or LC3 and LBPA double-positive amphisomes (Fig. 8B for RFP-LC3, Fig. S17 for endogenous LC3 and Fig. S18 for mRFP-GFP-LC3B vector). This confirms that the interaction of ZFYVE26 with RAB5 and RAB11 is required for proper fusion of autophagosomes with endosomes, while SPG11 has no role in this process.

ZFYVE26 interactions are not affected by the absence of SPG11 in AR-SPG11 cells

We analyzed whether ZFYVE26 and SPG11 depend on each other for their interactions. We first analyzed the effect of protein mutations on protein expression and we found that while ZFYVE26 levels were not affected by SPG11 mutations (Fig. 7A), ZFYVE26 mutations did affect SPG11 expression (Fig. 9A). Indeed, AR-SPG15 cells with the ZFYVE26^{L243P} mutation presented reduced SPG11 expression levels compared to control cells, and in AR-SPG15-mutated cells, with the S1312X and R1209fsX truncation mutations of ZFYVE26, where the protein product is absent, SPG11 levels were almost undetectable (Fig. 9A).

We then analyzed ZFYVE26 interactions in AR-SPG11 cells, where SPG11 is depleted, and we found that ZFYVE26 interactions were not affected by the absence of SPG11. Indeed, in AR-SPG11 cells, ZFYVE26 interacted with BECN1, PIK3C3, PIK3R4, UVRAG, RUBCN and with both RAB5A and RAB11 as in control cells (Fig. 9B and Fig. S19A). On the contrary, we found that SPG11 interactions required a functional ZFYVE26 protein. Indeed in AR-SPG15-mutated cells with ZFYVE26^{L243P}, the only AR-SPG15 cell line where SPG11 is expressed, SPG11 did not interact with mutated ZFYVE26^{L243P} and with the BECN1 complexes or with RAB5 or RAB11 (Fig. 9C and Fig. S19B).

Autophagy defects are less severe in AR-SPG11 compared to AR-SPG15 cells

Autophagy defects were reported in both AR-SPG11 and AR-SPG15 mutated cells [13,14,18]. We thus analyzed whether the differences we found between ZFYVE26 and SPG11 in terms of protein interactions and activation led to differences in autophagy regulation. Since a detailed characterisation of autophagy in AR-SPG15 cells is already reported in our previous work [14], here we used only one AR-SPG15 mutated cell line (S1312X truncation mutant) that recapitulates the phenotype of the cell lines used in that study. We used also the same control cells with similar results. Control cells, AR-SPG15 (S1312X) and AR-SPG11 mutated (SPG11Δ1, SPG11Δ2 and SPG11Δ3) cells were treated with EBSS to induce autophagy for different times and autophagy was

determined quantifying the autophagosomal marker LC3 and SQSTM1, a protein targeting poly-ubiquitinated protein to phagophores for degradation. LC3-II expression levels were enhanced during starvation in control cells and significantly enhanced further in AR-SPG15 cells [14]. In AR-SPG11 cells LC3-II levels were also significantly enhanced compared with control cells, although it was only half than that observed in AR-SPG15 cells (Fig. 10A). SQSTM1 levels were decreased in control cells, as expected because of autophagy induction, and were instead increased in AR-SPG15 cells, indicating defective autophagy, confirming previous data [14]. In AR-SPG11 mutated cells SQSTM1 degradation is delayed respect to control cells, but SQSTM1 levels were lower than those observed in AR-SPG15 cells. We then analyzed autophagosome accumulation in AR-SPG11 and AR-SPG15 mutated cells by immunofluorescence and we found that AR-SPG11 cells presented a lower number of LC3-positive vesicles (RFP-LC3 or endogenous LC3) compared with AR-SPG15 cells (Fig. 10B and Fig. S20).

These differences were confirmed analyzing the autophagic flux in AR-SPG15 and AR-SPG11 mutated cells by using BafA to inhibit autophagosome-lysosome fusion, as reported for AR-SPG15 cells in our previous work [14]. In basal condition BafA induced autophagosome accumulation with an increase in LC3-II levels in all cell lines, yet LC3-II levels in SPG11 cells were still lower than that of AR-SPG15 cells, confirming a less severe autophagosome accumulation (Fig. 10C). In autophagy-inducing conditions (starv), in the presence of BafA, all cell lines presented similar LC3-II levels confirming that LC3-II production and autophagy induction were not increased in AR-SPG11 mutated cells, as we already reported for AR-SPG15 cells [14].

These data indicate that the effect of SPG11 mutations on autophagy is less severe than that of AR-SPG15-related ZFYVE26 mutations and this can be explained by the absence of defects on RAB proteins and on the autophagosome-endosome fusion step.

Additionally, we found that AR-SPG15-related ZFYVE26 and SPG11 mutations have different effects also on endocytic trafficking and receptor degradation. We analyzed the effect of protein mutations on receptor-mediated endocytosis and delivery to lysosomes using Alexa Fluor-

coupled EGF as endocytic probe. EGF colocalization with early endosomes (EEA1) and lysosomes (LAMP1) was analyzed by confocal microscopy. In both AR-SPG15 and AR-SPG11 mutated cells, EGF accumulated in early endosomes (Fig. 11A) with a reduced delivery to lysosomes (Fig. 11B), confirming the presence of endosomal trafficking defects in both cells, yet also in this case, AR-SPG15 cells presented a more severe phenotype, with more EGF being localized in early endosomes compared with AR-SPG11 cells (Fig. 11C). Data were confirmed also by the analysis of EGFR internalization and degradation [40]. Mutated and control fibroblasts were serum starved for 16 h, after which EGFR endocytosis and degradation were induced by incubation with EGF from 0 to 2 h. Cells were then lysed at different time points and subjected to SDS-PAGE and western blot using an anti-EGFR antibody (Fig. S21). In both AR-SPG11 and AR-SPG15 mutated cells EGFR degradation was reduced compared to control cells, but the effect was more severe in AR-SPG15 cells. After 2 h of chase 75% of the internalized EGFR in control cells was degraded, while only 35 to 40% of the internalized EGFR was degraded in AR-SPG15 mutated cells (Fig. S21). In AR-SPG11 cells EGFR levels were higher than in control after 1 h of chase, but, similarly to control cells, most of the internalized EGFR was degraded after 2 h, suggesting that, at variance with AR-SPG15 cells, in AR-SPG11 cells EGFR degradation is only delayed.

Discussion

ZFYVE26 and SPG11 are both involved in the endolysosomal system. Recent studies show that they are also involved in autophagy to the point that accumulation of autophagosomes is observed in cells harbouring mutations in AR-SPG15 and AR-SPG11, respectively [13,14,18]. This is not surprising since the endosomal pathway and endocytosis are strictly interconnected with autophagy. The endosomal pathway plays a greater role in autophagy than just providing lysosomal enzymes for degradation [41]. Fusion of autophagosomes with early endosomes and MVB/late endosomes is required for the maturation of autophagosomes. Depletion of proteins involved in early endosome trafficking and maturation, like COPI, or in MVB/late endosomes formation, like the component of

the endosomal sorting complex required for transport (ESCRT), results in autophagosome accumulation [22,23]. The molecular machineries involved in the 2 pathways are also closely linked and coordinated with several groups of proteins involved in both autophagy and endocytosis, among these the BECN1 complexes and the RAB proteins [42]. The BECN1 complexes regulate both autophagosome formation and autophagosome and endosome maturation through the formation of the BECN1-PIK3C3-UVRAG complex [43,44]. Depletion of BECN1, PIK3C3 or UVRAG impairs both endocytosis and autophagy by inducing accumulation of endolysosomes and autophagosomes [43,44]. Intriguingly we found that BECN1, PIK3C3 and UVRAG interact with ZFYVE26 and that these interactions are lost in AR-SPG15 cells where ZFYVE26 is defective or absent and autophagosomes accumulate [14,17].

Analogously, loss of SPG11 in AR-SPG11 cells results in lysosomal depletion and impaired autophagy with autophagosome accumulation [19,13]. All these data indicate the relevance of ZFYVE26 and SPG11 in the endolysosomal and autophagic systems. Furthermore, the interactions between ZFYVE26 and SPG11 and the findings of autophagosome accumulation, lysosome enlargement and autophagic lysosome reformation defects in AR-SPG15 and AR-SPG11 cells and knockout mice [10,13,15,18,19], suggest that the 2 proteins have a common action in these pathways. Some studies however indicate that their actions differ to some extent; while silencing of either *SPG11* or *ZFYVE26* results in perturbed trafficking of the mannose 6-phosphate receptor, silencing of *ZFYVE26* leads to a more severe phenotype [10]. Moreover, only *ZFYVE26* silencing results in the tubulation of EEA1-positive endosomes and the presence of multilamellar bodies is detected only in AR-SPG15 mutated fibroblasts [10,18]. These data, while suggesting that ZFYVE26 and SPG11 are differently involved in the endolysosomal system and in autophagy, does not unravel their role and action. Here we provide clear evidence of the functional differences between these 2 proteins, through the characterisation of ZFYVE26 and SPG11 interactions with the small GTP-binding proteins RAB5A and RAB11.

RAB5 localizes on early endosomes and regulates receptor endocytosis, early endosome fusion, endosome association with microtubules and motility [30,32]. It colocalizes with both UVRAG and RUBCN on endosomes and interacts with BECN1 and PIK3C3 [31,37,40,45]. RAB11 is mainly localized on MVBs and on recycling endosomes and regulates endocytic and secretory pathways and the transport of many receptors and adhesion proteins, including EGFR (epidermal growth factor receptor) [25].

We demonstrated that ZFYVE26 interacts with both RAB5A and RAB11, that both RAB5A and RAB11 interact with BECN1 and BECN1 complex proteins PIK3C3, PIK3R4, UVRAG and RUBCN, and that these interactions are lost in the presence of AR-SPG15 mutations. We also found that AR-SPG15 mutations altered RAB5A and RAB11 biological functions, suggesting ZFYVE26 as a key player in the endosomal compartment. Two additional pieces of evidence reinforce this hypothesis further; first the reduction in the number of fused endosomes observed in AR-SPG15 cells is likely due to the decreased RAB5 activity. Indeed RAB5 activation is necessary for the recruitment of PIK3C3 on early endosomes and for the generation of PtdIns3P [45], which is required for several processes in the endosomal pathway, such as endosome fusion, endosome motility and recycling [30]. Second, it is known that RAB11, besides its role in the endocytic pathway, acts also in autophagosome maturation [34,46], being required for the fusion of autophagosomes with MVBs and the formation of amphisomes [34]. Lack of RAB11 indeed results in the accumulation of autophagosomes and late endosomes [35]. Upon autophagy induction, RAB11 induces the fusion between RAB11-decorated MVBs and autophagosomes by removing Hook from mature late endosomes (a negative regulator of endosome maturation) and translocating on autophagosomes [35]. The reduction in RAB11 activation and the loss of the interactions with PIK3C3 and HOOK1 observed in AR-SPG15 cells might impair endosome-autophagosome fusion thereby inducing accumulation of immature autophagosomes. Indeed we found that only few autophagosomes accumulated in AR-SPG15 cells were fused with MVBs and early endosomes.

We found that ZFYVE26 acts by binding to the GTP-bound form of RAB5A, as already demonstrated for BECN1, PIK3R4, PIK3C3 and EEA1. Thus, the effect of AR-SPG15 mutations on RAB activation levels cannot be direct. Rather, the effects on RAB activation must derive indirectly from altered pathways in AR-SPG15 cells. A likely possibility is an altered endocytosis. EGFR stimulates endocytosis activating RAB5A and there is a mutual relationship between the 2 partners: EGFR truncation or alterations fail to activate RAB5A and endocytosis and receptor degradation are inhibited in the absence of RAB5A [36]. An altered EGFR mediated endocytosis, like the one we see in AR-SPG15 cells, could be responsible of a reduced RAB5A activation.

The data summarized above support the hypothesis that ZFYVE26, through its PtdIns3P-binding FYVE domain and the binding with RAB proteins, localizes on RAB5 and RAB11-positive endosomal structures enriched in PtdIns3P (i.e. early endosomes and the internal vesicles of MVBs [28]) involved in autophagosome maturation, at the fusion step between autophagosomes and endosomes, where BECN1 and its binding partners PIK3C3, UVRAG and RUBCN are recruited (Fig. 12A). This is reminiscent of what had been already demonstrated in cytokinesis, where ZFYVE26 recruits BECN1 and the binding partners PIK3C3 and UVRAG to the midbody, to PtdIns3P enriched membranes [11,47]. The loss of the interactions between RAB proteins and BECN1 complexes determines endosome fusion and autophagosome fusion defects with impairment of the endocytic trafficking and the accumulation of immature autophagosomes.

ZFYVE26 has previously been reported to act in autophagic lysosome reformation (ALR), a process of lysosomal biogenesis from autolysosomes occurring after prolonged starvation [19,20]. Defects in ALR are reported for both AR-SPG15 and AR-SPG11 fibroblasts, with an increase in lysosomal size [18], decreased lysosome number and impaired recovery of lysosomes after prolonged starvation [13,19]. Our results are not in contrast with those observations. The effects of ZFYVE26 mutations on autophagosome-endosome fusion we observed in AR-SPG15 cells, were detected soon after autophagy induction. It is therefore conceivable that both autophagosome-endosome fusion defects in early stage and impaired ALR in later stage of autophagy, cooperate to

generate the AR-SPG15 phenotype. Indeed, the expression of a constitutively active form of RAB5 in AR-SPG15 cells rescues endosome-endosome fusion defects and the fusion between early endosomes and autophagosomes. However, it fails to yield a complete rescue of the autophagy defects observed in these cells, confirming the multivarious etiology of the defect, due to changes in both early and late stages of the pathway.

This work provides also novel information on SPG11, demonstrating that, like ZFYVE26, SPG11 interacts with RAB5A and RAB11 and with BECN1 and its partner proteins PIK3C3, UVRAG and RUBCN. However, unlike ZFYVE26, mutations in SPG11 neither altered RAB proteins interactions nor affected RAB5A and RAB11 activation state. As an expected consequence, in AR-SPG11 mutated cells we did not detect any defect in autophagosome-endosome fusion process. Moreover, we found that SPG11 stability and interactions depend on ZFYVE26: the mutations of ZFYVE26 affect both SPG11 expression levels and interactions, while SPG11 mutations have no effect on ZFYVE26.

These findings imply that AR-SPG15 related ZFYVE26 and SPG11 mutations have different biological roles. Indeed, the comparison of the autophagy defects in AR-SPG11 and AR-SPG15 mutated cells revealed that autophagy impairment in AR-SPG11 cells is significantly lower than in AR-SPG15. This less severe phenotype can be justified by the absence of effects of AR-SPG11 mutations on RAB proteins interactions and activation and on the autophagosome-endosome fusion process. We also found differences in terms of endosome to autophagosome and lysosome delivery, investigated by tracking EGFR movement and degradation. A more severe EGFR accumulation in early endosome and a reduced degradation of the receptor are indeed observed in AR-SPG15, while in AR-SPG11 cells, EGFR degradation is only delayed, thus confirming the previously reported differences in the effects of ZFYVE26 and SPG11 on endosomal processes [10]. It is also possible that SPG11 depletion is better tolerated by sensitive cells, such as motor neurons, and that autophagic dysfunction and accumulation of lysosomal structures only occur at late stages of the disease. Conversely, localization and stability of AP5, the

other component of the ZFYVE26-SPG11-AP5 complex, are strictly dependent upon the functionality of the other 2 proteins [10], though AP5 mutations do not induce autophagosome accumulation but rather lead to endolysosome accumulation [48]. Taken together these findings support the hypothesis that the components of the ZFYVE26-SPG11-AP5 complex share common features but have substantial differential functions and roles in health and disease conditions to be considered while planning therapeutic approaches.

In conclusion, we propose a model (Fig. 12), integrating our results and the available information, where the function of ZFYVE26 and SPG11 is now recomposed in a wider and more comprehensive picture, that explains the defective activities observed in AR-SPG15 and AR-SPG11 cells. SPG11 or ZFYVE26 loss leads to autophagosome accumulation, lysosome enlargement and autophagic lysosome reformation defects, but only ZFYVE26 has a role in the steps functionally connecting autophagy and the endocytic pathways, thereby determining a more severe autophagy defect (Fig. 12). In this view, ZFYVE26 mutations are expected to lead to multiple and more heterogeneous effects on cellular processes compared to SPG11 mutations, therefore less tolerable by neuronal cells. This may also contribute to explain the different mutation frequencies observed for the 2 overlapping HSP subtypes, AR-SPG15 (5 to 7%) and AR-SPG11 (21 to 26%) [49,4], and eventually the pleiomorphic nature of SPG11-related disease conditions, i.e. HSP, amyotrophic lateral sclerosis 5 (ALS5) and recessive axonal Charcot-Marie-Tooth (CMT) involving central and peripheral nervous system [50,51].

Materials and Methods

Patients

AR-SPG15 patients and AR-SPG11 patients analysis and clinical data are reported in our previous works [8,14,38,39]. The overview of the clinical data is reported in Table S1. Blood samples and clinical data from affected and unaffected subjects were obtained under a protocol of informed

consent approved by the Ethics Committee of the E. Medea Scientific Institute, who approved the entire study, and in accordance with the Helsinki Declaration of 1975.

In this study we analyzed 3 different mutations of the ZFYVE26 protein (L243P, S1312X and R1209fsX) and 3 different mutations of the SPG11 protein (SPG11Δ1: c.4307_4308delAA, p.W221X; SPG11Δ2: [c.3121C>T/p.R1041*]+[c.4636-3A>G] [38], SPG11Δ3: [c.1891+1G>T]+[c.7000G>C/p.A2334P] [39]).

Cell cultures and treatments

Fibroblasts cell lines were established from skin biopsies obtained from AR-SPG15 and AR-SPG11 patients, as described [14]. Fibroblasts were maintained in Dulbecco Modified Eagle Medium (DMEM; Invitrogen/Thermo Fisher Scientific, 41965062) supplemented with 10% fetal bovine serum (Euroclone, ECS0180DH), 100 U/ml penicillin/streptomycin and 2 mM L-glutamine (Invitrogen/Thermo Fisher Scientific, 15140122 and 25030024). HeLa cells were grown in the same medium.

Cells were transiently transfected using Lipofectamine 2000 (Invitrogen/Thermo Fisher Scientific, 11668027). Untransfected cells are not mock-transfected cells. Autophagy was induced by amino acid and serum starvation in Earle Balanced Salt Solution (EBSS, Euroclone, ECB4055L) for the indicated times [52]. To induce autophagosome accumulation and block the fusion with lysosomes cells were pre-treated for 30 min with 200 nM bafilomycin A_1 (BafA) (Sigma-Aldrich, B1793) in complete medium, and successively incubated in EBSS in the presence of 200 nM (BafA) for 30 min [53].

RNA interference

The shRNA plasmids for *ZFYVE26*/*SPG15* silencing were purchased from SABiosciences Corporation (KH07631G) and were characterised in our previous work [14]. In the experiments we used an shRNA with a silencing efficiency of 80% [14]. For *SPG11* silencing we used FlexiTube

siRNA for human *SPG11* with a 3'-Alexa Fluor 488 modification (Qiagen, SI04230632). Silencing efficiency was analyzed in HeLa cells transiently transfected with the siRNA or with control siRNA (Qiagen, 1022076) by quantitative Real Time PCR. RNA was prepared using Trizol (Invitrogen/Thermo Fisher Scientific, 15596026), and 1 μg/sample was reverse-transcribed into cDNA using the Superscript First Strand Synthesis System for RT-PCR kit (Invitrogen/Thermo Fisher Scientific, 11904018) and random hexamers. The expression levels of *SPG11* were analyzed by quantitative Real Time PCR on an ABI PRISM® 7900HT Fast Real-Time PCR Systems (Applied Biosystems/Thermo Fisher Scientific, Waltham, MA, USA) by using specific gene expression assays (Applied Biosystems/Thermo Fisher Scientific, Hs00276752_m1). B2M/β2 microglubulin (Applied Biosystems/Thermo Fisher Scientific, Hs99999907_m1) was used for normalization. Untransfected cells were used as endogenous control. Data were analyzed using the delta-delta-Ct method.

Antibodies and vectors

Antibodies against RAB7 (9367), RAB11A/B (5589), BECN1 (3738), PIK3C3 (4263), PIK3R4 (14580), LC3B (2775), ATG14 (5504), rabbit IgG isotype control sepharose bead conjugate (3423) and mouse anti-rabbit IgG conformation-specific HRP conjugate (5127) were purchased from Cell Signaling Technology. Anti-RAB5A (sc309, sc166600), EGFR (sc-373746), ZFYVE26/Spastizin (sc79372), ACTB/β-actin (sc47778) and EEA1 (sc6415) Abs were purchased from Santa Cruz Biotechnology. Anti-RUBCN (ab92388), HOOK1 (ab77422), RAB11A/B (ab3612) and GFP (ab290) Abs were purchased from Abcam. Anti-ZFYVE26/Spastizin (SAB3500005), SPG11/Spatacsin (HPA040412), AP5Z1 (adaptor related protein complex 5 zeta 1 subunit) (HPA035693), UVRAG (SAB4200005), EEA1 (E4156), SQSTM1/p62 (P0067 and WH0008878M1), LC3B (L7543) and RAB7 (R8779) Abs were purchased from Sigma-Aldrich. The anti-LBPA (Z-SLBPA) Ab was purchased from Echelon Biosciences Incorporated.

GFP-RAB11 WT was a gift from Richard Pagano (Addgene, 12674) [54]. mCherry-RAB5A(CA) ($RAB5A^{Q79L}$) (Addgene, 35138), GFP-RAB5A(CA) ($RAB5A^{Q79L}$) (Addgene, 35140) and GFP-RAB5A(DN) ($RAB5A^{S34N}$) (Addgene, 35141) were a gift from Sergio Grinstein [55]. mRFP-GFP-LC3B (ptfLC3B) vector was a gift from Tamotsu Yoshimori (Addgene, 21074) [56]. pCMV6-RFP-MAP1LC3B vector (RC100053) was purchased from Origene.

Confocal immunofluorescence

Cells were usually fixed with 4% paraformaldehyde for 10 min and permeabilized with phosphate-buffered saline (PBS; Euroclone, ECB4053L) containing 0.1% saponin (Sigma-Aldrich, S4521) and 1% bovine serum albumin (Sigma-Aldrich, A9647) for 30 min. For endogenous LC3 staining and the analysis with mRFP-GFP-LC3B vector, cells were fixed with cold methanol for 5 min and permeabilized with PBS containing 0.1% Triton X-100 (Sigma-Aldrich, T8787). Samples were then incubated for 2 h with primary Abs and revealed using the secondary Abs Alexa Fluor 488, 546 and 647 (Invitrogen/Thermo Fisher Scientific, A10040, A21206, A10036, A21202, A31573, A21447, A11056). For the staining of LC3-positive vesicles, cells were transfected with the pCMV6-RFP-MAP1LC3B vector. For the staining of RAB11 we used the anti-RAB11A/B Ab from Abcam or we expressed the GFP-RAB11 WT vector. To stain recycling endosomes HeLa cells were serum starved for 2 h and incubated with 10 μg/ml Alexa Fluor 555-Transferrin (TF) (Invitrogen/Thermo Fisher Scientific, T-35352) in serum-free medium for 1 h at 4°C followed by incubation at 37°C for 25 min [27]. Cells were then fixed and processed by immunofluorescence. Images were acquired using a Leica TCS SP2 AOBS confocal laser scanning microscope (Leica Microsystems GmbH, Wetzlar, Germany) with a 63x oil immersion lens at 1024x1024 pixel resolution. Vesicles were counted manually and the investigator was blinded as to the nature of the sample analyzed. Pearson correlation coefficients for proteins colocalization were determined using NIH ImageJ/Fiji software.

Immunoprecipitation and protein level analysis

Cells were lysed in ice-cold lysis buffer (20 mM Tris-HCl, pH 7.4, 150 mM NaCl, 10% glycerol, 5 mM EGTA, 1 mM EDTA, 1% Triton X-100, 50 mM NaF, 20 mM Na_3VO_4, 1 mM PMSF and protease inhibitor cocktail [Sigma-Aldrich, P8340]) and incubated on ice for 10 min [52]. Cells were sonicated and centrifuged at 14500 g for 10 min at 4°C. Supernatants were assayed and an equal amount of total proteins for each cell line was immunoprecipitated with the indicated primary Ab overnight at 4°C. Protein A-Sepharose (GE Healthcare-Italia, GEH17078001) was then added to each sample and rotated at 4°C for 1 h. Total protein extracts from untreated HeLa cells and from control fibroblasts were immunoprecipitated with an Ab against rabbit IgG isotype control conjugated with sepharose beads to determine nonspecific immunoprecipitation complexes. Immunocomplexes were washed 3 times with lysis buffer, eluted in 5x sample buffer plus 1 mM DTT at 95°C for 5 min and subjected to SDS-PAGE and western blot as described [57]. RAB7 and RAB11 proteins were revealed by using a mouse anti-rabbit IgG conformation-specific Ab that does not bind the denaturated 25-kDa rabbit IgG light chain of the Abs used for all the immunoprecipitations. RAB5A protein was revealed by using an anti-RAB5A antibody produced in mouse. Quantification of results obtained from coimmunoprecipitation experiments were performed as follow. Bands were quantified with NIH ImageJ/Fiji software using the "Gel Analysis" functions, accordingly to manufacturer instruction. The frame size for each protein (in a row) was determined drawing a region of interest that included the largest band of the row. The same frame size was then used across all the column of the row. Background correction was performed enclosing the relevant peaks on plots with the line tool. The area of the enclosed peaks was measured for each column. The amount of coimmunoprecipitated proteins was then normalized to the amount of proteins available for coimmunoprecipitation (input). This value was normalized to the amount of the protein immunoprecipitated directly by the antibody used in the IP.

RAB5A and RAB11 activation assays

RAB5A and RAB11 activation were analyzed by using RAB5A and RAB11 Activation Assay Kits (Abcam, ab173244 and ab173255), according to the manufacturer's instructions. Activation was induced with EGF (Invitrogen/Thermo Fisher Scientific, PHG0311). Briefly, cells were serum starved for 2 h and incubated with 200 ng/ml EGF for 15 min in DMEM, 20 mM HEPES, pH 7.5, 0.2% BSA. Cells were then lysed in Assay buffer plus protease inhibitor cocktail and total extracts were quantified and immunoprecipitated with a configuration-specific monoclonal Ab that specifically recognizes RAB5A-GTP or RAB11-GTP, but not their GDP-bound forms. The active GTP-bound RAB5A or RAB11 proteins were pulled down with protein A/G agarose, loaded on 12% polyacrylamide gels and detected with anti-RAB5A or -RAB11 polyclonal Abs.

Receptor-mediated endocytosis

Endocytosis was determined using Alexa Fluor-coupled EGF as endocytic probe and analyzing its delivery to lysosomes. Control and mutated fibroblasts were serum starved for 2 h and incubated with 2 µg/ml Alexa Fluor 555-EGF (Invitrogen/Thermo Fisher Scientific, E-35350) for 15 min in uptake medium (DMEM, 20 mM HEPES, pH 7.5, 2% BSA), followed by incubation in uptake medium alone for 45 min, for lysosome delivery [58]. Cells were fixed and the colocalization of EGF with early endosomes (EEA1) and lysosomes (LAMP1) was analyzed by confocal microscopy.

EGFR degradation assay

Fibroblast cells were cultured in 6-well plates and grown to 80% confluence. Cells were washed with PBS and serum starved for 16 h. EGFR degradation was induced by incubation with 200 ng/ml EGF (Invitrogen/Thermo Fisher Scientific, PHG0311) in DMEM containing 20 mM HEPES, pH 7.5 and 0.2% BSA, for different times as described [37]. Cells were then lysed in lysis buffer and subjected to SDS-PAGE and western blot.

Endosome fusion

Endosome fusion was investigated using a fluorescence assay in living cells as described [37]. ZFYVE26 mutated and control cells were incubated with 1 mg/ml Oregon Green 488-avidin and 1 mg/ml Alexa Fluor dextran 568 or 647 (Invitrogen/Thermo Fisher Scientific, A6374, D22911 and D22914), as internal control, in uptake medium (1 mM $CaCl_2$, 1 mM $MgCl_2$, 10 mM glucose) for 10 min. Cells were then washed in PBS and incubated 30 min with medium alone to label late endosomes. Cells were then incubated with 16 mg/ml biotin-BSA (Thermo Scientific Pierce, 29130) in uptake medium for 10 min to label early endosomes, fixed and processed for confocal microscopy. Biotin-avidin binding, which resulted from endosome fusion, induced a significant increase in Oregon Green 488 fluorescence. Fused vesicles (green) were counted and expressed as percentage of total vesicles (dextran-positive). Vesicles were counted manually and the investigator was blinded as to the nature of the sample analyzed.

Statistical analysis

The results are expressed as means ± standard error of the mean (SEM); *n* represents the number of individual experiments. Statistical analysis was carried out using the Student t test for unpaired variables (two-tailed), double or triple asterisks refer to statistical probabilities ($P<0.01$ and <0.001, respectively), measured in the various experimental conditions as detailed in the legend of the figures. *P* values of less than 0.05 were considered significant.

Abbreviations

ALR, autophagic lysosome reformation; AP5, adaptor related protein complex 5; AR, autosomal-recessive; HSP, hereditary spastic paraplegia/paraparesis; ATG14, autophagy related 14; BafA, bafilomycin A_1; BECN1, beclin 1; EBSS, Earle balanced salt solution; EEA1, early endosome antigen 1; EGF, epidermal growth factor; EGFR, epidermal growth factor receptor; GDP, guanosine diphosphate; GFP, green fluorescent protein; GTP, guanosine triphosphate; HSP, hereditary spastic

paraplegias; LBPA, lysobisphosphatidic acid; MAP1LC3B/LC3B, microtubule associated protein 1 light chain 3 beta; MVBs, multivesicular bodies; PIK3C3, phosphatidylinositol 3-kinase, catalytic subunit type 3; PIK3R4, phosphoinositide-3-kinase regulatory subunit 4; PtdIns3P, phosphatidylinositol-3-phosphate; RFP, red fluorescent protein; RUBCN, RUN and cysteine rich domain containing beclin 1 interacting protein; shRNA, short hairpin RNA; SQSTM1/p62, sequestosome 1; TCC: thin corpus callosum; TF, transferrin; UVRAG, UV radiation resistance associated.

Disclosure of potential conflict of interest.

The Authors report that there is no conflict of interest.

Acknowledgments

The Authors wish to thank the patients and their families for participation to the study.

Confocal images acquisition was performed in ALEMBIC, an advanced microscopy laboratory at the San Raffaele Scientific Institute.

Funding

This work was supported by the Italian Ministry of health under the frame of E-Rare-2, the ERA-Net for Research on Rare Diseases" grant NEUROLIPID, under the 5XMille Funds and the grant n. RC 2014-2017 to MTB.

References

[1]. Fink JK. Hereditary spastic paraplegia. Curr Neurol Neurosci Rep. 2006 Jan;6(1):65-76. Review. PMID: 16469273.

[2]. Depienne C, Fedirko E, Faucheux JM, Forlani S, Bricka B, Goizet C, Lesourd S, Stevanin G, Ruberg M, Durr A, et al. A de novo SPAST mutation leading to somatic mosaicism is associated

with a later age at onset in HSP. Neurogenetics. 2007 Aug;8(3):231-3. doi: 10.1007/s10048-007-0090-4. PMID: 17597328.

[3]. Novarino G, Fenstermaker AG, Zaki MS, Hofree M, Silhavy JL, Heiberg AD, Abdellateef M, Rosti B, Scott E, Mansour L, et al. Exome sequencing links corticospinal motor neuron disease to common neurodegenerative disorders. Science. 2014 Jan 31;343(6170):506-11. doi: 10.1126/science.1247363. PMID: 24482476.

[4]. Schüle R, Wiethoff S, Martus P, Karle KN, Otto S, Klebe S, Klimpe S, Gallenmüller C, Kurzwelly D, Henkel D, et al. Hereditary spastic paraplegia: Clinicogenetic lessons from 608 patients. Ann Neurol. 2016 Apr;79(4):646-58. doi: 10.1002/ana.24611. PMID: 26856398.

[5]. Stevanin G, Azzedine H, Denora P, Boukhris A, Tazir M, Lossos A, Rosa AL, Lerer I, Hamri A, Alegria P, et al. Mutations in SPG11 are frequent in autosomal recessive spastic paraplegia with thin corpus callosum, cognitive decline and lower motor neuron degeneration. Brain. 2008 Mar;131(Pt3):772-84. doi: 10.1093/brain/awm293. PMID: 18079167.

[6]. Schüle R, Schlipf N, Synofzik M, Klebe S, Klimpe S, Hehr U, Winner B, Lindig T, Dotzer A, Riess O, et al. Frequency and phenotype of SPG11 and SPG15 in complicated hereditary spastic paraplegia. J Neurol Neurosurg Psychiatry. 2009 Dec;80(12):1402-4. doi: 10.1136/jnnp.2008.167528. PMID: 19917823.

[7]. Pensato V, Castellotti B, Gellera C, Pareyson D, Ciano C, Nanetti L, Salsano E, Piscosquito G, Sarto E, Eoli M, et al. Overlapping phenotypes in complex spastic paraplegias SPG11, SPG15, SPG35 and SPG48. Brain. 2014 Jul;137(Pt 7):1907-20. doi: 10.1093/brain/awu121. PMID: 24833714.

[8]. Hanein S, Martin E, Boukhris A, Byrne P, Goizet C, Hamri A, Benomar A, Lossos A, Denora P, Fernandez J, et al. Identification of the SPG15 gene, encoding spastizin, as a frequent cause of complicated autosomal-recessive spastic paraplegia, including Kjellin syndrome. Am J Hum Genet. 2008 Apr;82(4):992-1002. doi: 10.1016/j.ajhg.2008.03.004. PMID: 18394578.

[9]. Stevanin G, Santorelli FM, Azzedine H, Coutinho P, Chomilier J, Denora PS, Martin E, Ouvrard Hernandez AM, Tessa A, Bouslam N, et al. Mutations in SPG11, encoding spatacsin, are a major cause of spastic paraplegia with thin corpus callosum. Nat Genet. 2007 Mar;39(3):366-72. doi: 10.1038/ng1980. PMID: 17322883.

[10]. Hirst J, Borner GH, Edgar J, Hein MY, Mann M, Buchholz F, Antrobus R, Robinson MS. Interaction between AP-5 and the hereditary spastic paraplegia proteins SPG11 and SPG15. Mol Biol Cell. 2013 Aug;24(16):2558-69. doi: 10.1091/mbc.E13-03-0170. PMID: 23825025.

[11]. Sagona AP, Nezis IP, Pedersen NM, Liestøl K, Poulton J, Rusten TE, Skotheim RI, Raiborg C, Stenmark H. PtdIns(3)P controls cytokinesis through KIF13A-mediated recruitment of FYVE-CENT to the midbody. Nat Cell Biol. 2010 Apr;12(4):362-71. doi: 10.1038/ncb2036. PMID: 20208530.

[12]. Murmu RP, Martin E, Rastetter A, Esteves T, Muriel MP, El Hachimi KH, Denora PS, Dauphin A, Fernandez JC, Duyckaerts C, et al. Cellular distribution and subcellular localization of spatacsin and spastizin, two proteins involved in hereditary spastic paraplegia. Mol Cell Neurosci. 2011 Jul;47(3):191-202. doi: 10.1016/j.mcn.2011.04.004. PMID: 21545838.

[13]. Varga RE, Khundadze M, Damme M, Nietzsche S, Hoffmann B, Stauber T, Koch N, Hennings JC, Franzka P, Huebner AK, et al. In Vivo Evidence for Lysosome Depletion and Impaired Autophagic Clearance in Hereditary Spastic Paraplegia Type SPG11. PLoS Genet. 2015 Aug 18;11(8):e1005454. doi: 10.1371/journal.pgen.1005454. PMID: 26284655.

[14]. Vantaggiato C, Crimella C, Airoldi G, Polishchuk R, Bonato S, Brighina E, Scarlato M, Musumeci O, Toscano A, Martinuzzi A, et al. Defective autophagy in spastizin mutated patients with hereditary spastic paraparesis type 15. Brain. 2013 Oct;136(Pt10):3119-39. doi: 10.1093/brain/awt227. PMID: 24030950.

[15]. Khundadze M, Kollmann K, Koch N, Biskup C, Nietzsche S, Zimmer G, Hennings JC, Huebner AK, Symmank J, Jahic A, et al. A hereditary spastic paraplegia mouse model supports a

role of ZFYVE26/SPASTIZIN for the endolysosomal system. PLoS Genet. 2013;9(12):e1003988. doi: 10.1371/journal.pgen.1003988. PMID: 24367272.

[16]. Słabicki M, Theis M, Krastev DB, Samsonov S, Mundwiller E, Junqueira M, Paszkowski-Rogacz M, Teyra J, Heninger AK, Poser I, et al. A genome-scale DNA repair RNAi screen identifies SPG48 as a novel gene associated with hereditary spastic paraplegia. PLoS Biol. 2010 Jun 29;8(6):e1000408. doi: 10.1371/journal.pbio.1000408. PMID: 20613862.

[17]. Vantaggiato C, Clementi E, Bassi MT. ZFYVE26/SPASTIZIN: a close link between complicated hereditary spastic paraparesis and autophagy. Autophagy. 2014 Feb;10(2):374-5. doi: 10.4161/auto.27173. PMID: 24284334.

[18]. Renvoisé B, Chang J, Singh R, Yonekawa S, FitzGibbon EJ, Mankodi A, Vanderver A, Schindler A, Toro C, Gahl WA, et al. Lysosomal abnormalities in hereditary spastic paraplegia types SPG15 and SPG11. Ann Clin Transl Neurol. 2014 Jun 1;1(6):379-389. PMID: 24999486.

[19]. Chang J, Lee S, Blackstone C. Spastic paraplegia proteins spastizin and spatacsin mediate autophagic lysosome reformation. J Clin Invest. 2014 Dec;124(12):5249-62. doi: 10.1172/JCI77598. PMID: 25365221.

[20]. Yu L, McPhee CK, Zheng L, Mardones GA, Rong Y, Peng J, Mi N, Zhao Y, Liu Z, Wan F, et al. Termination of autophagy and reformation of lysosomes regulated by mTOR. Nature. 2010 Jun 17;465(7300):942-6. doi: 10.1038/nature09076. PMID: 20526321.

[21]. Hyttinen JM, Niittykoski M, Salminen A, Kaarniranta K. Maturation of autophagosomes and endosomes: a key role for Rab7. Biochim Biophys Acta. 2013 Mar;1833(3):503-10. doi: 10.1016/j.bbamcr.2012.11.018. Review. PMID: 23220125.

[22]. Razi M, Chan EY, Tooze SA. Early endosomes and endosomal coatomer are required for autophagy. J Cell Biol. 2009 Apr 20;185(2):305-21. doi: 10.1083/jcb.200810098. PMID: 19364919.

[23]. Filimonenko M, Stuffers S, Raiborg C, Yamamoto A, Malerød L, Fisher EM, Isaacs A, Brech A, Stenmark H, Simonsen A. Functional multivesicular bodies are required for autophagic

clearance of protein aggregates associated with neurodegenerative disease. J Cell Biol. 2007 Nov 5;179(3):485-500. doi: 10.1083/jcb.200702115. PMID: 17984323.

[24]. Chen X, Wang Z. Regulation of intracellular trafficking of the EGF receptor by Rab5 in the absence of phosphatidylinositol 3-kinase activity. EMBO Rep. 2001 Jan;2(1):68-74. PMID: 11252727.

[25]. Kelly EE, Horgan CP, McCaffrey MW. Rab11 proteins in health and disease. Biochem Soc Trans. 2012 Dec 1;40(6):1360-7. doi: 10.1042/BST20120157. Review. PMID: 23176481.

[26]. Kanagaraj P, Gautier-Stein A, Riedel D, Schomburg C, Cerdà J, Vollack N, Dosch R. Souffle/Spastizin controls secretory vesicle maturation during zebrafish oogenesis. PLoS Genet. 2014 Jun 26;10(6):e1004449. doi: 10.1371/journal.pgen.1004449. PMID: 24967841.

[27]. Nagabhushana A, Chalasani ML, Jain N, Radha V, Rangaraj N, Balasubramanian D, Swarup G. Regulation of endocytic trafficking of transferrin receptor by optineurin and its impairment by a glaucoma-associated mutant. BMC Cell Biol. 2010 Jan 19;11:4. doi: 10.1186/1471-2121-11-4. PMID: 20085643 27.

[28]. Gillooly DJ, Morrow IC, Lindsay M, Gould R, Bryant NJ, Gaullier JM, Parton RG, Stenmark H. Localization of phosphatidylinositol 3-phosphate in yeast and mammalian cells. EMBO J. 2000 Sep 1;19(17):4577-88. doi: 10.1093/emboj/19.17.4577. PMID: 10970851.

[29]. Alonso R, Mazzeo C, Rodriguez MC, Marsh M, Fraile-Ramos A, Calvo V, Avila-Flores A, Merida I, Izquierdo M. Diacylglycerol kinase α regulates the formation and polarisation of mature multivesicular bodies involved in the secretion of Fas ligand-containing exosomes in T lymphocytes. Cell Death Differ. 2011 Jul;18(7):1161-73. doi: 10.1038/cdd.2010.184. PMID: 21252909.

[30]. Stenmark H, Parton RG, Steele-Mortimer O, Lütcke A, Gruenberg J, Zerial M. Inhibition of rab5 GTPase activity stimulates membrane fusion in endocytosis. EMBO J. 1994 Mar 15;13(6):1287-96. PMID: 8137813.

[31]. Ravikumar B, Imarisio S, Sarkar S, O'Kane CJ, Rubinsztein DC. Rab5 modulates aggregation and toxicity of mutant huntingtin through macroautophagy in cell and fly models of Huntington disease. J Cell Sci. 2008 May 15;121(Pt 10):1649-60. doi: 10.1242/jcs.025726. PMID: 18430781.

32. Simonsen A, Lippé R, Christoforidis S, Gaullier JM, Brech A, Callaghan J, Toh BH, Murphy C, Zerial M, Stenmark H. EEA1 links PI(3)K function to Rab5 regulation of endosome fusion. Nature. 1998 Jul 30;394(6692):494-8. doi: 10.1038/28879. PMID: 9697774.

[33]. Nielsen E, Severin F, Backer JM, Hyman AA, Zerial M. Rab5 regulates motility of early endosomes on microtubules. Nat Cell Biol. 1999 Oct;1(6):376-82. doi: 10.1038/14075. PMID: 10559966.

[34]. Fader CM, Sánchez D, Furlán M, Colombo MI. Induction of autophagy promotes fusion of multivesicular bodies with autophagic vacuoles in k562 cells. Traffic. 2008 Feb;9(2):230-50. doi: 10.1111/j.1600-0854.2007.00677.x. PMID: 17999726.

[35]. Szatmári Z, Kis V, Lippai M, Hegedus K, Faragó T, Lorincz P, Tanaka T, Juhász G, Sass M. Rab11 facilitates cross-talk between autophagy and endosomal pathway through regulation of Hook localization. Mol Biol Cell. 2014 Feb;25(4):522-31. doi: 10.1091/mbc.E13-10-0574. PMID: 24356450.

[36]. Barbieri MA, Roberts RL, Gumusboga A, Highfield H, Alvarez-Dominguez C, Wells A, Stahl PD. Epidermal growth factor and membrane trafficking. EGF receptor activation of endocytosis requires Rab5a. J Cell Biol. 2000 Oct 30;151(3):539-50. doi: 10.1083/jcb.151.3.539. PMID: 11062256.

[37]. Liang C, Lee JS, Inn KS, Gack MU, Li Q, Roberts EA, Vergne I, Deretic V, Feng P, Akazawa C, et al. Beclin1-binding UVRAG targets the class C Vps complex to coordinate autophagosome maturation and endocytic trafficking. Nat Cell Biol. 2008 Jul;10(7):776-87. doi: 10.1038/ncb1740. PMID: 18552835.

[38]. Rubegni A, Storti E, Tessa A, Federico A, Santorelli FM. Hereditary spastic paraplegia type 11 with a very late onset. J Neurol. 2015 Aug;262(8):1987-9. doi: 10.1007/s00415-015-7854-9. PMID: 26183056.

[39]. Giannoccaro MP, Liguori R, Arnoldi A, Donadio V, Avoni P, Bassi MT. Atypical late-onset hereditary spastic paraplegia with thin corpus callosum due to novel compound heterozygous mutations in the SPG11 gene. J Neurol. 2014 261(9):1825–1827. doi: 10.1007/s00415-014-7443-3. PMID: 25059394.

[40]. Sun Q, Westphal W, Wong KN, Tan I, Zhong Q. Rubicon controls endosome maturation as a Rab7 effector. Proc Natl Acad Sci U S A. 2010 Nov 9;107(45):19338-43. doi: 10.1073/pnas.1010554107. PMID: 20974968.

[41]. Tooze SA, Abada A, Elazar Z. Endocytosis and autophagy: exploitation or cooperation? Cold Spring Harb Perspect Biol. 2014 May 1;6(5):a018358. doi: 10.1101/cshperspect.a018358. Review. PMID: 24789822.

[42]. Szatmári Z, Sass M. The autophagic roles of Rab small GTPases and their upstream regulators: a review. Autophagy. 2014 Jul;10(7):1154-66. doi: 10.4161/auto.29395. Review. PMID: 24915298.

[43]. Thoresen SB, Pedersen NM, Liestøl K, Stenmark H. A phosphatidylinositol 3-kinase class III sub-complex containing PIK3R4, VPS34, Beclin 1, UVRAG and BIF-1 regulates cytokinesis and degradative endocytic traffic. Exp Cell Res. 2010 Dec 10;316(20):3368-78. doi: 10.1016/j.yexcr.2010.07.008. PMID: 20643123.

[44]. McKnight NC, Zhong Y, Wold MS, Gong S, Phillips GR, Dou Z, Zhao Y, Heintz N, Zong WX, Yue Z. Beclin 1 is required for neuron viability and regulates endosome pathways via the UVRAG-VPS34 complex. PLoS Genet. 2014 Oct 2;10(10):e1004626. doi: 10.1371/journal.pgen.1004626. PMID: 25275521.

[45]. Christoforidis S, Miaczynska M, Ashman K, Wilm M, Zhao L, Yip SC, Waterfield MD, Backer JM, Zerial M. Phosphatidylinositol-3-OH kinases are Rab5 effectors. Nat Cell Biol. 1999 Aug;1(4):249-52. doi: 10.1038/12075. PMID: 10559924.

[46]. Fader CM, Colombo MI. Autophagy and multivesicular bodies: two closely related partners. Cell Death Differ. 2009 Jan;16(1):70-8. doi: 10.1038/cdd.2008.168. Review. PMID: 19008921.

[47]. Sagona AP, Nezis IP, Bache KG, Haglund K, Bakken AC, Skotheim RI, Stenmark H. A tumor-associated mutation of FYVE-CENT prevents its interaction with Beclin 1 and interferes with cytokinesis. PLoS One. 2011 Mar 24;6(3):e17086. doi: 10.1371/journal.pone.0017086. PubMed PMID: 21455500.

[48]. Hirst J, Edgar JR, Esteves T, Darios F, Madeo M, Chang J, Roda RH, Dürr A, Anheim M, Gellera C, et al. Loss of AP-5 results in accumulation of aberrant endolysosomes: defining a new type of lysosomal storage disease. Hum Mol Genet. 2015 Sep 1;24(17):4984-96. doi: 10.1093/hmg/ddv220. PMID: 26085577.

[49]. Tesson C, Koht J, Stevanin G. Delving into the complexity of hereditary spastic paraplegias: how unexpected phenotypes and inheritance modes are revolutionizing their nosology. Hum Genet. 2015 Jun;134(6):511-38. doi: 10.1007/s00439-015-1536-7. Review. PMID: 25758904.

[50]. Orlacchio A, Babalini C, Borreca A, Patrono C, Massa R, Basaran S, Munhoz RP, Rogaeva EA, St George-Hyslop PH, Bernardi G, et al. SPATACSIN mutations cause autosomal recessive juvenile amyotrophic lateral sclerosis. Brain. 2010 Feb;133(Pt 2):591-8. doi: 10.1093/brain/awp325. PMID: 20110243.

[51]. Montecchiani C, Pedace L, Lo Giudice T, Casella A, Mearini M, Gaudiello F, Pedroso JL, Terracciano C, Caltagirone C, Massa R, et al. ALS5/SPG11/KIAA1840 mutations cause autosomal recessive axonal Charcot-Marie-Tooth disease. Brain. 2016 Jan;139(Pt1):73-85. doi: 10.1093/brain/awv320. PMID: 26556829.

[52]. Matsunaga K, Morita E, Saitoh T, Akira S, Ktistakis NT, Izumi T, Noda T, Yoshimori T. Autophagy requires endoplasmic reticulum targeting of the PI3-kinase complex via Atg14L. J Cell Biol. 2010 Aug 23;190(4):511-21. doi: 10.1083/jcb.200911141. PMID: 20713597.

[53]. Vergne I, Roberts E, Elmaoued RA, Tosch V, Delgado MA, Proikas-Cezanne T, Laporte J, Deretic V. Control of autophagy initiation by phosphoinositide 3-phosphatase Jumpy. EMBO J. 2009 Aug 5;28(15):2244-58. doi: 10.1038/emboj.2009.159. PMID: 19590496.

[54]. Choudhury A, Dominguez M, Puri V, Sharma DK, Narita K, Wheatley CL, Marks DL, Pagano RE. Rab proteins mediate Golgi transport of caveola-internalized glycosphingolipids and correct lipid trafficking in Niemann-Pick C cells. J Clin Invest. 2002 Jun. 109(12):1541-50. doi: 10.1172/JCI15420. PMID:12070301

[55]. Bohdanowicz M, Balkin DM, De Camilli P, Grinstein S. Recruitment of OCRL and Inpp5B to phagosomes by Rab5 and APPL1 depletes phosphoinositides and attenuates Akt signaling. Mol Biol Cell. 2012 Jan;23(1):176-87. doi: 10.1091/mbc.E11-06-0489. PMID:22072788

[56]. Kimura S, Noda T, Yoshimori T. Dissection of the autophagosome maturation process by a novel reporter protein, tandem fluorescent-tagged LC3. Autophagy. 2007 Sep-Oct;3(5):452-60. doi: 10.4161/auto.4451. PMID: 17534139.

[57]. Vantaggiato C, Redaelli F, Falcone S, Perrotta C, Tonelli A, Bondioni S, Morbin M, Riva D, Saletti V, Bonaglia MC, et al. A novel CLN8 mutation in late-infantile-onset neuronal ceroid lipofuscinosis (LINCL) reveals aspects of CLN8 neurobiological function. Hum Mutat. 2009 Jul;30(7):1104-16. doi: 10.1002/humu.21012. PMID: 19431184.

[58]. Tabata K, Matsunaga K, Sakane A, Sasaki T, Noda T, Yoshimori T. Rubicon and PLEKHM1 negatively regulate the endocytic/autophagic pathway via a novel Rab7-binding domain. Mol Biol Cell. 2010 Dec;21(23):4162-72. doi: 10.1091/mbc.E10-06-0495. PMID: 20943950.

Figure legends.

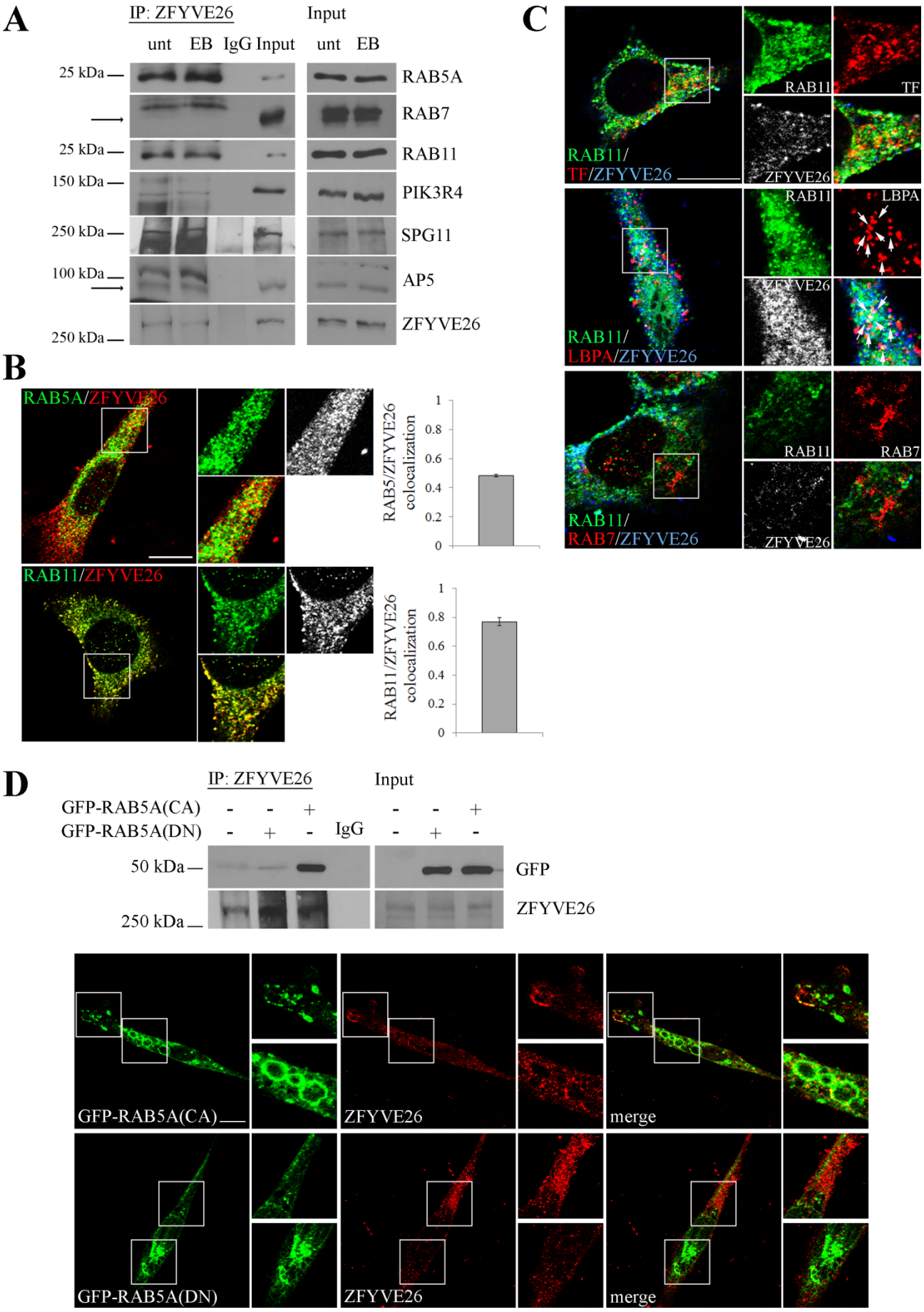

Figure 1. ZFYVE26 interactions with RAB5A and RAB11 in HeLa cells. (**A**) Total protein extracts were prepared from HeLa cells untreated (unt) or starved with EBSS (EB) for 2 h and then subjected to immunoprecipitation (IP) with anti-ZFYVE26 Ab. Proteins were loaded onto 6% and 12% SDS-polyacrylamide gels. Total protein extracts (5%) used for the IP were loaded as positive control (Input). Total protein extracts were immunoprecipitated also with an Ab against rabbit IgG isotype as negative control (IgG). Specific bands are indicated by the arrows. Shown is a representative blot out of 3 replicates. (**B**) ZFYVE26 colocalizes with RAB5A and RAB11. HeLa cells were fixed and immunostained with anti-ZFYVE26 (red) and anti-RAB5A or -RAB11A/B (green) Abs. Yellow in the merge images indicates colocalization. The small panels show a higher magnification of the area indicated in the squares. Pearson correlation coefficients for ZFYVE26 colocalization with RAB5A or RAB11 were determined in at least 30 cells/staining and reported in the graphs. Scale bar: 10 μm. (**C**) ZFYVE26 and RAB11 colocalize on LBPA-positive structures. HeLa cells were fixed and immunostained with anti-ZFYVE26 (blue), anti-RAB11A/B (green) and with the MVB marker LBPA or the late endosome and lysosome marker RAB7 (red) Abs. To stain recycling endosomes cells were incubated with Alexa Fluor 555-Transferrin (TF) for 1 h at 4°C followed by incubation at 37°C for 25 min. The small panels show a higher magnification of the area indicated in the squares. Colocalization of ZFYVE26 and RAB11 with LBPA (white) is indicated by the arrows in the magnification area. No colocalization was detected with TF and RAB7. Scale bar: 10 μm. (**D**) ZFYVE26 interacts with constitutively active RAB5A (RAB5A[CA]). HeLa cells were transfected with the active (GFP-RAB5A[CA]) or the inactive (GFP-RAB5A[DN]) forms of RAB5A and 24 h later total extracts were immunoprecipitated with anti-ZFYVE26 Ab and revealed with an anti-GFP Ab. An Ab against rabbit IgG isotype was used as negative control (IgG). Only the active GFP-RAB5A(CA) protein was immunoprecipitated. Total protein extracts (5%) used for the IP were loaded as positive control (Input). Interaction was confirmed by immunofluorescence. HeLa cells were transfected with GFP-RAB5A(CA) or GFP-RAB5A(DN) and immunostained with anti-ZFYVE26 Ab (red). RAB5A(CA) and ZFYVE26

colocalize on enlarged early endosomes (yellow in the merge). The small panels show a higher magnification of the area indicated in the squares. Scale bar: 10 μm.

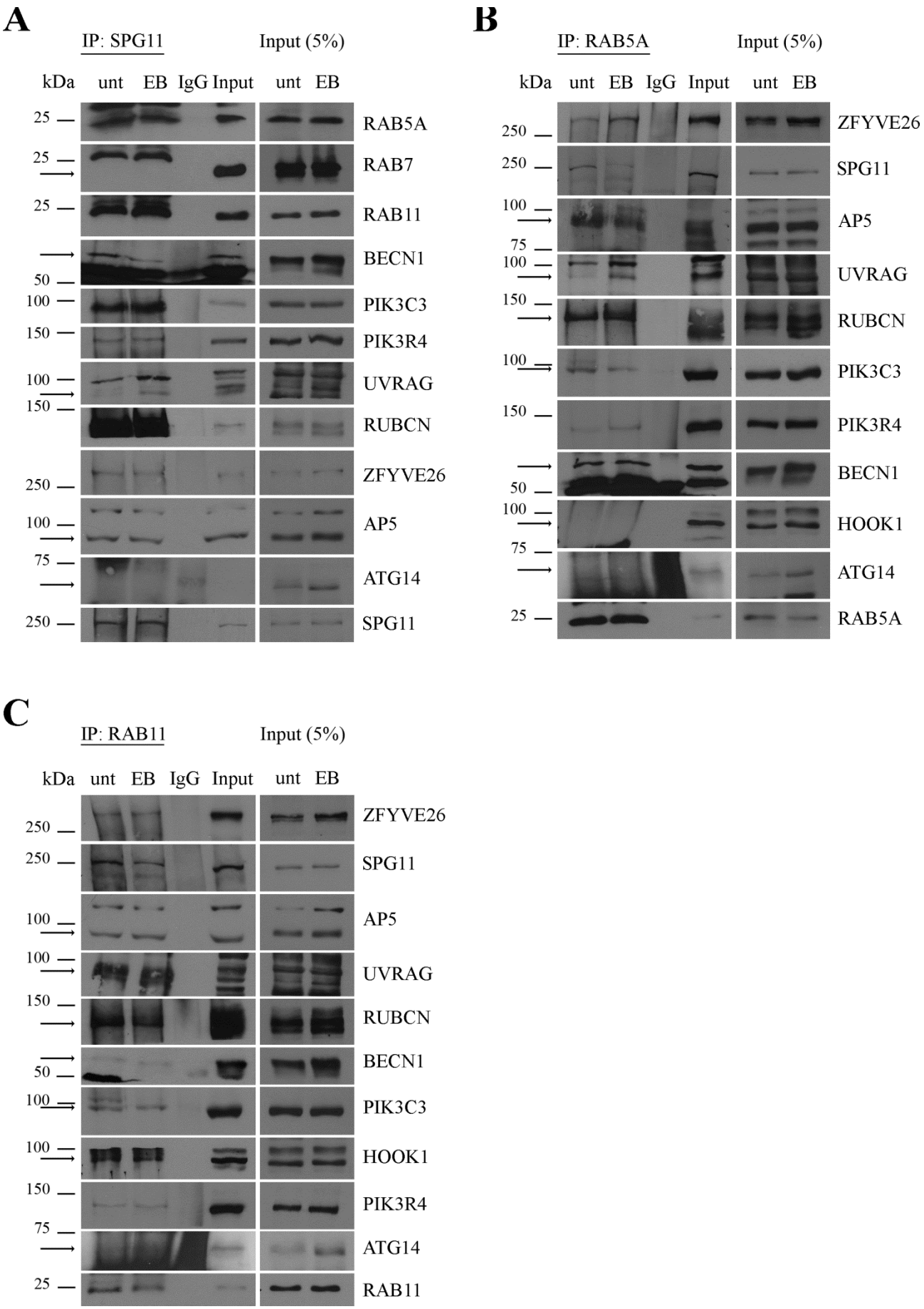
A
IP: SPG11
Input (5%)
kDa unt EB IgG Input unt EB
25
RAB5A
25
RAB7
25
RAB11
50
BECN1
100
PIK3C3
150
PIK3R4
100
150
UVRAG
RUBCN
250
ZFYVE26
100
AP5
75
ATG14
250
SPG11
B
IP: RAB5A
Input (5%)
kDa unt EB IgG Input unt EB
250
ZFYVE26
250
SPG11
100
75
AP5
100
UVRAG
150
RUBCN
100
PIK3C3
150
PIK3R4
50
BECN1
100
HOOK1
75
ATG14
25
RAB5A
C
IP: RAB11
Input (5%)
kDa unt EB IgG Input unt EB
250
ZFYVE26
250
SPG11
100
AP5
100
UVRAG
150
RUBCN
50
BECN1
100
PIK3C3
100
HOOK1
150
PIK3R4
75
ATG14
25
RAB11

Figure 2. SPG11, RAB5A and RAB11 interactions in HeLa cells. Total protein extracts were prepared from HeLa cells untreated (unt) or starved with EBSS (EB) for 2 h and then subjected to immunoprecipitation (IP) with anti-SPG11 (**A**), anti-RAB5A (**B**) or RAB11A/B (**C**) Abs. Proteins were loaded onto 6% and 12% SDS-polyacrylamide gels. Total protein extracts (5%) used for the IP were loaded as positive control (Input). Total protein extracts were immunoprecipitated also with an Ab against rabbit IgG isotype as negative control (IgG). Specific bands are indicated by the arrows. Shown is a representative blot out of 3 replicate blots. Replicates and quantification for SPG11 in the RAB5A IP are shown in Fig. S2. Original uncropped UVRAG gels from panel A and B are shown in Fig. S3. Original uncropped AP5 gels are shown in Fig. S6.

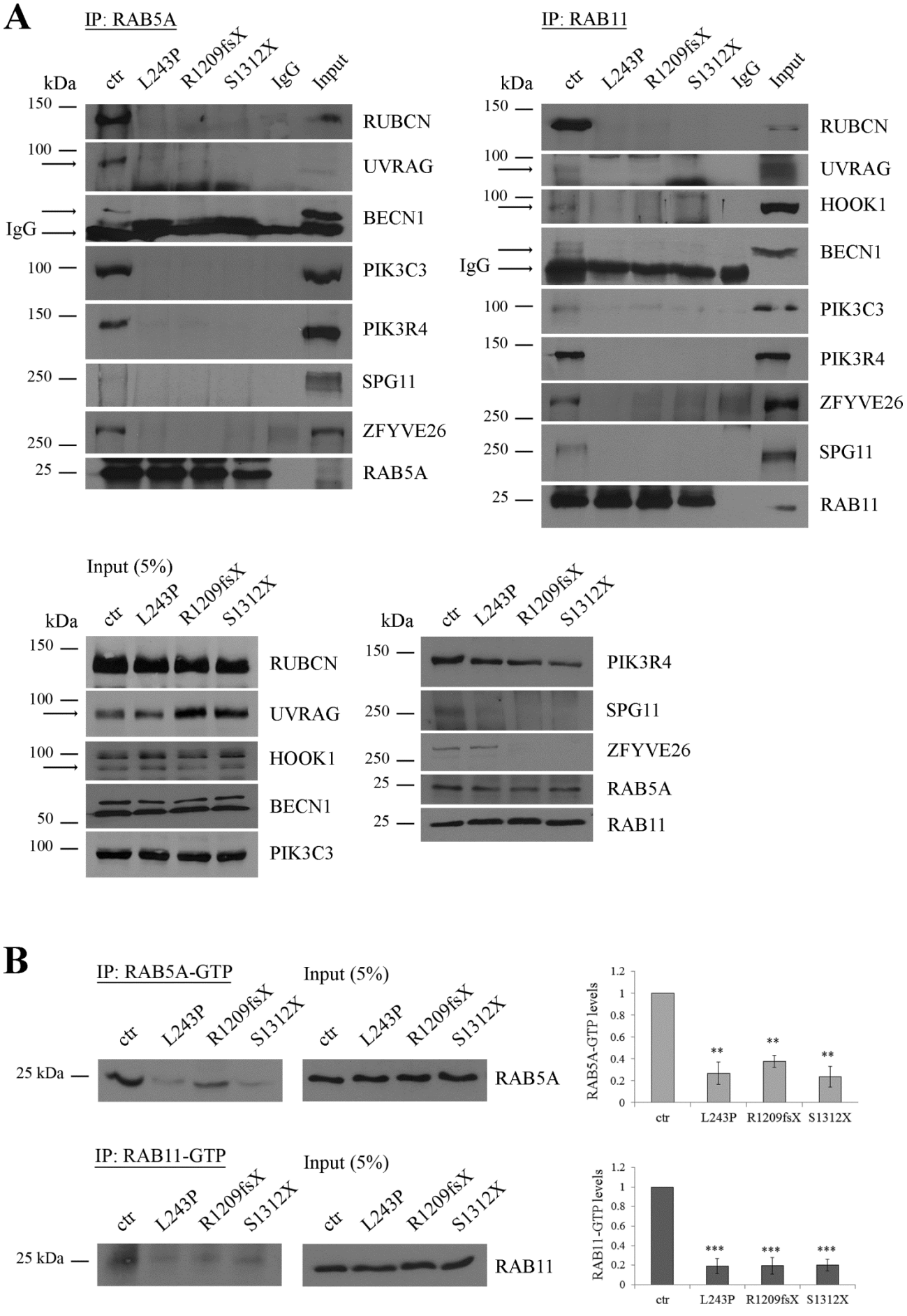
A
IP: RAB5A
kDa
ctr
L243P
R1209fsX
S1312X
IgG
Input
150
100
IgG
100
150
250
250
25
RUBCN
UVRAG
BECN1
PIK3C3
PIK3R4
SPG11
ZFYVE26
RAB5A
IP: RAB11
kDa
ctr
L243P
R1209fsX
S1312X
IgG
Input
150
100
100
IgG
100
150
250
250
25
RUBCN
UVRAG
HOOK1
BECN1
PIK3C3
PIK3R4
ZFYVE26
SPG11
RAB11
Input (5%)
kDa
ctr
L243P
R1209fsX
S1312X
150
100
100
50
100
RUBCN
UVRAG
HOOK1
BECN1
PIK3C3
kDa
ctr
L243P
R1209fsX
S1312X
150
250
250
25
25
PIK3R4
SPG11
ZFYVE26
RAB5A
RAB11
B
IP: RAB5A-GTP
Input (5%)
ctr
L243P
R1209fsX
S1312X
25 kDa
RAB5A
RAB5A-GTP levels
1.2
1
0.8
0.6
0.4
0.2
0
**
**
**
ctr
L243P
R1209fsX
S1312X
IP: RAB11-GTP
Input (5%)
ctr
L243P
R1209fsX
S1312X
25 kDa
RAB11
RAB11-GTP levels
1.2
1
0.8
0.6
0.4
0.2
0
***
***
***
ctr
L243P
R1209fsX
S1312X

Figure 3. AR-SPG15 mutations alter RAB5A and RAB11 interactions and activation state. (**A**) Total protein extracts were prepared from controls and AR-SPG15 cells with the L243P, S1312X and R1209fsX mutations of ZFYVE26, and subjected to immunoprecipitation (IP) with anti-RAB5A or anti-RAB11A/B Abs. Proteins were loaded onto 6% and 12% SDS-polyacrylamide gels. An Ab against rabbit IgG isotype was used as negative control (IgG). Specific bands are indicated by the arrows. The 50-kDa rabbit IgG heavy chain is indicated (IgG). Total protein extracts (5%) used for the IP were loaded as positive control (Input). Shown is a representative blot out of 3 replicates. Protein quantification is shown in Fig. S9. (**B**) RAB5A and RAB11 activation assay. Controls and AR-SPG15 cells with the L243P, S1312X and R1209fsX mutations of ZFYVE26 were serum starved for 2 h and incubated with 200 ng/ml EGF for 15 min. Total protein extracts were subjected to immunoprecipitation (IP) with monoclonal Abs that specifically recognize RAB5A-GTP or RAB11-GTP, but not their GDP-bound forms. Proteins were loaded onto a 12% SDS-polyacrylamide gels and revealed with rabbit anti-RAB5A or -RAB11 Abs. Total protein extracts (5%) used for the IP were loaded as positive control (Input). Shown is a representative blot out of 3 replicates. Immunoprecipitated RAB proteins levels were quantified, normalized to input levels and expressed as fold increase of control cells. The graphs show the mean ± SEM of replicates (*** $P<0.001$; ** $P<0.01$).

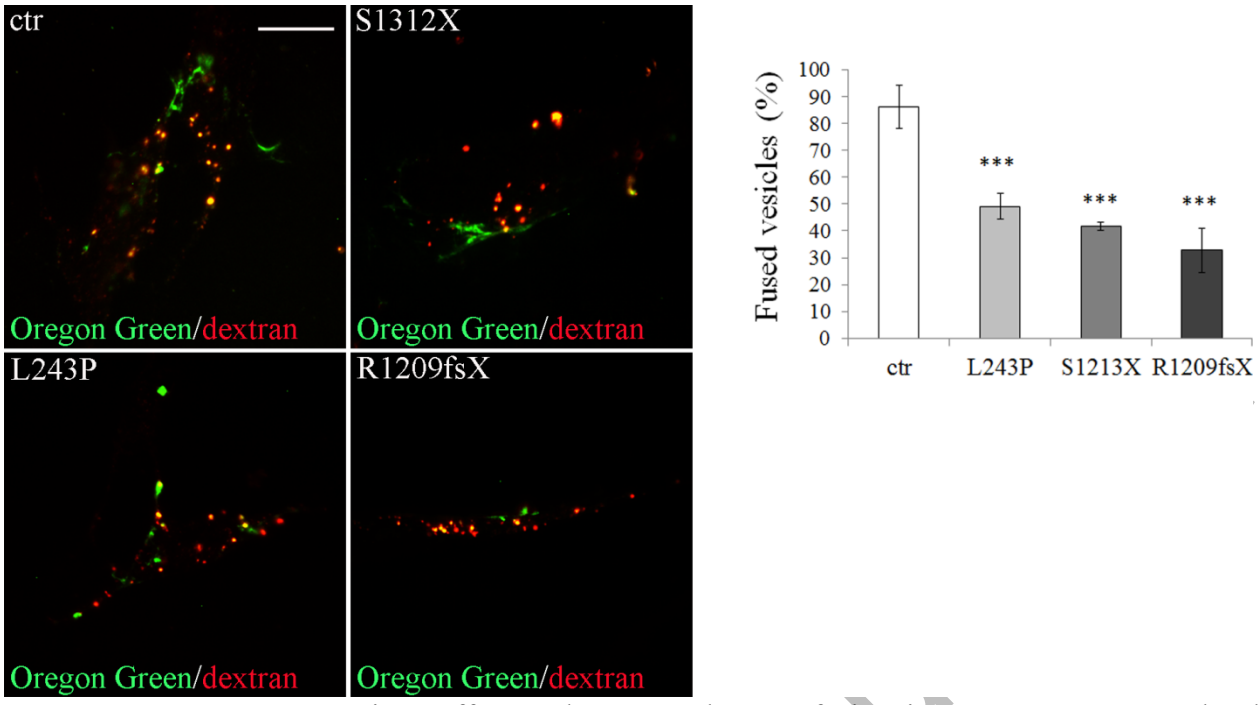

Figure 4. ZFYVE26 mutations affect endosome-endosome fusion in AR-SPG15 mutated cells. Controls (ctr), and AR-SPG15 cells with the L243P, S1312X and R1209fsX mutations of ZFYVE26 were incubated for 10 min with Oregon Green 488-avidin and Alexa Fluor 568 dextran, as internal control, followed by an incubation of 30 min to label late endosomes. Then cells were incubated with biotin-BSA in uptake medium for 10 min to label early endosomes, fixed and processed for confocal microscopy. The fusion between avidin- and biotin-labelled endosomes induced a significant increase in Oregon Green 488 fluorescence. Green fused vesicles were counted, normalized to total dextran-positive vesicles (red) and expressed as percentage. Scale bar: 10 mm.

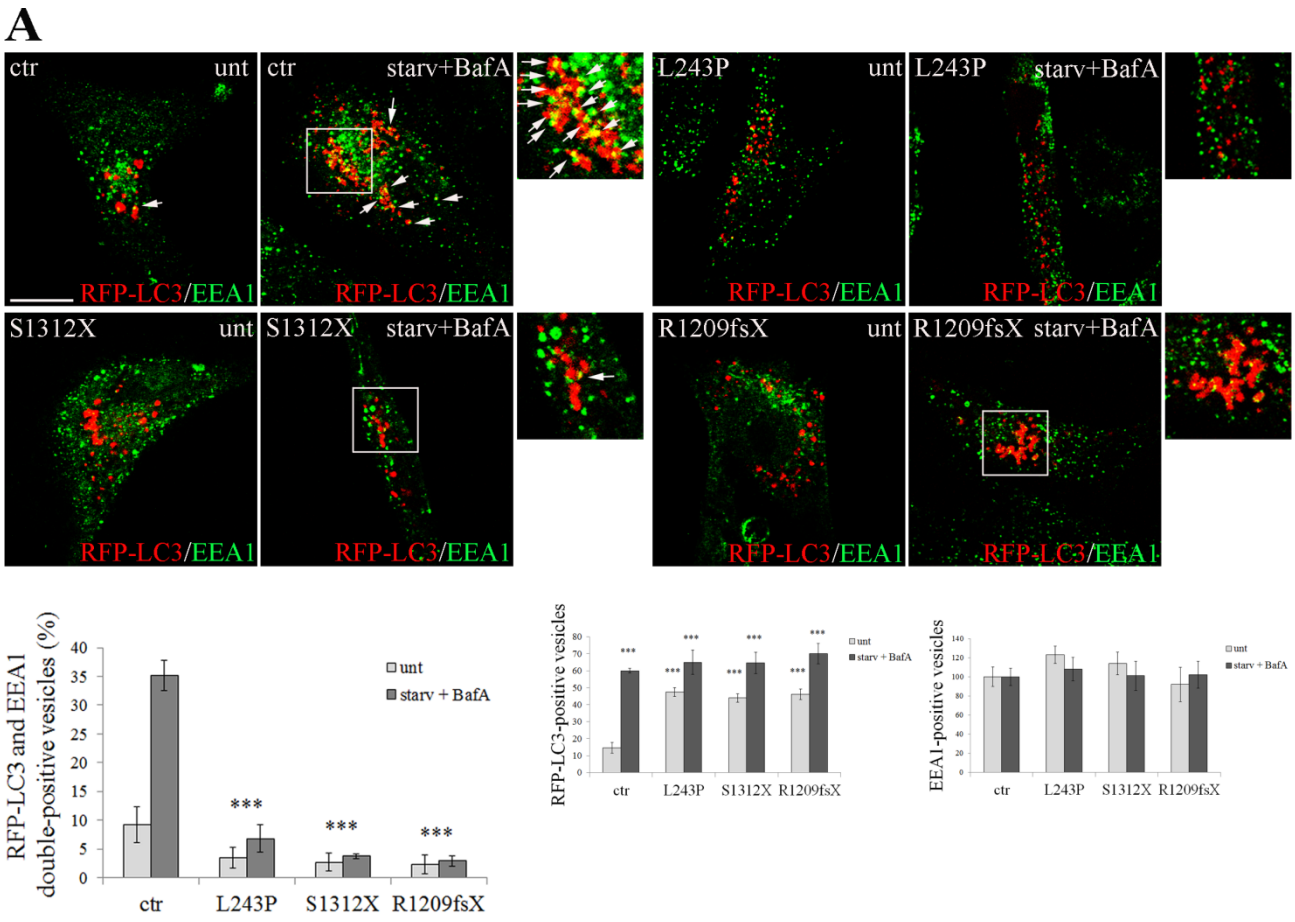
A
ctr
unt
starv+BafA
L243P
S1312X
R1209fsX
RFP-LC3/EEA1
RFP-LC3 and EEA1 double-positive vesicles (%)
unt
starv + BafA
***
ctr
L243P
S1312X
R1209fsX
RFP-LC3-positive vesicles
EEA1-positive vesicles

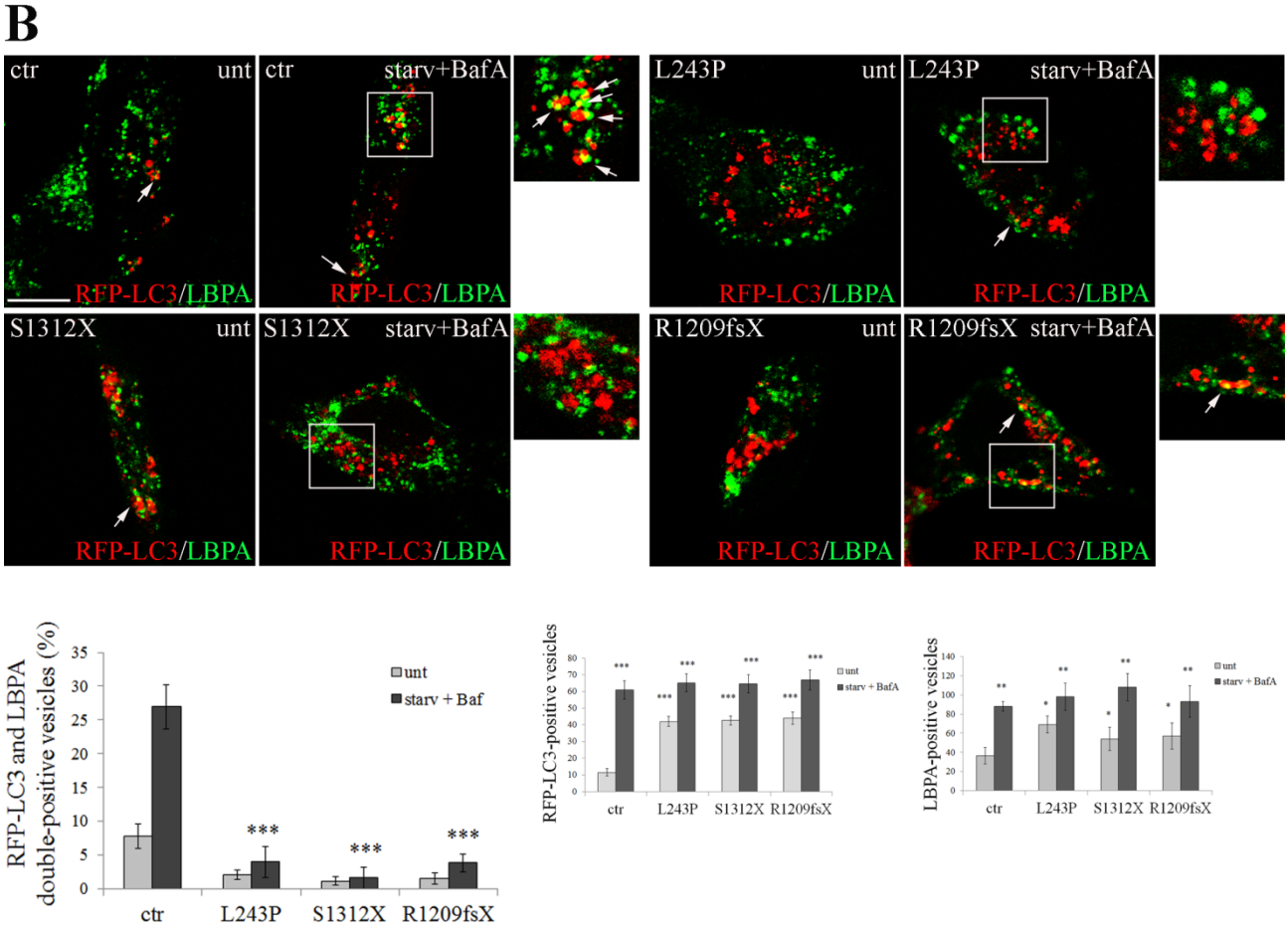
B
ctr
unt
starv+BafA
L243P
S1312X
R1209fsX
RFP-LC3/LBPA
RFP-LC3 and LBPA double-positive vesicles (%)
unt
starv + Baf
***
ctr
L243P
S1312X
R1209fsX
RFP-LC3-positive vesicles
LBPA-positive vesicles

Figure 5. ZFYVE26 mutations affect autophagosome-endosome fusion in AR-SPG15 mutated cells. (**A**) Autophagosome-early endosome fusion. Controls and AR-SPG15 cells with the L243P, S1312X and R1209fsX mutations of ZFYVE26 were transfected with pCMV6-RFP-MAP1LC3B to stain autophagosomes and incubated without (unt) or with EBSS and 200 nM BafA for 30 min (starv+BafA), fixed and subjected to immunofluorescence. Colocalization of autophagosomes (red) with the early endosomal marker EEA1 (green) was analyzed. The small panels on the right show a higher magnification of the area indicated in the square. Arrows indicates colocalization. Scale bar: 10 μm. RFP-LC3 and EEA1 double-positive vesicles were counted, normalized to total RFP-LC3-positive vesicles and expressed as percentage of the total. Total RFP-LC3- and EEA1-positive vesicle numbers are shown on the right. The graphs show the mean ± SEM of 3 independent experiments for a total of at least 30 cells for each sample (*** $P<0.001$). (**B**) Autophagosome-MVB fusion. Controls and AR-SPG15 cells the L243P, S1312X and R1209fsX mutations of ZFYVE26 were transfected with pCMV6-RFP-MAP1LC3B to stain autophagosomes and incubated without (unt) or with EBSS and 200 nM BafA for 30 min (starv+BafA), fixed and subjected to immunofluorescence. Colocalization of autophagosomes (red) with the MVB marker LBPA (green) was analyzed. The small panels on the right show a higher magnification of the area indicated in the square. Arrows indicates colocalization (yellow). Scale bar: 10 μm. RFP-LC3 and LBPA double-positive vesicles were counted, normalized to total RFP-LC3-positive vesicles and expressed as percentage of the total. Total RFP-LC3- and LBPA-positive vesicle numbers are shown on the right. The graphs show the mean ± SEM of 3 independent experiments for a total of at least 30 cells for each sample (*** $P<0.001$; * $P<0.05$).

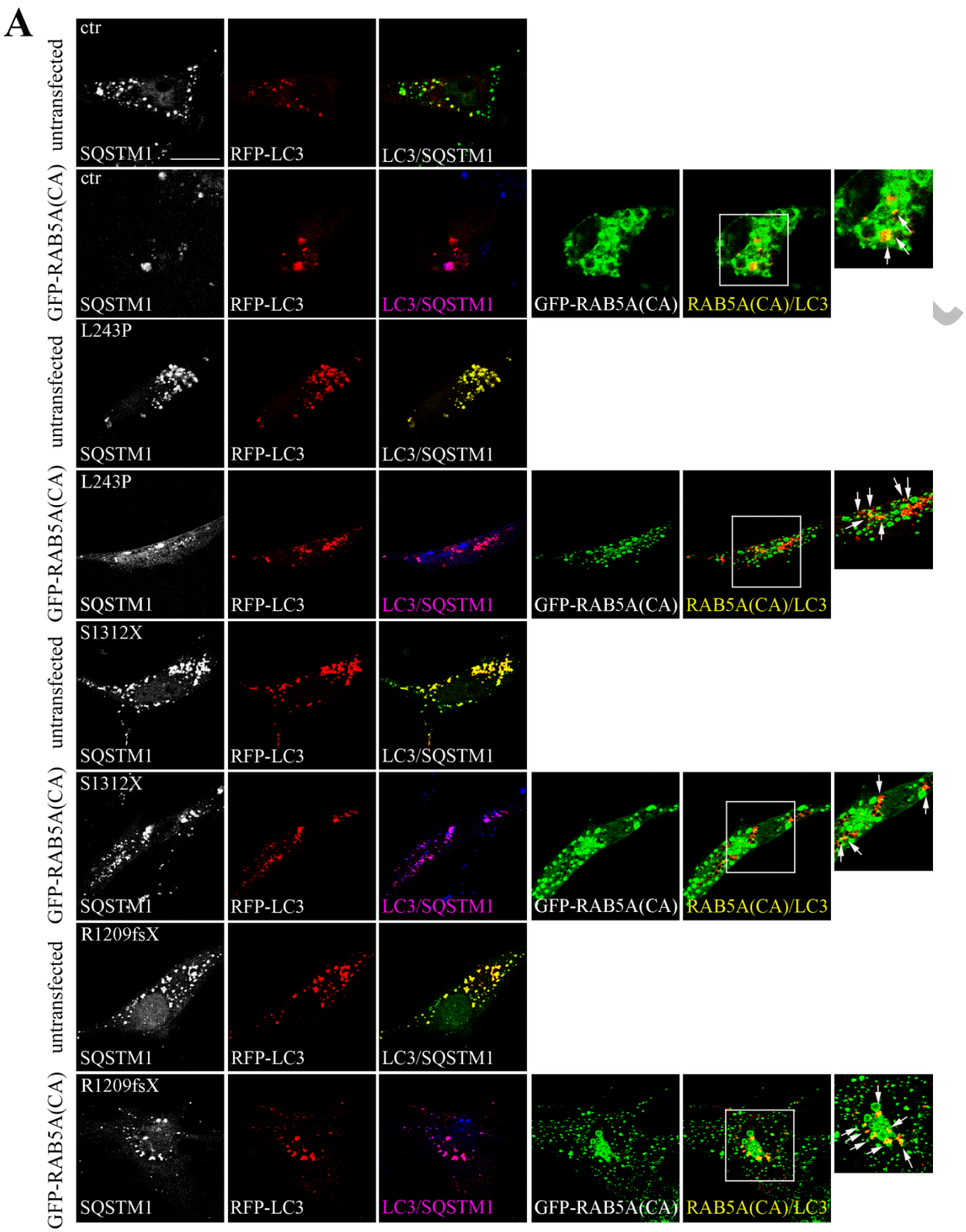
A
untransfected
GFP-RAB5A(CA)
ctr
L243P
S1312X
R1209fsX
SQSTM1
RFP-LC3
LC3/SQSTM1
GFP-RAB5A(CA)
RAB5A(CA)/LC3
B
RFP-LC3-positive vesicles
unt
GFP-RAB5A(CA)
ctr
L243P
S1312X
R1209fsX
C
RFP-LC3 and RAB5A(CA) double-positive vesicles (%)

Figure 6. Constitutively active RAB5A(CA) partially rescues the autophagy defect in AR-SPG15 cells. **(A)** Control and AR-SPG15 cells with ZFYVE26 mutations were untransfected or transfected with the GTP-bound mutant $RAB5A^{Q79L}$ (RAB5A[CA]) with a GFP tag and with the pCMV6-RFP-MAP1LC3B vector for the staining of autophagosomes. Cells were then fixed and immunostained with anti-SQSTM1 Ab (red in untransfected cells and blue in transfected cells). Scale bar: 10 μm. (**B**) Total RFP-LC3-positive vesicles from panel A were counted and are shown in the graph. The graphs show the mean ± SEM of 3 independent experiments for a total of at least 30 cells for each sample (*** $P<0.001$; * $P<0.05$). (**C**) Constitutively active RAB5A(CA) rescues autophagosome-early endosome fusion in AR-SPG15 cells. RFP-LC3 and RAB5A(CA) double-positive vesicles were counted from panel A, normalized to total RFP-LC3 vesicles and expressed as percentage of the total.

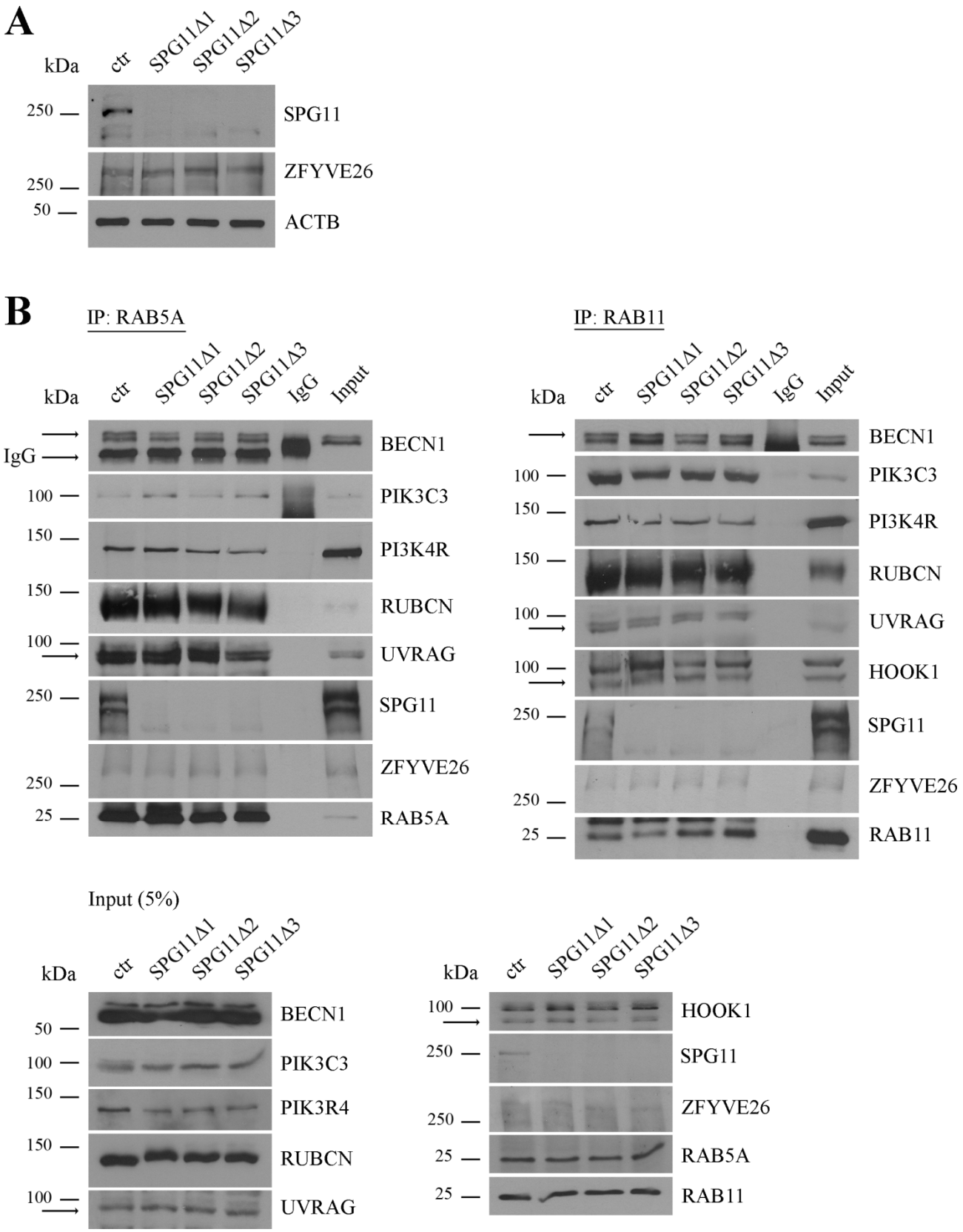

Figure 7. Effect of SPG11 mutations on RAB5A and RAB11 interactions. **(A)** SPG11 levels in SPG11 mutated cells. Total extracts from AR-SPG11 cells (with SPG11Δ1, SPG11Δ2 and SPG11Δ3 mutations) were run onto 6% SDS-polyacrylamide gel and stained with an anti-SPG11

Ab directed against the N terminal of the protein. While SPG11 is expressed in control cells, no signal is observed in AR-SPG11 mutated cells, indicating that SPG11 mutations lead to the absence of the protein. The same extracts were incubated with anti-ZFYVE26 Ab. SPG11 mutations do not affect ZFYVE26 expression levels. (**B**) SPG11 mutations do not alter RAB5A and RAB11 interactions. Total protein extracts from controls and AR-SPG11 mutated cells were subjected to immunoprecipitation (IP) with anti-RAB5A or -RAB11A/B Abs and loaded onto 6% or 12% SDS-polyacrylamide gels. IgG: control cell extract immunoprecipitated with an Ab against rabbit IgG isotype as negative control. Specific bands are indicated by the arrows. Total protein extracts (5%) used for the IP were loaded as positive control (Input). Shown is a representative blot out of 3 replicates. Protein quantification is shown in Fig. S15.

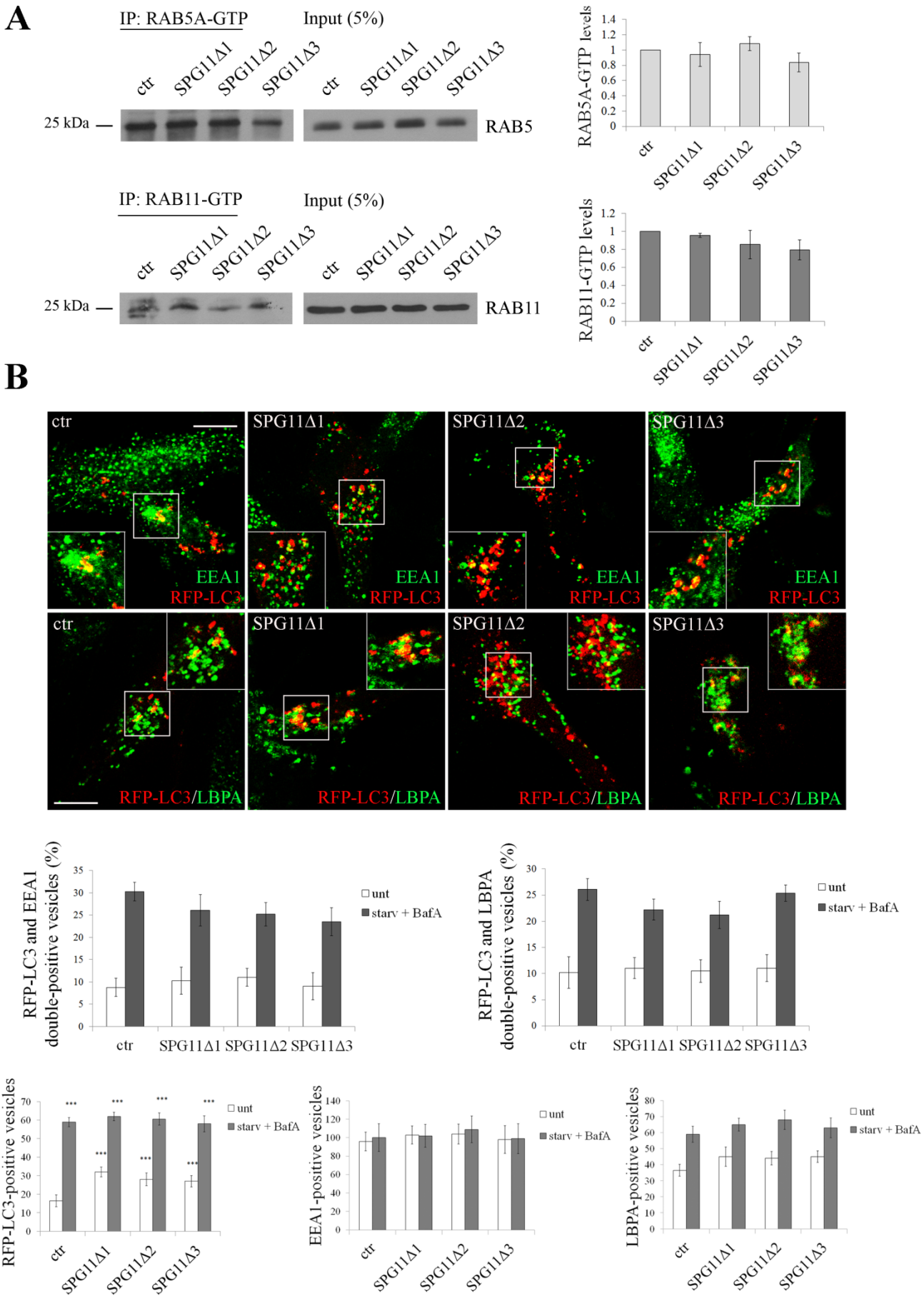
A
IP: RAB5A-GTP
Input (5%)
ctr
SPG11Δ1
SPG11Δ2
SPG11Δ3
25 kDa
RAB5
RAB5A-GTP levels
IP: RAB11-GTP
RAB11
RAB11-GTP levels
B
EEA1
RFP-LC3
RFP-LC3/LBPA
RFP-LC3 and EEA1 double-positive vesicles (%)
RFP-LC3 and LBPA double-positive vesicles (%)
unt
starv + BafA
RFP-LC3-positive vesicles
EEA1-positive vesicles
LBPA-positive vesicles

Figure 8. Effect of SPG11 mutations on RAB5A and RAB11 activity and on autophagosome-endosome fusion in AR-SPG11 mutated cells. (**A**) SPG11 mutations do not alter RAB5A and RAB11 activation. Control and AR-SPG11 mutated cells were serum starved for 2 h and incubated with 200 ng/ml EGF for 15 min. Total protein extracts were subjected to immunoprecipitation (IP) with monoclonal Abs that specifically recognizes RAB5A-GTP or RAB11-GTP, but not the GDP-bound forms of the proteins. Proteins were loaded on a 12% SDS-polyacrylamide gels and resolved with rabbit anti-RAB5A or -RAB11 Abs. Total protein extracts (5%) used for the IP were loaded as positive control (Input). Shown is a representative blot out of 3 replicates. Immunoprecipitated RAB proteins levels were quantified, normalized to input levels and expressed as fold increase of control cells. The graphs show the mean ± SEM of replicates. (**B**) SPG11 mutations do not alter autophagosome-endosome fusion. Controls and AR-SPG11 mutated cells were transfected with pCMV6-RFP-MAP1LC3B to stain autophagosomes and incubated with EBSS and 200 nM BafA for 30 min, fixed and subjected to immunofluorescence. Colocalization of autophagosomes (red) with the early endosomal marker EEA1 (green) or with the MVB marker LBPA (green) was analyzed. The small panels show a higher magnification of the area indicated in the squares. Scale bar: 10 mm. Untreated conditions were also analyzed (images not shown). RFP-LC3 and EEA1 or RFP-LC3 and LBPA double-positive vesicles were counted from untreated (unt) and treated (starv+BafA) cells, normalized to total RFP-LC3-positive vesicles and expressed as percentage of the total. Total RFP-LC3-, EEA1- and LBPA-positive vesicle numbers are shown. The graphs show the mean ± SEM of 3 independent experiments for a total of at least 30 cells for each sample (*** $P<0.001$; ** $P<0.01$).

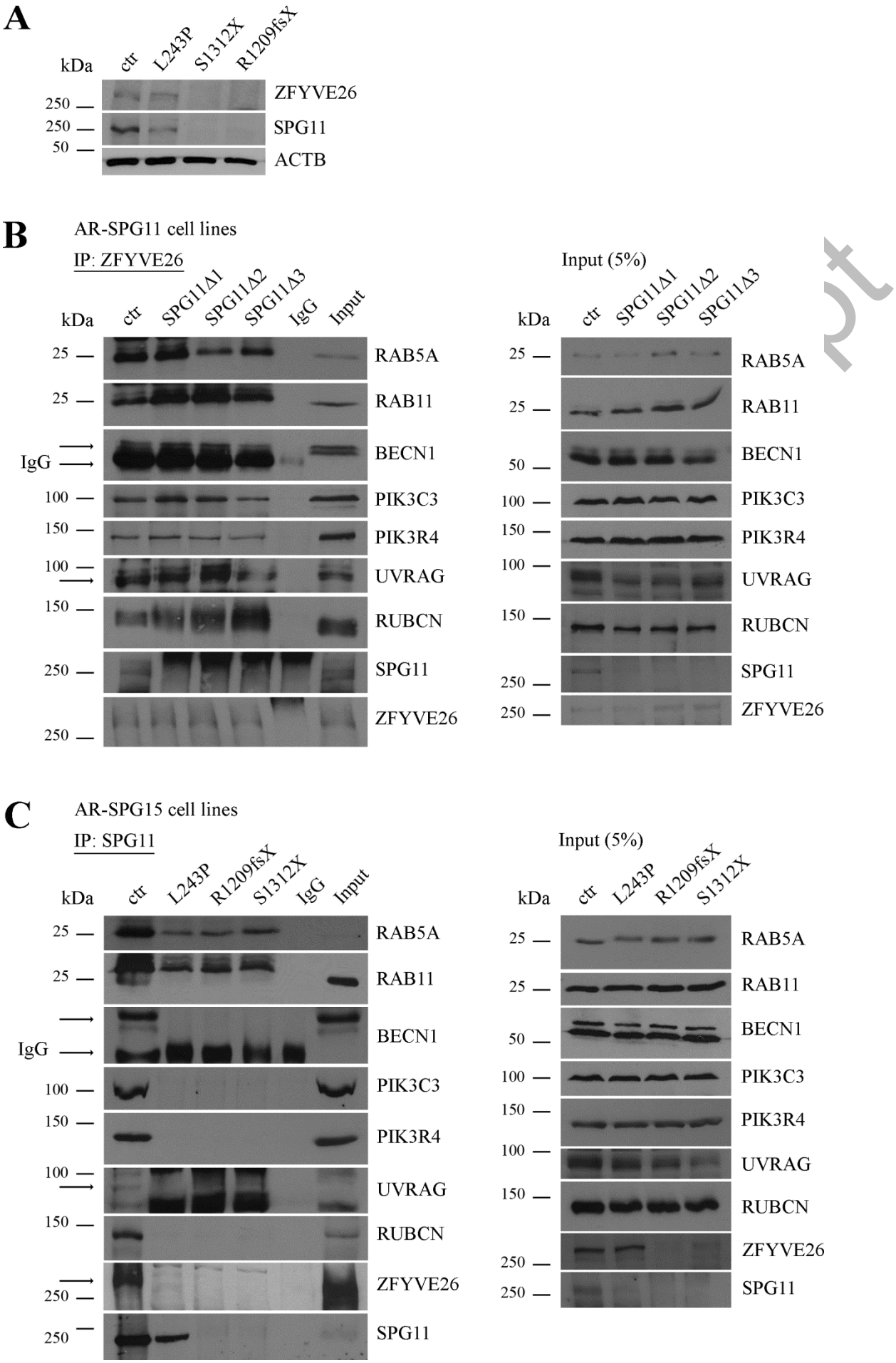
A
kDa
ctr
L243P
S1312X
R1209fsX
250
250
50
ZFYVE26
SPG11
ACTB
B
AR-SPG11 cell lines
IP: ZFYVE26
kDa
ctr
SPG11Δ1
SPG11Δ2
SPG11Δ3
IgG
Input
25
25
IgG
100
150
100
150
250
250
RAB5A
RAB11
BECN1
PIK3C3
PIK3R4
UVRAG
RUBCN
SPG11
ZFYVE26
Input (5%)
kDa
ctr
SPG11Δ1
SPG11Δ2
SPG11Δ3
25
25
50
100
150
100
150
250
250
RAB5A
RAB11
BECN1
PIK3C3
PIK3R4
UVRAG
RUBCN
SPG11
ZFYVE26
C
AR-SPG15 cell lines
IP: SPG11
kDa
ctr
L243P
R1209fsX
S1312X
IgG
Input
25
25
IgG
100
150
100
150
250
250
RAB5A
RAB11
BECN1
PIK3C3
PIK3R4
UVRAG
RUBCN
ZFYVE26
SPG11
Input (5%)
kDa
ctr
L243P
R1209fsX
S1312X
25
25
50
100
150
100
150
250
250
RAB5A
RAB11
BECN1
PIK3C3
PIK3R4
UVRAG
RUBCN
ZFYVE26
SPG11

Figure 9. Reciprocal effect of SPG11 and ZFYVE26 mutations on ZFYVE26 and SPG11 interactions. (**A**) SPG11 protein levels in AR-SPG15 cells with ZFYVE26 mutations. Total extracts from AR-SPG15 cells were run onto 6% SDS-polyacrylamide gel and stained with an anti-ZFYVE26 and -SPG11 Abs. AR-SPG15 mutations affect SPG11 expression levels. (**B**) Effect of SPG11 mutations on ZFYVE26 interactions in AR-SPG11 cells. Total protein extracts from controls and AR-SPG11 mutated cells (SPG11Δ1, SPG11Δ2 and SPG11Δ3 mutations) were subjected to immunoprecipitation (IP) with anti-ZFYVE26 Ab and loaded onto 6% and 12% SDS-polyacrylamide gels. SPG11 mutations do not affect ZFYVE26 interactions. IgG: control cell extract immunoprecipitated with an Ab against rabbit IgG isotype as negative control. Specific bands are indicated by the arrows. Where present, the 50 kDa rabbit IgG heavy chain is also indicated. Shown is a representative blot out of 3 replicates. Total protein extracts (5%) used for the IP were loaded as positive control (Input). Protein quantification is shown in Fig. S19A. (**C**) Effect of ZFYVE26 mutations on SPG11 interactions in AR-SPG15 cells. Total protein extracts from controls and AR-SPG15 cells with the L243P, S1312X and R1209fsX mutations of ZFYVE26 were subjected to immunoprecipitation (IP) with anti-SPG11 Ab and loaded onto 6% and 12% SDS-polyacrylamide gels. Total protein extracts (5%) used for the IP were loaded as positive control (Input). ZFYVE26 alter SPG11 expression and interactions. Some unspecific RAB5 IP independent of SPG11 or ZFYVE26 was observed. Protein quantification is shown in Fig. S19B.

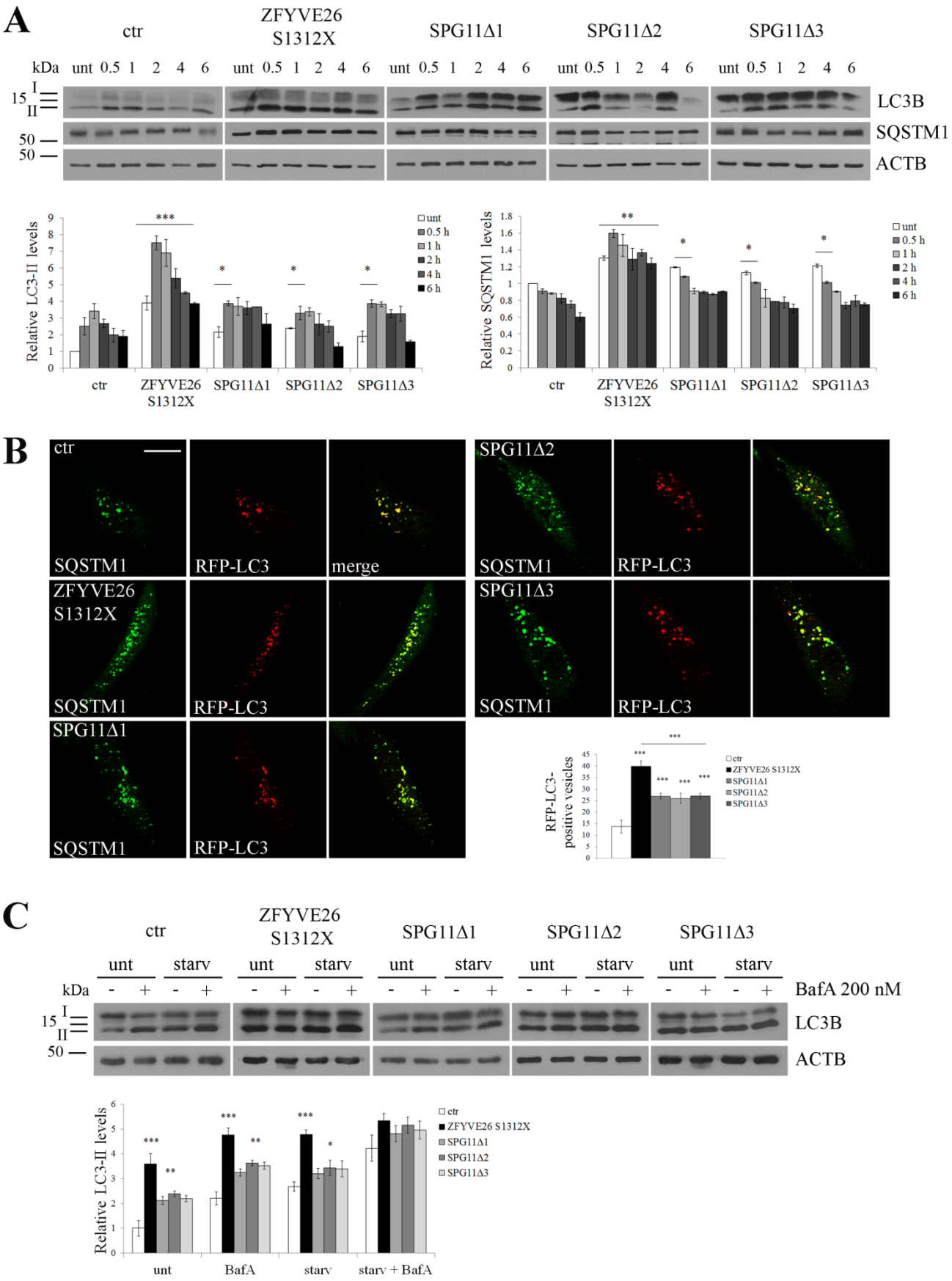

Figure 10. Autophagy in AR-SPG11 and AR-SPG15 mutated cells. (**A**) SPG11 mutations induce a lower increase in LC3-II levels compared with ZFYVE26 mutations. Controls, AR-SPG11 mutated

(SPG11Δ1, SPG11Δ2 and SPG11Δ3) cells and AR-SPG15 cells with the S1312X mutation of ZFYVE26 were starved with EBSS for different times, from 30 min to 6 h to induce autophagy. Untreated and treated cells were lysed and total protein extracts were run onto 12 or 10% SDS-polyacrylamide gels and probed with anti-LC3B, -SQSTM1 and -ACTB Abs. For quantification, mutated samples were processed in parallel with controls. Arrows indicate the 2 LC3-I and LC3-II forms of LC3. LC3-II and SQSTM1 levels were quantified, normalized to ACTB levels and expressed as fold increase of control. The graphs show the mean ± SEM of 3 independent experiments (*** $P<0.001$; ** $P<0.01$; * $P<0.05$). (**B**) SPG11 mutations induce a reduced autophagosome accumulation compared with ZFYVE26 mutations. Controls (ctr), AR-SPG11 cells (SPG11Δ1, SPG11Δ2 and SPG11Δ3 mutations) and AR-SPG15 cells with the S1312X mutation of ZFYVE26 were transfected with pCMV6-RFP-MAP1LC3B for the staining of autophagosomal vesicles (red) and 24 h later were fixed and immunostained with anti-SQSTM1 (green) Ab. Yellow in the merged images indicates colocalization of SQSTM1 and RFP-LC3. Total RFP-LC3-positive vesicle number is shown in the graph. The graphs show the mean ± SEM of 3 independent experiments for a total of at least 30 cells for each sample. Upper line indicates the *P* values for the Student t test performed between cells with AR-SPG15 and AR-SPG11 mutations (*** $P<0.001$). Scale bar: 10 μm. (**C**) Autophagic flux in AR-SPG11 and AR-SPG15 mutated cells**.** Controls (ctr), AR-SPG11 cells (SPG11Δ1, SPG11Δ2 and SPG11Δ3) and AR-SPG15 cells with the S1312X mutation of ZFYVE26 were incubated in complete medium (unt) or in EBSS (starv) for 30 min in the presence (+) or in the absence (-) of 200 nM BafA. Total protein extracts were run on 12% SDS-polyacrylamide gels and probed with anti-LC3B and -ACTB Abs. Shown is a representative blot out of 3 replicates. LC3-II levels were quantified, normalized to ACTB levels and expressed as fold increase of control. The graphs show the mean ± SEM of 3 independent experiments (*** $P<0.001$; ** $P<0.01$; * $P<0.05$).

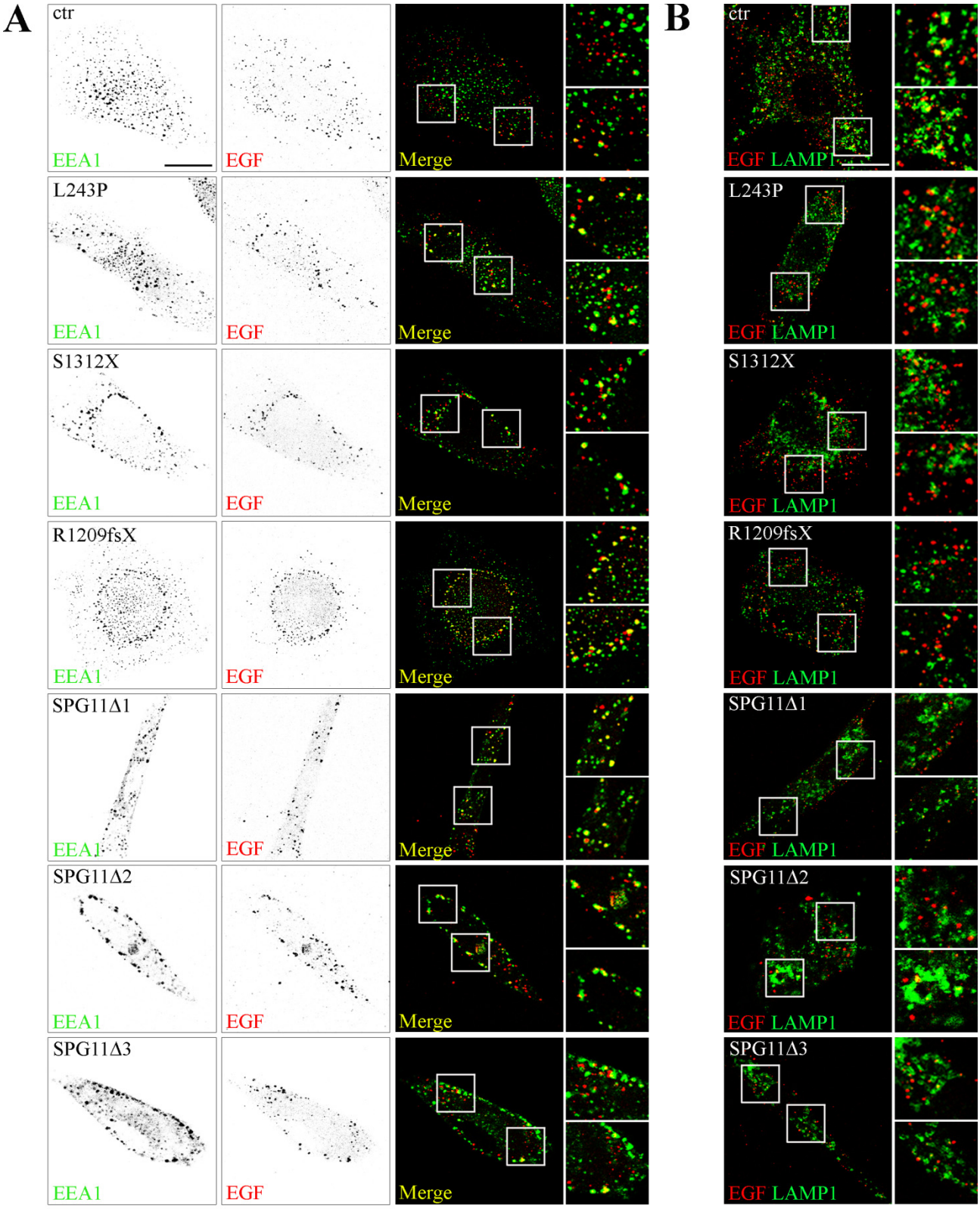
A
ctr
EEA1
EGF
Merge
L243P
S1312X
R1209fsX
SPG11Δ1
SPG11Δ2
SPG11Δ3
B
EGF LAMP1
C
EGF and EEA1 double-positive vesicles
EGF and LAMP1 double-positive vesicles
ctr
ZFYVE26 L243P
ZFYVE26 S1312X
ZFYVE26 R1209fsX
SPG11Δ1
SPG11Δ2
SPG11Δ3

Figure 11. Analysis of the effects of ZFYVE26 and SPG11 mutations on endocytic trafficking**.** Controls (ctr), AR-SPG15 and AR-SPG11 mutated cells were serum starved for 2 h and incubated with 2 μg/ml Alexa Fluor 555-EGF for 15 min in uptake medium and incubated for 45 min in EGF-free medium for lysosome delivery. Cells were fixed and EGF (red) colocalization with early endosomes (EEA1) (**A**) and lysosomes (LAMP1) (green) (**B**) was analyzed by confocal microscopy. Yellow in the merge indicates colocalization. The small panels show a higher magnification of the area indicated in the squares. Scale bar: 10 mm. (**C**) EGF and EEA1,as well as EGF and LAMP1 colocalized vesicles were counted, normalized to EGF-positive vesicles and expressed as fold increase of control. The graphs show the mean ± SEM of 3 independent experiments for a total of at least 30 cells for each sample. A Student t test was performed between AR-SPG15 or AR-SPG11 values of each individual mutation and control value (** $P<0.01$) and between values of the AR-SPG15 and AR-SPG11 mutations (** $P<0.01$).

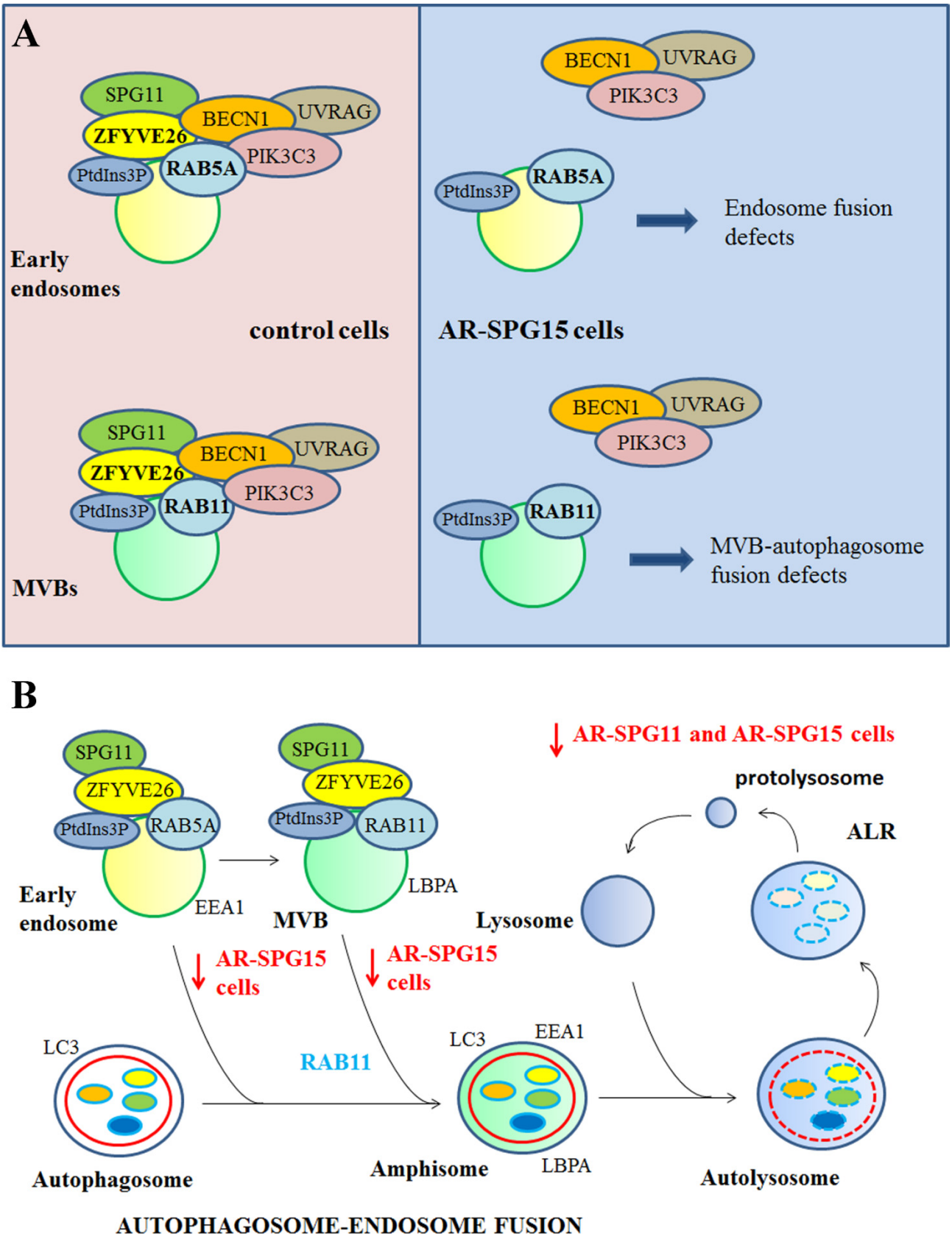

Figure 12. ZFYVE26 and SPG11 in autophagy and endolysosomal pathway. **(A)** In control cells ZFYVE26, through its PtdIns3P-binding FYVE domain, recruits BECN1 and its binding partners PIK3C3, UVRAG and RUBCN on RAB5A and RAB11-positive endosomal structures enriched in

PtdIns3P, i.e. early endosomes and the internal vesicles of MVBs [28]. In AR-SPG15 cells, where ZFYVE26 is mutated or absent, RAB proteins are less activated and do not interact with the BECN1 complexes. These in turn induce endosome fusion and autophagosome fusion defects with impairment of the endocytic trafficking and accumulation of immature autophagosomes. (**B**) Autophagy and endocytosis are strictly interconnected: autophagosome maturation requires the fusion of autophagosomes with endosomes [21]. In particular, autophagosomes fuse with early endosomes and MVBs to form amphisomes that later fuse with lysosomes for cargo degradation. Both autophagosomes and amphisomes share the autophagy marker LC3. After fusion with endosomes, amphisomes present also the early endosomal and MVBs markers EEA1 and LBPA. Fusion between MVBs and autophagosomes is mediated by RAB11 [35]. Amphisomes subsequently fuse with lysosomes to form autolysosomes for cargo degradation. After prolonged starvation new lysosomes form from autolysosomes through the autophagic lysosome reformation process (ALR) [20]. Both ZFYVE26 and SPG11 are involved in ALR such that AR-SPG15 and AR-SPG11 mutated cells present defects in lysosome reformation with depletion of free lysosomes and accumulation of autolysosomes [13,19]. Since only ZFYVE26 is involved in endosome-autophagosome fusion, only AR-SPG15 mutated cells present defects in autophagosome-endosome fusion with accumulation of amphisomes.

Table S1. Overview of clinical and molecular features of AR-SPG15 and AR-SPG11 patients.

Patient/ Features	**P664-I**	**P582**	**F761/3**		**P1**	**PII-3**
HSP subtype/ mutation	AR-SPG15/ ZFYVE26 L243P	AR-SPG15/ ZFYVE26 S1312X	AR-SPG15/ ZFYVE26 R1209fsX	AR-SPG11/ SPG11Δ1 (W221X)	AR-SPG11/ SPG11Δ2 (R1041X)	AR-SPG11/ SPG11Δ3 (A2334P)
Reference	[14]	[14]	[8]	this work	[38]	[39]
Gender	F	F	M	M	M	M
Age at onset (y)/ symptoms at onset	38/ walking difficulties and rigidity at LL	14/ walking difficulties and rigidity at LL	12/ walking difficulties and rigidity at LL	8/ learning disability and difficulties while running	47/ walking difficulties and urinary disturbances	42/ walking difficulties and urinary disturbances
Disease duration (y)	17	13	26	20	5	5
Disability score (n/7)	7	6	6	5	3	2-3
Clinical features	Severe spastic paraparesis, moderate mental deterioration	Severe spastic paraparesis, trunk ataxia, sever axonal neurophaty, mild mental deterioration	Severe spastic paraparesis, axonal neuropathy, pseudo bulbar dysarthria	Spastic paraparesis	Spastic paraparesis, axonal polyneuropathy	Spastic paraparesis, very mild mental deterioration
Cerebral MRI	TCC, white matter hyperintensity	Diffuse periventricular hyperintensity and TCC	TCC, periventricular white matter changes, marked cortical atrophy, mild cerebellar atrophy	TCC, cerebellar atrophy, white matter changes	TCC, periventricular white matter changes	TCC, periventricular frontal white matter hyperintensity

LL: lower limbs; TCC: thin corpus callosum, y: years.

Disability assessed on a 7 point scale: 1, minimal disability (slight stiffness of the legs); 2, mild disability (unable to run, but full autonomy); 3, moderate disability when walking (reduced perimeter, frequent falls); 4, severe disability (unilateral support required to walk); 5, bilateral support required to walk; 6, wheelchair bound; 7, bedridden.

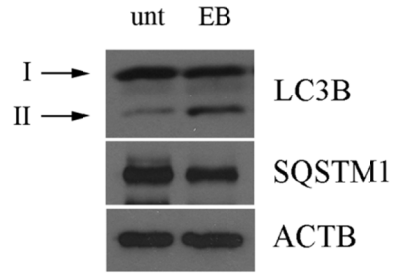

Figure S1. Autophagy induction in EBSS-treated HeLa cells. HeLa cells were treated with EBSS for 2 h. Untreated and treated cells were lysed and total protein extracts were run on 12 or 10% SDS-polyacrylamide gels and probed with anti-LC3B, SQSTM1 and ACTB Abs. Arrows indicate the LC3-I and LC3-II forms. Treatment with EBSS induces an increase in LC3-II levels and a decrease in SQSTM1 levels, as expected.

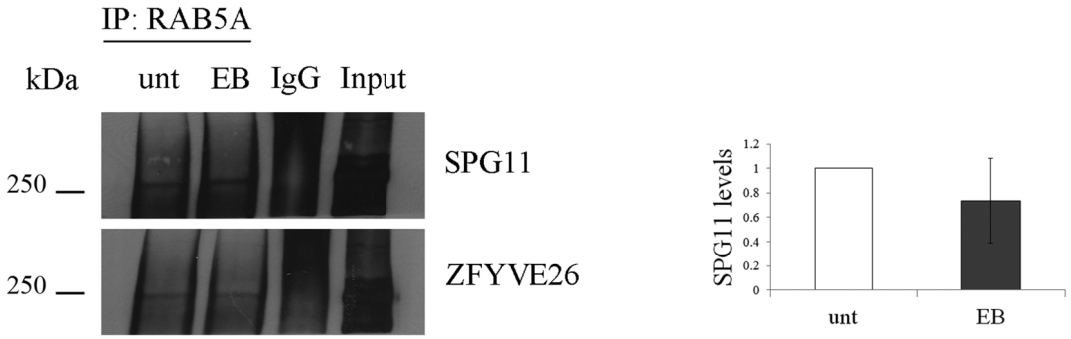

Figure S2. Shown are the 2 replicates of the analysis of SPG11 and RAB5A interaction in HeLa cells. SPG11 levels were quantified from Fig. 2B and from the 2 replicates above and showed in the graph. There is no difference in the amount of SPG11 immunoprecipitated in untreated (unt) and starved (EB) conditions in HeLa cells.

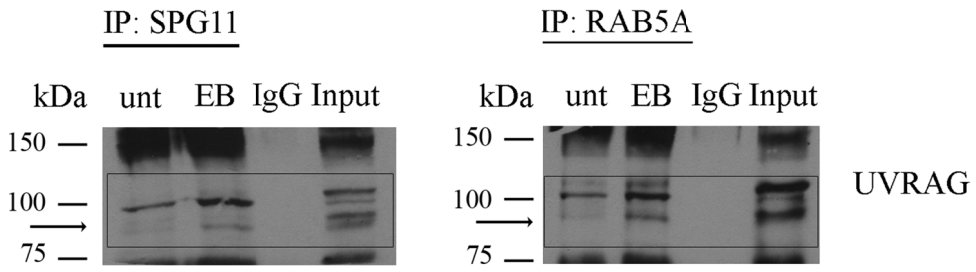

Figure S3. Original uncropped UVRAG gels of Figure 2A and 2B.

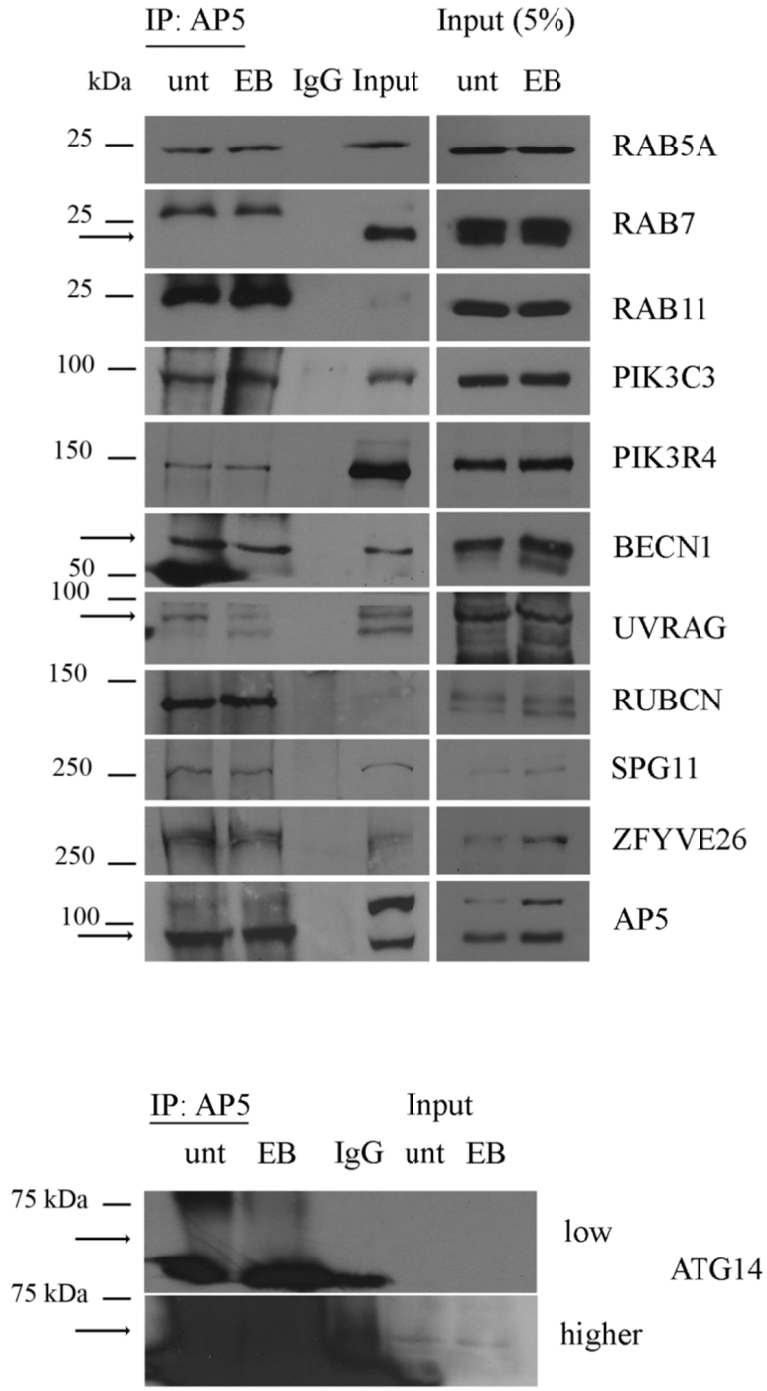

Figure S4. AP5 interacts with RAB5 and RAB11 in HeLa cells. Total protein extracts were prepared from HeLa cells untreated (unt) or starved with EBSS (EB) and then subjected to immunoprecipitation (IP) with anti AP5 Ab. Proteins were loaded on 6% and 12% SDS-polyacrylamide gels. Total protein extracts (5%) used for the IP were loaded as positive control (Input). An Ab against rabbit IgG isotype was used as negative control (IgG). Specific bands are

indicated by the arrows. For ATG14 are shown a low and a higher exposure to detect proteins in the IP and the input sections of the gels. Original uncropped AP5 gel is shown in Fig. S6.

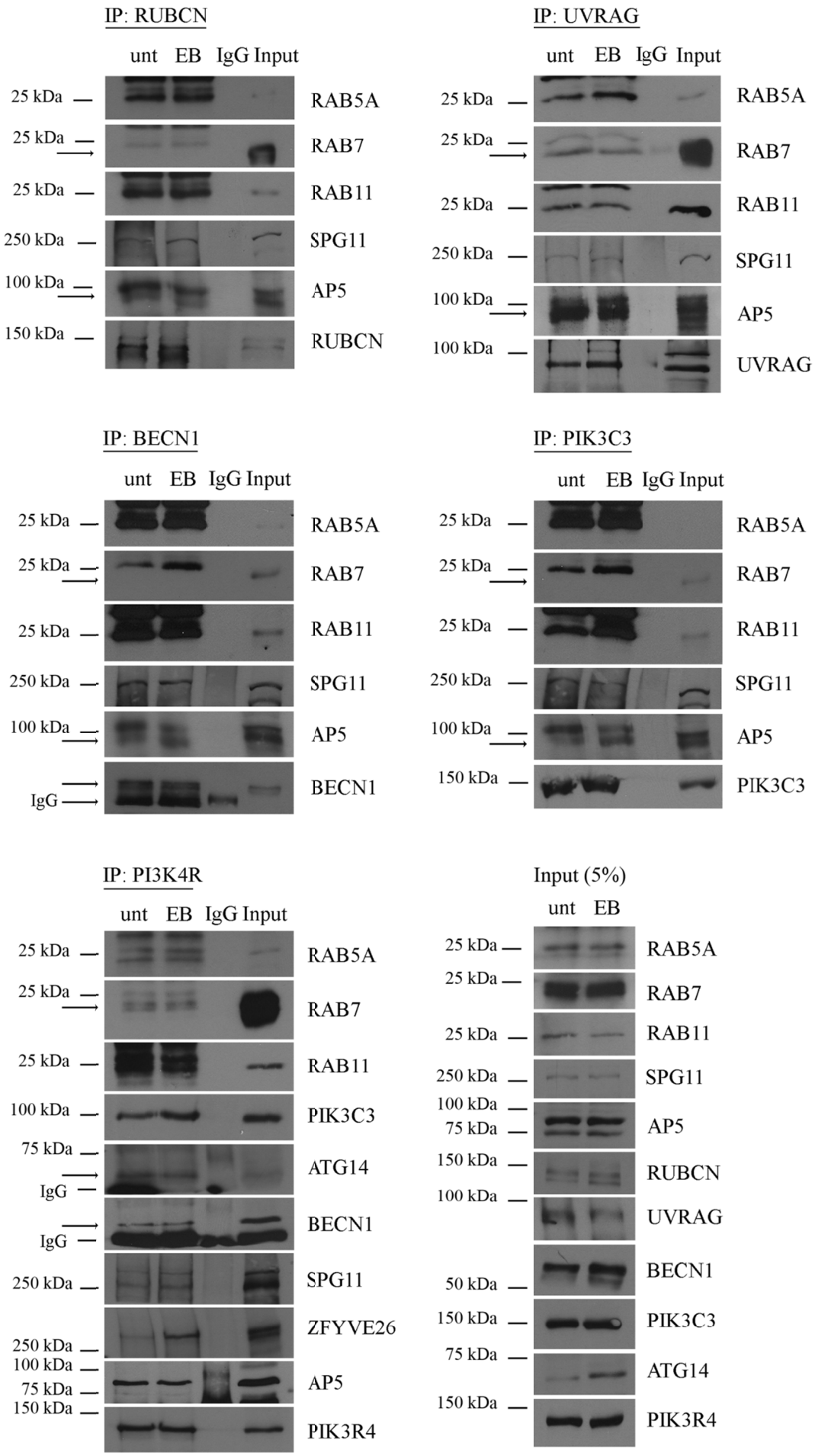
IP: RUBCN
unt EB IgG Input
25 kDa
RAB5A
25 kDa
RAB7
25 kDa
RAB11
250 kDa
SPG11
100 kDa
AP5
150 kDa
RUBCN
IP: UVRAG
unt EB IgG Input
25 kDa
RAB5A
25 kDa
RAB7
25 kDa
RAB11
250 kDa
SPG11
100 kDa
AP5
100 kDa
UVRAG
IP: BECN1
unt EB IgG Input
25 kDa
RAB5A
25 kDa
RAB7
25 kDa
RAB11
250 kDa
SPG11
100 kDa
AP5
IgG
BECN1
IP: PIK3C3
unt EB IgG Input
25 kDa
RAB5A
25 kDa
RAB7
25 kDa
RAB11
250 kDa
SPG11
100 kDa
AP5
150 kDa
PIK3C3
IP: PI3K4R
unt EB IgG Input
25 kDa
RAB5A
25 kDa
RAB7
25 kDa
RAB11
100 kDa
PIK3C3
75 kDa
ATG14
IgG
IgG
BECN1
250 kDa
SPG11
ZFYVE26
250 kDa
100 kDa
75 kDa
150 kDa
AP5
PIK3R4
Input (5%)
unt EB
25 kDa
RAB5A
25 kDa
RAB7
25 kDa
RAB11
250 kDa
SPG11
100 kDa
75 kDa
AP5
150 kDa
RUBCN
100 kDa
UVRAG
50 kDa
BECN1
150 kDa
PIK3C3
75 kDa
ATG14
150 kDa
PIK3R4

Figure S5. RUBCN, UVRAG, BECN1, PIK3C3 and PIK3R4 interactions in HeLa cells. Total protein extracts were prepared from HeLa cells untreated (unt) or starved with EBSS (EB) for 2 h and then subjected to immunoprecipitation (IP) with anti-RUBCN, -UVRAG, -BECN1, -PIK3C3 and -PIK3R4 Abs. Proteins were loaded on 6% and 12% SDS-polyacrylamide gels. RUBCN, UVRAG, BECN1, PIK3C3 and PIK3R4 interact with RAB5A, RAB11, SPG11 and AP5. Protein interactions with ZFYVE26 have been extensively demonstrated in our previous work [14]. Total protein extracts (5%) used for the IP were loaded as positive control (Input). Total protein extracts were immunoprecipitated with an Ab against rabbit IgG isotype as negative control (IgG). Specific bands are indicated by the arrows. The 50-kDa rabbit IgG heavy chain is indicated (IgG heavy) where present. Shown is a representative blot out of 3 replicates. Original uncropped AP5 gels are shown in Fig. S6.

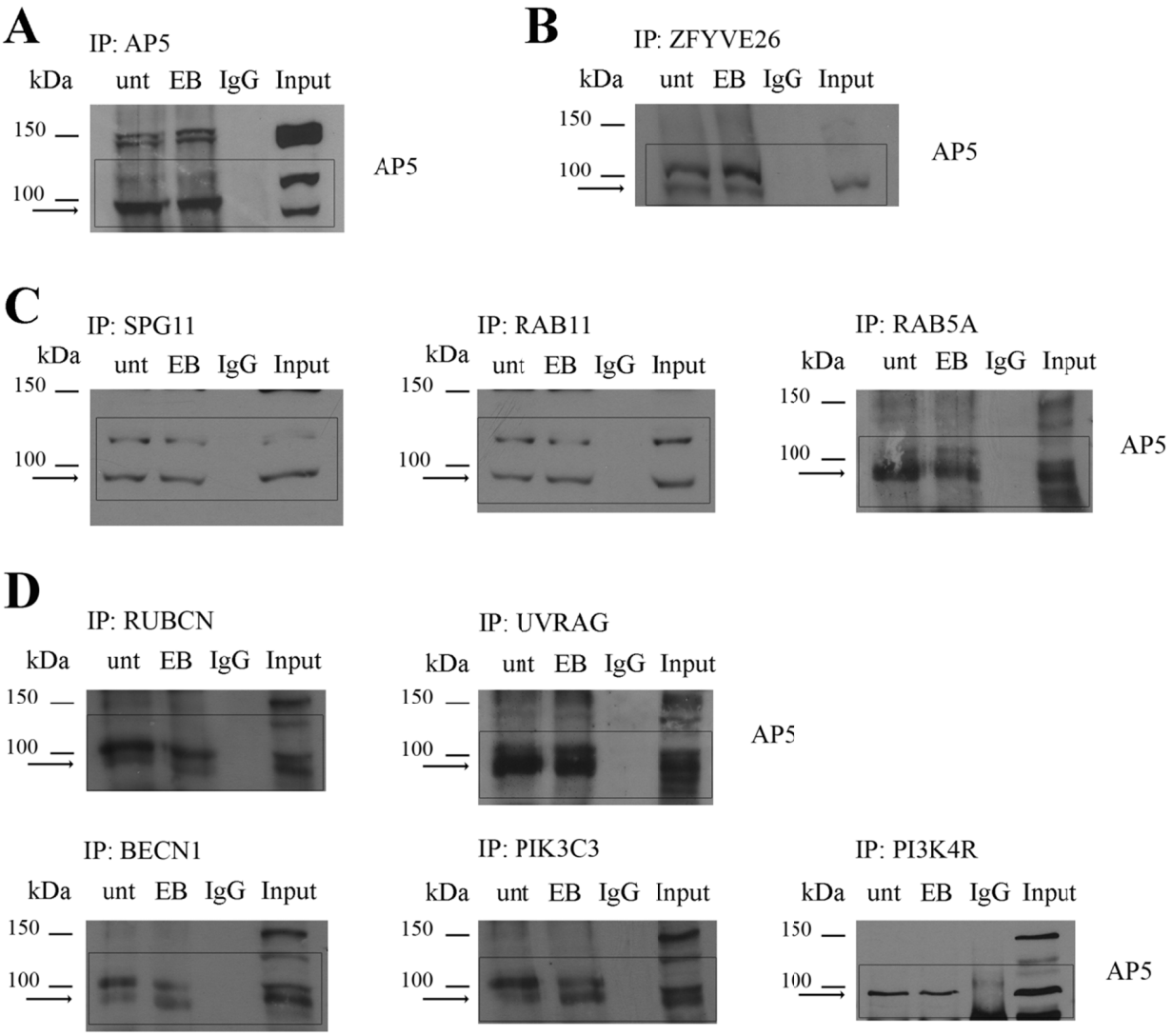

Figure S6. Original uncropped gels of AP5 immunoprecipitation in HeLa cells of Fig. S4 (**A**), Fig. 1A (**B**), Fig. 2 (**C**) and Fig. S5 (**D**).

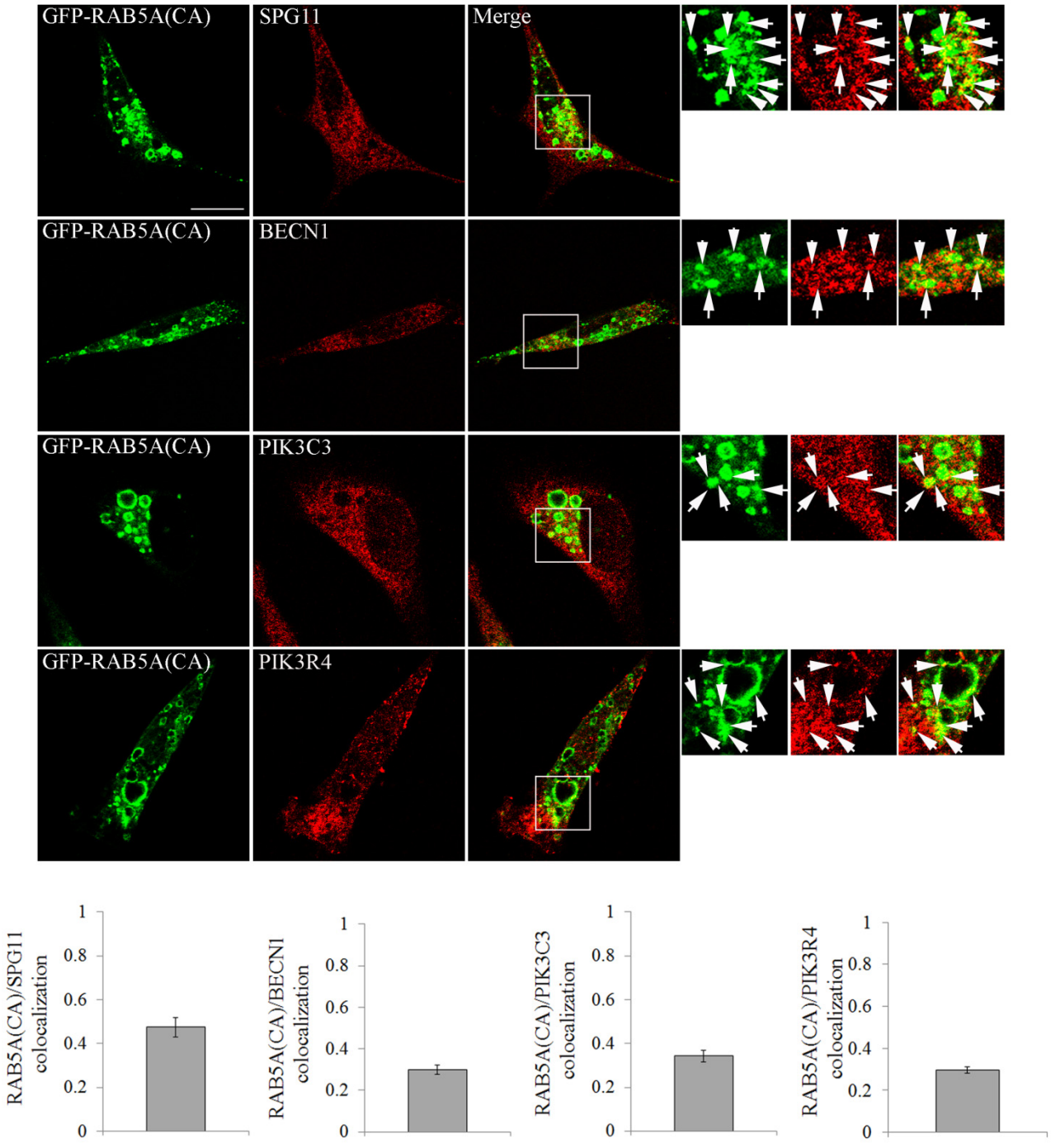

Figure S7. SPG11, BECN1, PIK3C3 and PIK3R4 colocalize with RAB5A(CA). HeLa cells were transfected with GFP-RAB5A(CA), fixed and immunostained with anti-SPG11, -BECN1, -PIK3C3 and -PIK3R4 (red) Abs. A representative image is shown. The small panels show a higher magnification of the area indicated in the squares. Arrows indicate colocalization (yellow). Pearson correlation coefficients for proteins colocalization were determined in at least 30 cells/staining and reported in the graphs. Scale bar: 10 μm.

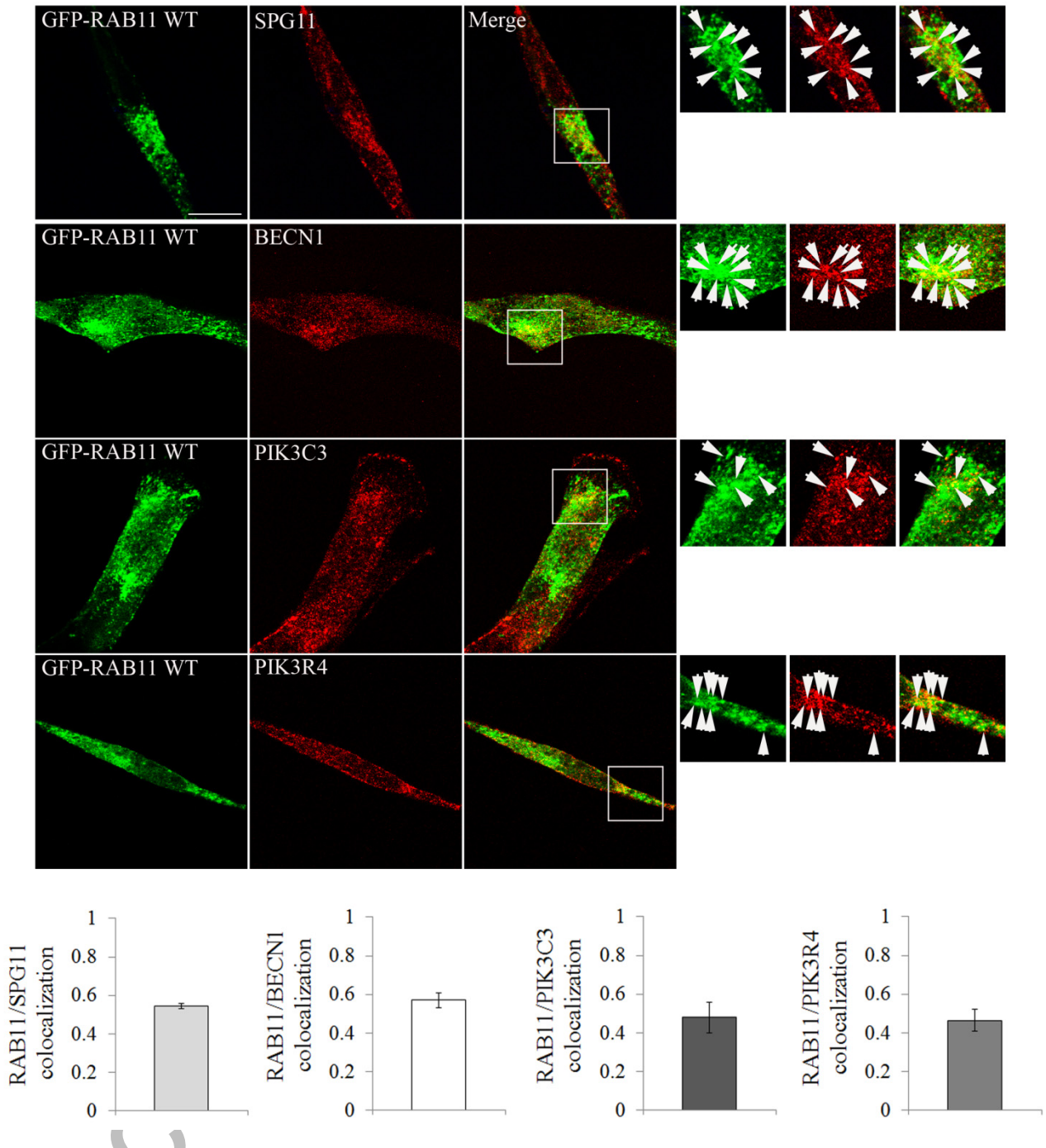

Figure S8. SPG11, BECN1, PIK3C3 and PIK3R4 colocalize with RAB11. HeLa cells were transfected with GFP-RAB11 WT, fixed and immunostained with anti-SPG11, -BECN1, -PIK3C3 and -PIK3R4 (red) Abs. Show is a representative image. The small panels show a higher magnification of the area indicated in the squares. Arrows indicate colocalization (yellow). Pearson correlation coefficients for proteins colocalization were determined in at least 30 cells/staining and reported in the graphs. Scale bar: 10 μm.

A

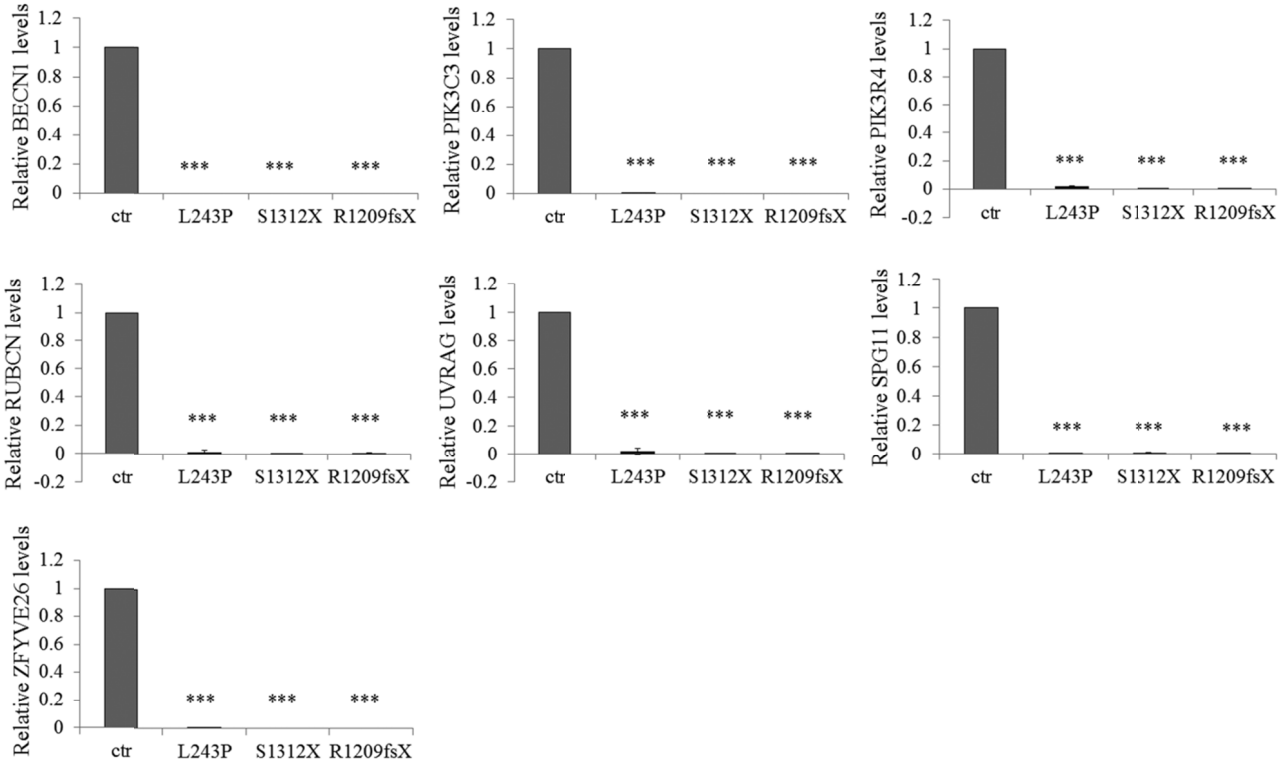
Relative BECN1 levels
Relative PIK3C3 levels
Relative PIK3R4 levels
Relative RUBCN levels
Relative UVRAG levels
Relative SPG11 levels
Relative ZFYVE26 levels
ctr
L243P
S1312X
R1209fsX
***

B

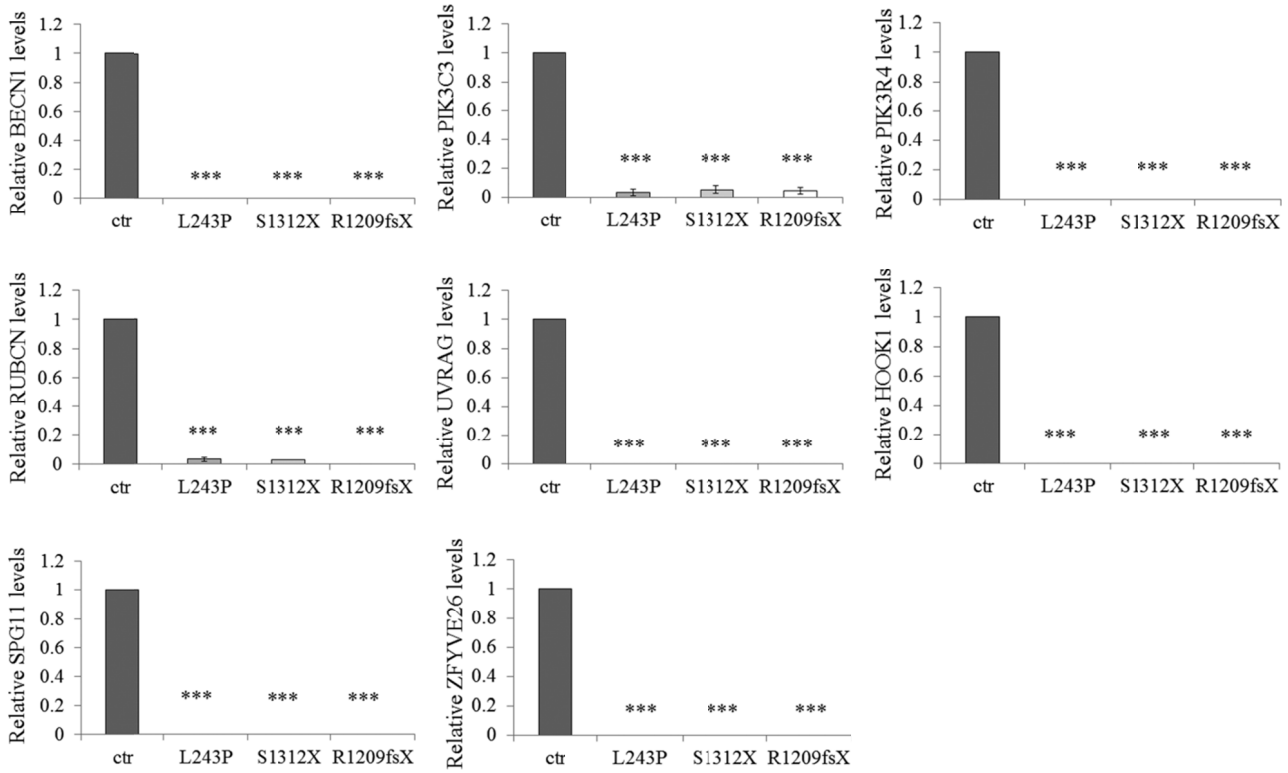
Relative BECN1 levels
Relative PIK3C3 levels
Relative PIK3R4 levels
Relative RUBCN levels
Relative UVRAG levels
Relative HOOK1 levels
Relative SPG11 levels
Relative ZFYVE26 levels
ctr
L243P
S1312X
R1209fsX
***

Figure S9. Quantification of proteins coimmunoprecipitated with RAB5A and RAB11 in SPG15 cells. (**A**) Proteins from Fig. 3A and from 2 replicates were quantified, normalized to total protein available for immunoprecipitation (input) and to immunoprecipitated RAB5A levels, and expressed as fold increase of control. (**B**) Proteins from Fig. 3A and from 2 replicates were quantified, normalized to total protein available for immunoprecipitation (input) and to immunoprecipitated RAB11 levels, and expressed as fold increase of control. The graphs show the mean ± SEM (*** $P<0.001$).

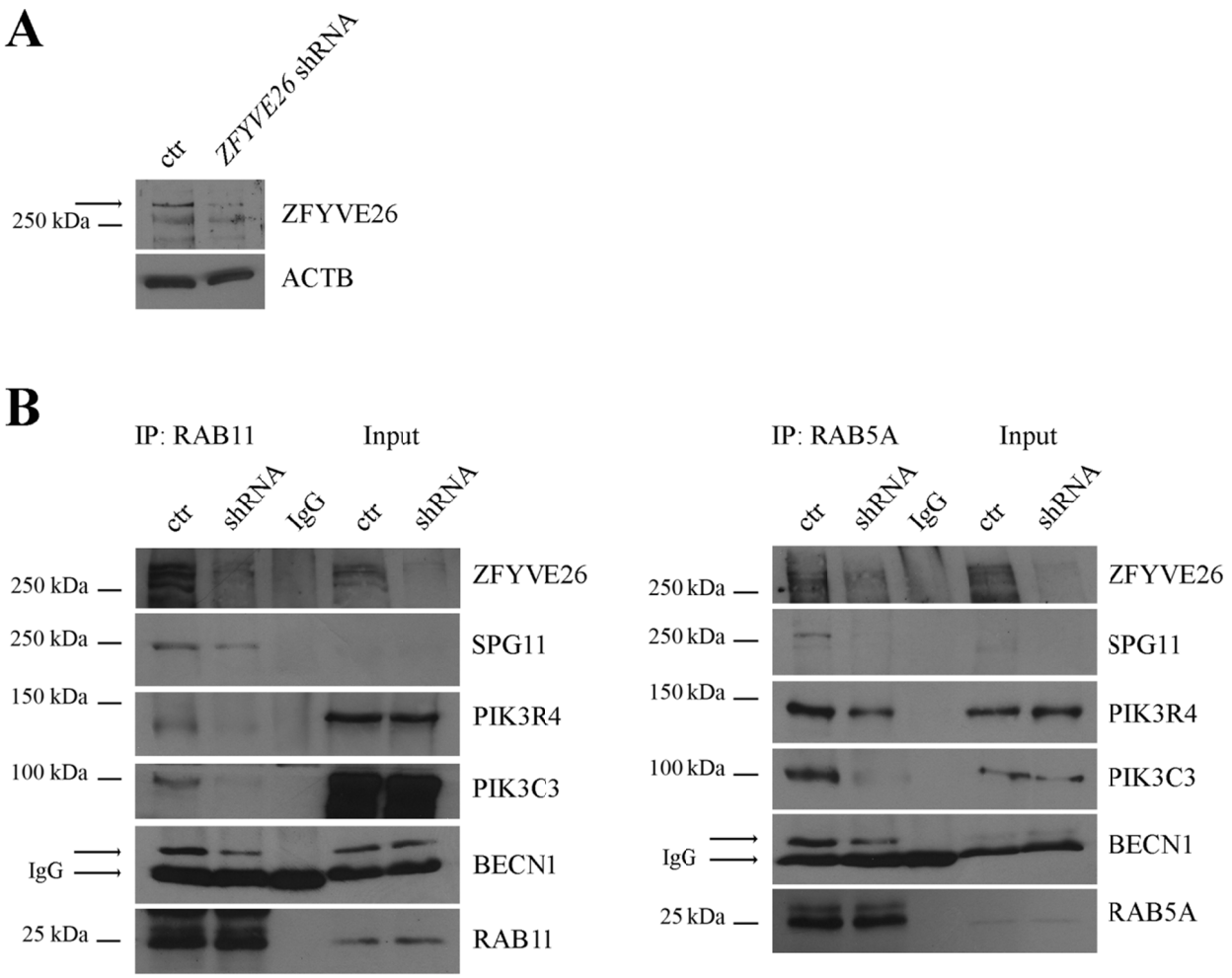

Figure S10. Effect of *ZFYVE26* silencing on RAB5A and RAB11 interactions. HeLa cells were transfected with a *ZFYVE26* shRNA with high silencing efficiency [14], or with a scrambled (ctr) and 48 h later cells were lysed. (**A**) 70 µg of total protein extracts were loaded on a 6% SDS-polyacrylamide gel and probed with anti-ZFYVE26 Ab to show the residual ZFYVE26 levels in *ZFYVE26* shRNA-transfected cells. (**B**) Total protein extracts from *ZFYVE26* shRNA-transfected cells were then subjected to immunoprecipitation (IP) with anti-RAB5A or -RAB11A/B Abs. Silencing of *ZFYVE26* affects the interaction of RAB5A and RAB11 with SPG11, PIK3C3, PIK3R4 and BECN1. Total protein extracts (5%) used for the IP were loaded as positive control (Input). Total protein extracts were immunoprecipitated with an Ab against rabbit IgG isotype as negative control (IgG). The 50 kDa rabbit IgG heavy chain is indicated (IgG heavy) where present.

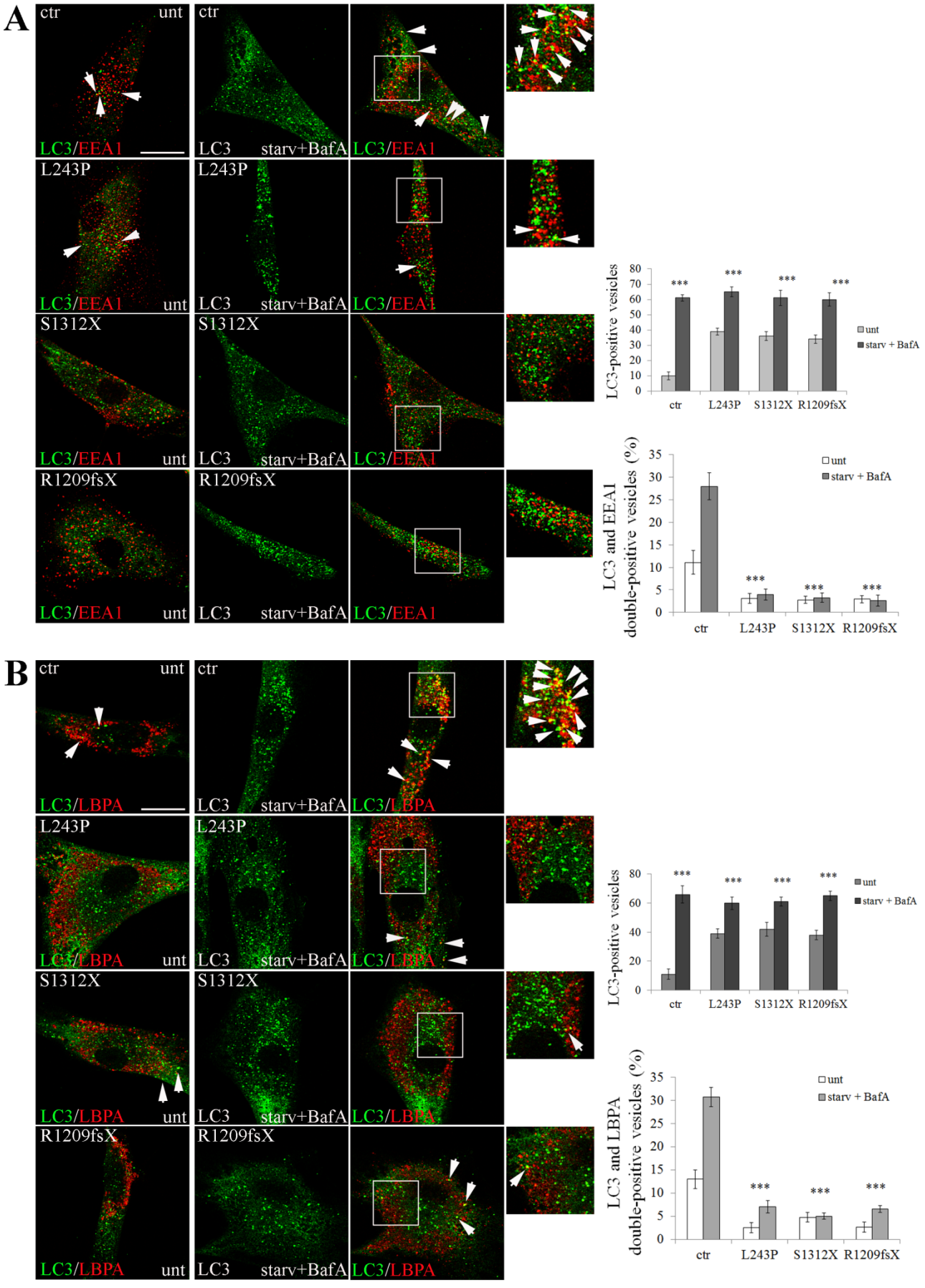
A
ctr
unt
LC3/EEA1
LC3
starv+BafA
L243P
S1312X
R1209fsX
LC3-positive vesicles
unt
starv + BafA
ctr
L243P
S1312X
R1209fsX
LC3 and EEA1 double-positive vesicles (%)
B
LC3/LBPA
LC3-positive vesicles
LC3 and LBPA double-positive vesicles (%)

Figure S11. ZFYVE26 mutations affect autophagosome-endosome fusion in AR-SPG15 mutated cells. Controls and AR-SPG15 cells with the L243P, S1312X and R1209fsX mutations of ZFYVE26 were incubated with or without (unt) EBSS and 200 nM bafilomycin A_1 (BafA) for 30 min (starv+BafA), fixed and stained with anti-LC3B (green) and the early endosomal marker EEA1 (red) (**A**) or the MVBs marker LBPA (red) (**B**) Abs. Colocalization of autophagosomes with early endosomes and with MVBs was analyzed. The small panels on the right show a higher magnification of the area indicated in the square. Arrows indicates colocalization (yellow). Scale bar: 10 μm. LC3 and EEA1 or LC3 and LBPA double-positive vesicles were counted, normalized to total LC3-positive vesicles and expressed as percentage of the total. Total LC3-positive vesicle number is also shown. The graphs show the mean ± SEM of 3 independent experiments for a total of at least 30 cells for each sample (*** $P<0.001$).

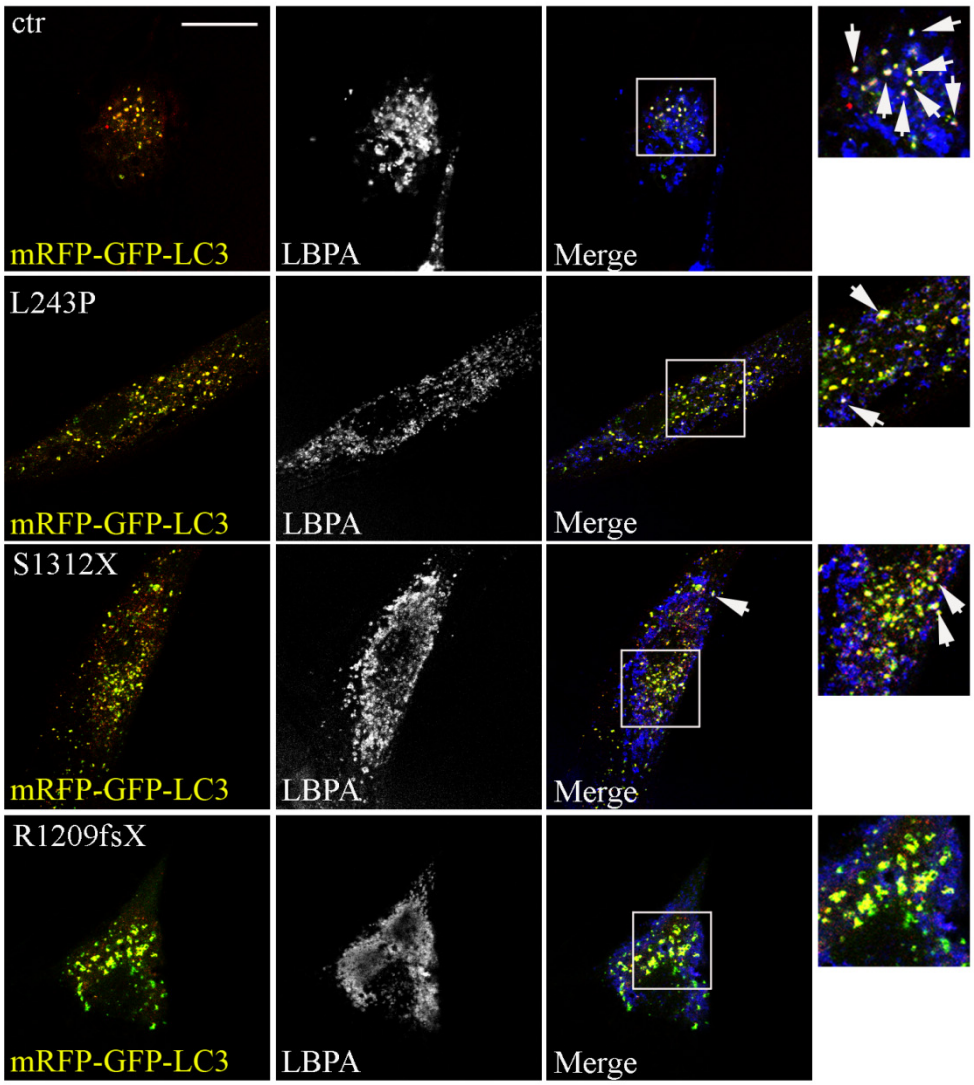
ctr
mRFP-GFP-LC3
LBPA
Merge
L243P
mRFP-GFP-LC3
LBPA
Merge
S1312X
mRFP-GFP-LC3
LBPA
Merge
R1209fsX
mRFP-GFP-LC3
LBPA
Merge

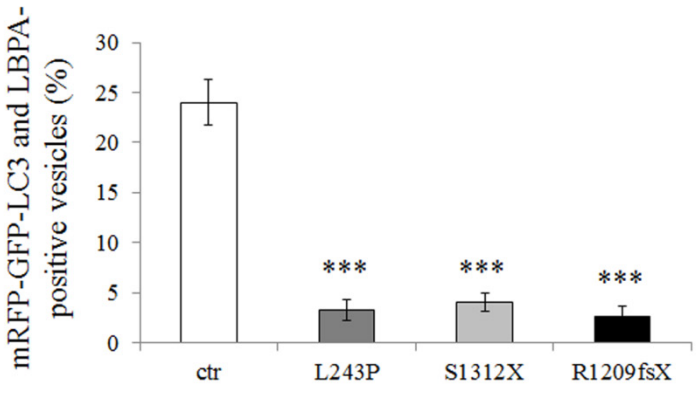
mRFP-GFP-LC3 and LBPA-positive vesicles (%)
30
25
20
15
10
5
0
***
***
***
ctr
L243P
S1312X
R1209fsX

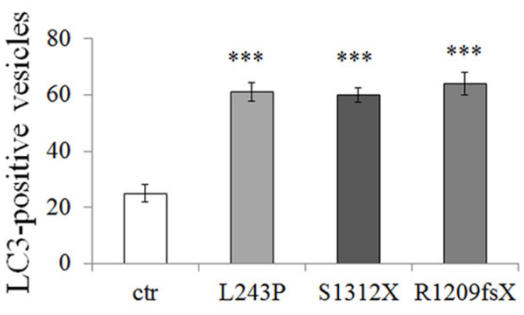
LC3-positive vesicles
80
60
40
20
0
***
***
***
ctr
L243P
S1312X
R1209fsX

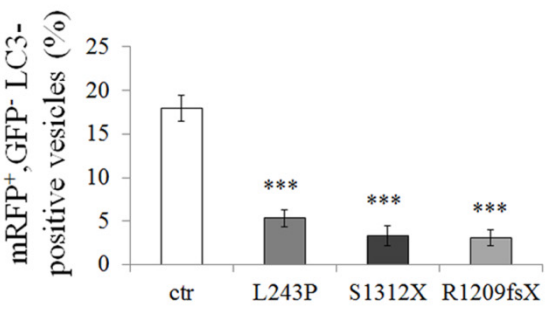
mRFP+,GFP- LC3-positive vesicles (%)
25
20
15
10
5
0
***
***
***
ctr
L243P
S1312X
R1209fsX

Figure S12. ZFYVE26 mutations affect autophagosome-MVBs fusion in AR-SPG15 mutated cells. Controls and AR-SPG15 cells with the L243P, S1312X and R1209fsX mutations of ZFYVE26 were transfected with mRFP-GFP-LC3B (ptfLC3B) vector, incubated with EBSS for 30 min, fixed and stained with anti-LBPA (blue) Ab. Red and green channels were merged and mRFP-GFP-LC3-positive autophagosomes are shown in yellow. Colocalization of autophagosomes with MVBs was analyzed. The small panels on the right show a higher magnification of the area indicated in the square. Arrows indicates colocalization (white). Scale bar: 10 μm. $mRFP^+$ GFP^+ LC3-positive vesicles (yellow) positive for LBPA (mRFP-GFP-LC3 and LBPA, white) were counted, normalized to total LC3-positive vesicles and expressed as percentage of the total. Total LC3 vesicle number is shown in the graph on the right. $mRFP^+$ GFP^- LC3-positive vesicles (only red), corresponding to acidified autophagosomes, were also counted, normalized to total LC3-positive vesicles and expressed as percentage of the total. The graphs show the mean ± SEM of 3 independent experiments for a total of at least 30 cells for each sample (*** $P<0.001$).

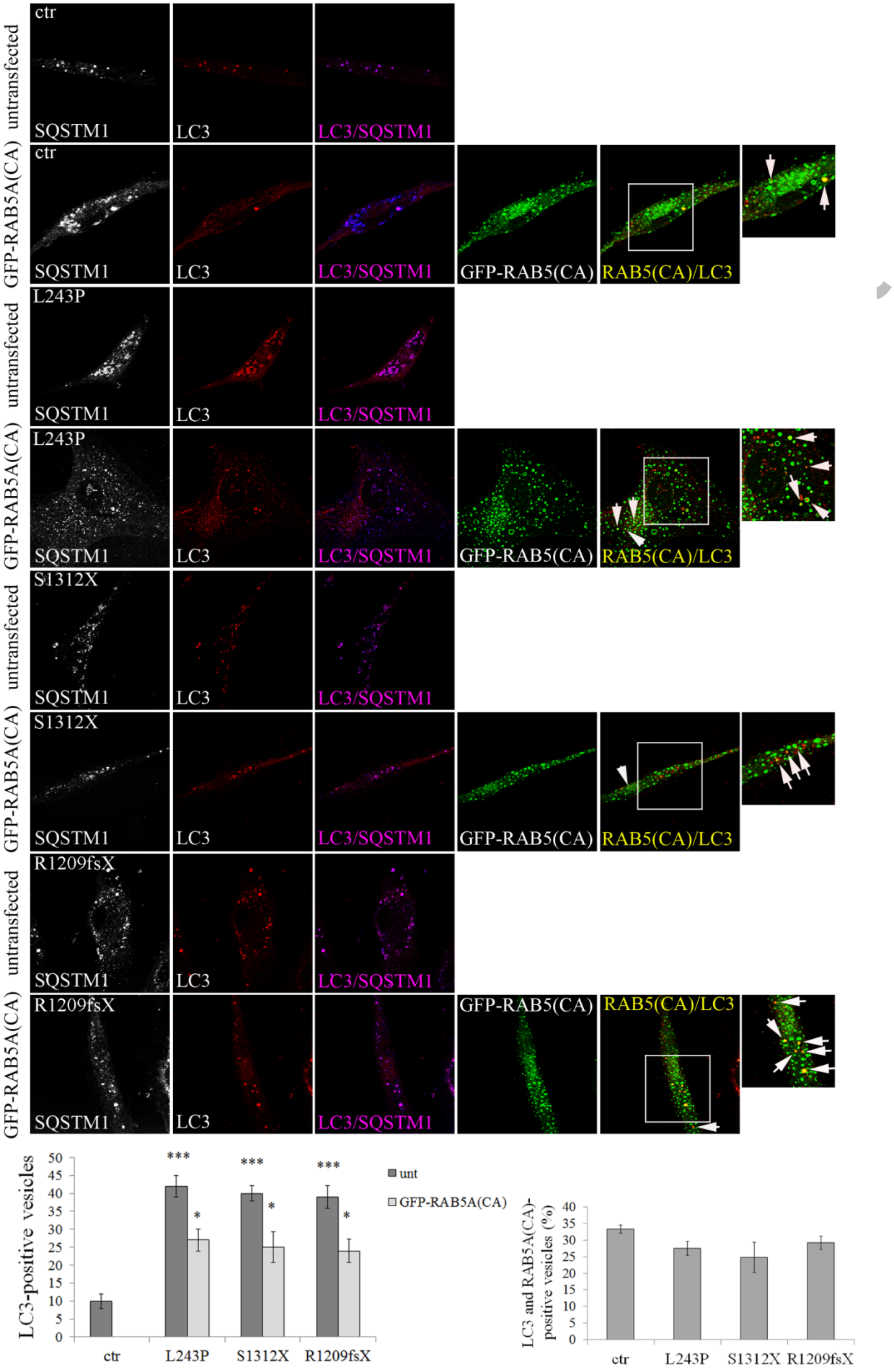
ctr
SQSTM1
LC3
LC3/SQSTM1
GFP-RAB5(CA)
RAB5(CA)/LC3
L243P
S1312X
R1209fsX
untransfected
GFP-RAB5A(CA)
LC3-positive vesicles
unt
GFP-RAB5A(CA)
***
*
LC3 and RAB5A(CA)-positive vesicles (%)

Figure S13. Constitutively active RAB5A(CA) partially rescues the autophagy defect in ZFYVE26 cells. Control and ZFYVE26 mutated cells were untransfected or transfected with the GTP-bound mutant RAB5A^{Q79L} (RAB5A[CA]) with a GFP tag, fixed and immunostained with anti-LC3B (red) and -SQSTM1 Abs (blue). Total LC3-positive vesicles were counted and are shown in the graph. LC3 and RAB5A(CA) double-positive vesicles were counted, normalized to total LC3-positive vesicles and expressed as percentage of the total. The graphs show the mean ± SEM of 3 independent experiments for a total of at least 30 cells for each sample (*** $P<0.001$; * $P<0.05$).

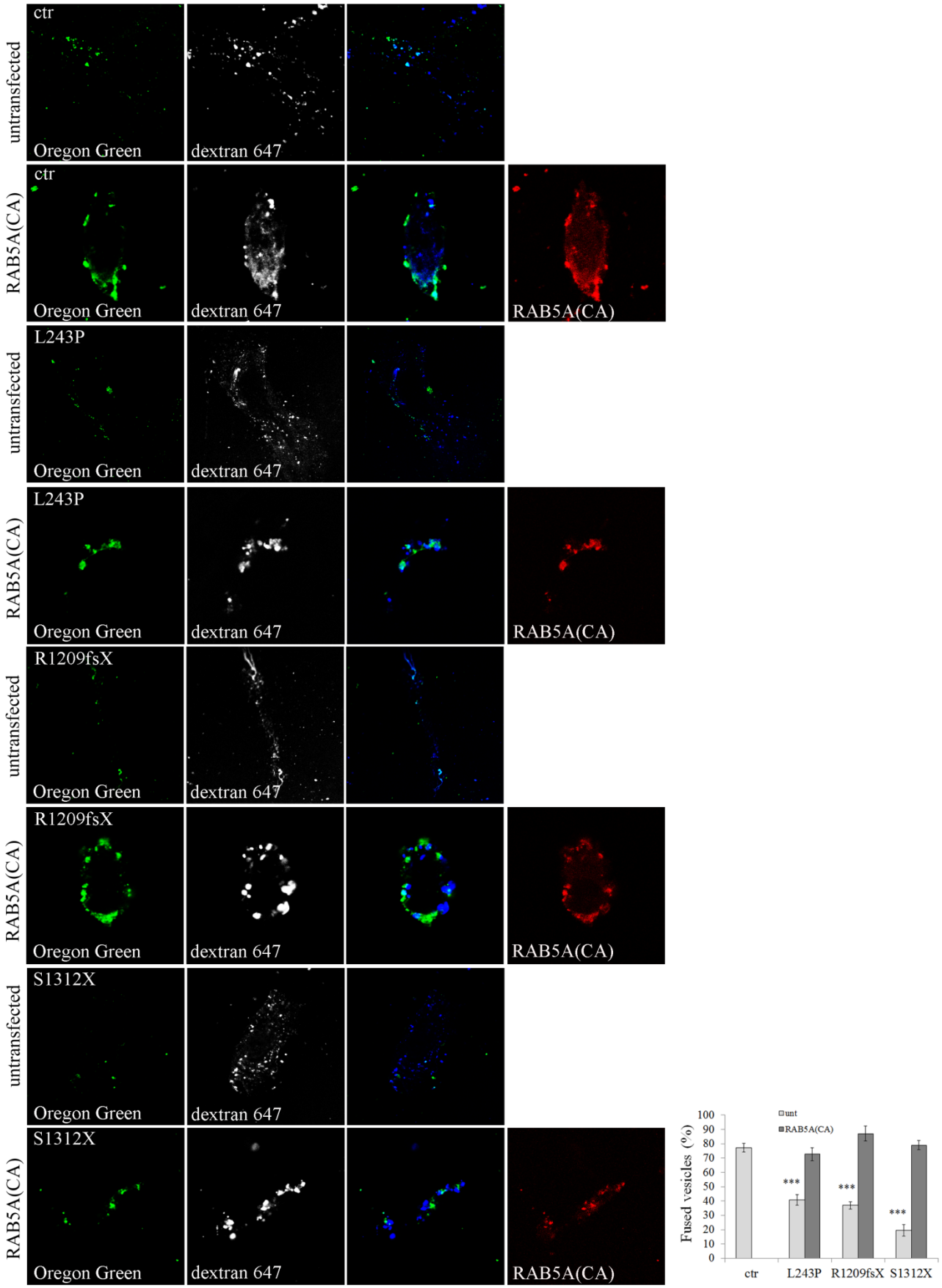
untransfected
RAB5A(CA)
ctr
L243P
R1209fsX
S1312X
Oregon Green
dextran 647
RAB5A(CA)
unt
RAB5A(CA)
Fused vesicles (%)
100
90
80
70
60
50
40
30
20
10
0
***
ctr
L243P
R1209fsX
S1312X

Figure S14. Constitutively active RAB5A(CA) rescues endosome-endosome fusion in ZFYVE26 mutated cells. Control and ZFYVE26 mutated cells were transfected with or without mCherryRAB5A^{Q79L} (RAB5A[CA]). 24 h later cells were incubated for 10 min with Oregon Green 514-avidin and Alexa Fluor 647 dextran, as internal control, followed by an incubation of 30 min to label late endosomes. Then cells were incubated with biotin-BSA in uptake medium for 10 min to label early endosomes, fixed and processed for confocal microscopy. The fusion between avidin- and biotin-labelled endosomes induced a significant increase in Oregon Green 514 fluorescence. Green fused vesicles were counted, normalized to total dextran-positive vesicles (blue) and expressed as percentage. Scale bar: 10 μm. The graphs show the mean ± SEM of 3 independent experiments for a total of at least 30 cells for each sample (*** $P<0.001$). ZFYVE26 mutated cells transfected with RAB5A(CA) and control cells exhibited the same percentage of fused vesicles.

A

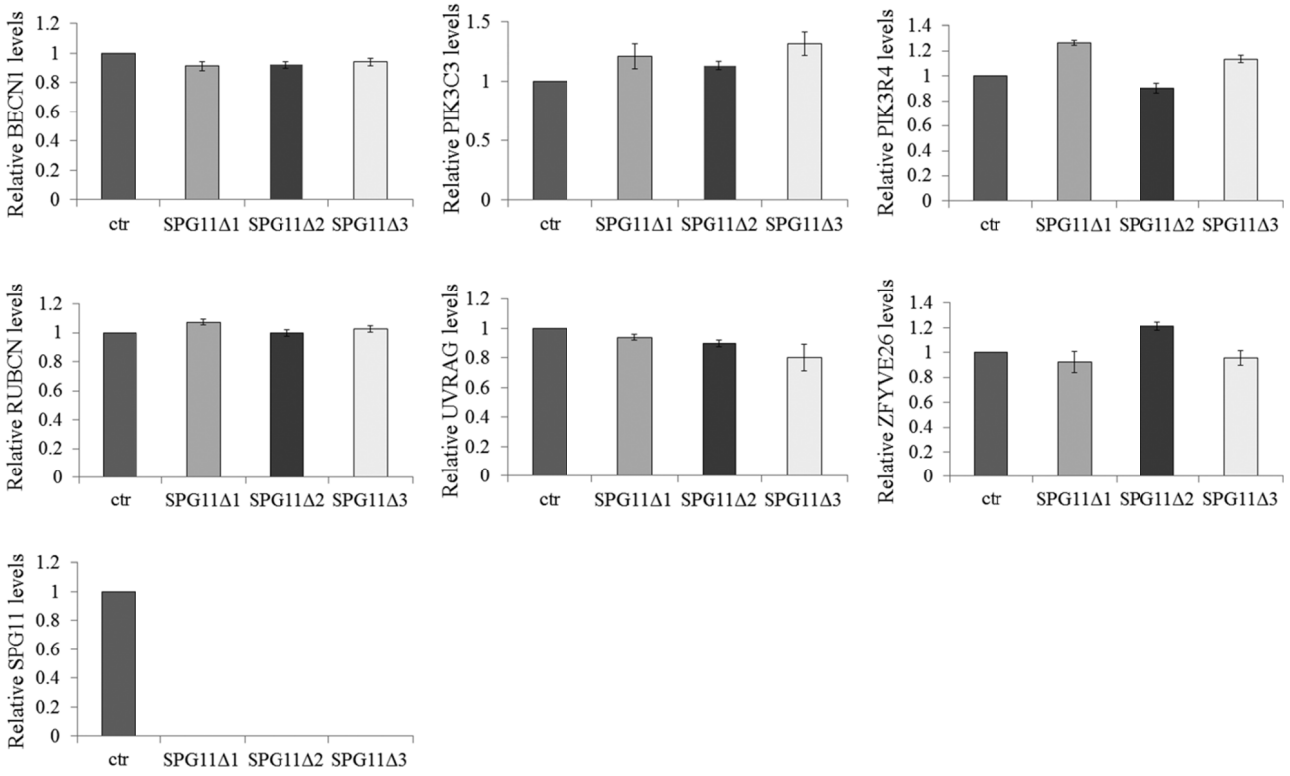
Relative BECN1 levels
Relative PIK3C3 levels
Relative PIK3R4 levels
Relative RUBCN levels
Relative UVRAG levels
Relative ZFYVE26 levels
Relative SPG11 levels
ctr
SPG11Δ1
SPG11Δ2
SPG11Δ3

B

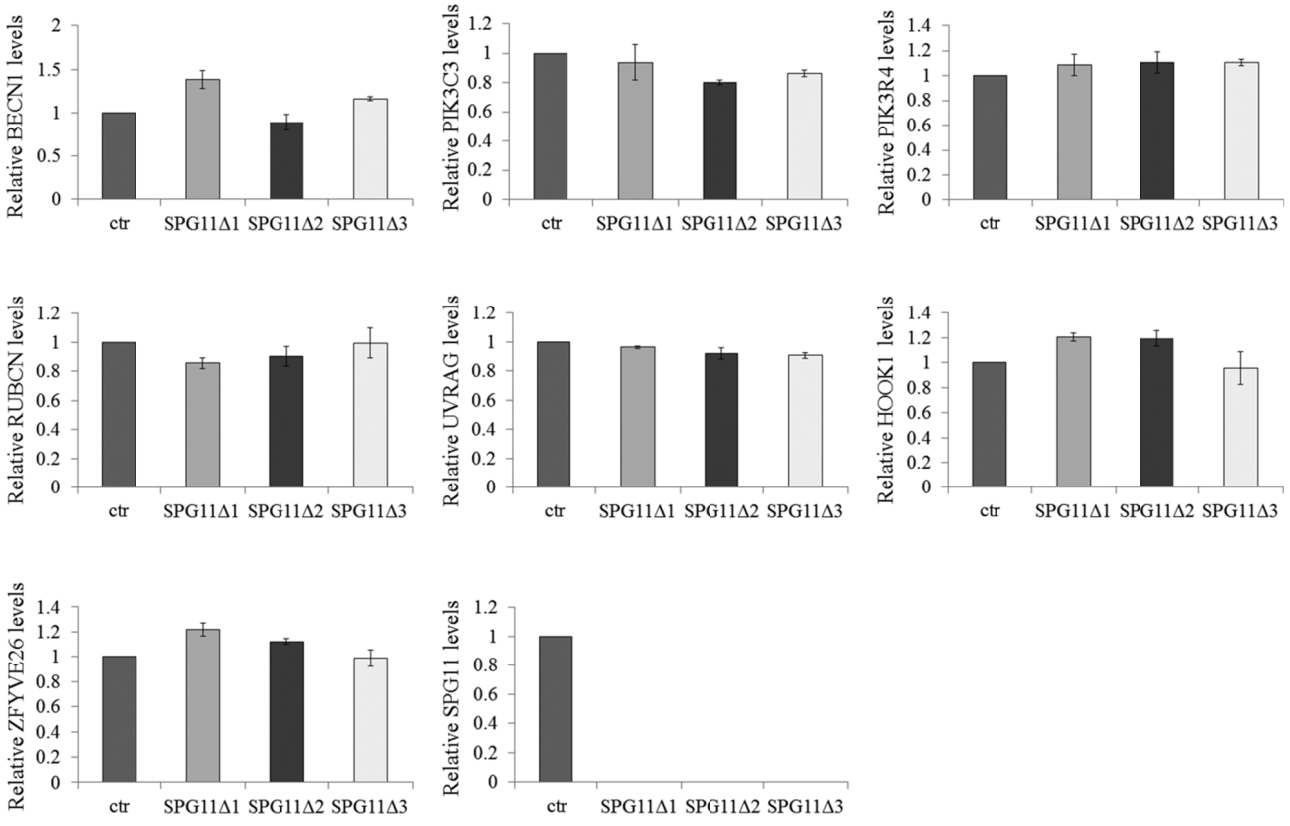
Relative BECN1 levels
Relative PIK3C3 levels
Relative PIK3R4 levels
Relative RUBCN levels
Relative UVRAG levels
Relative HOOK1 levels
Relative ZFYVE26 levels
Relative SPG11 levels
ctr
SPG11Δ1
SPG11Δ2
SPG11Δ3

Figure S15. Quantification of proteins coimmunoprecipitated with RAB5A and RAB11 in AR-SPG11 mutated cells. (**A**) Proteins from Fig. 7B and from 2 replicates were quantified, normalized to total protein available for immunoprecipitation (input) and immunoprecipitated RAB5A levels. (**B**) Proteins from Fig. 7B and from 2 replicates 2 quantified, normalized to total protein available for immunoprecipitation (input) and to immunoprecipitated RAB11 levels, and expressed as fold increase of control. The graphs show the mean ± SEM (*** $P<0.001$).

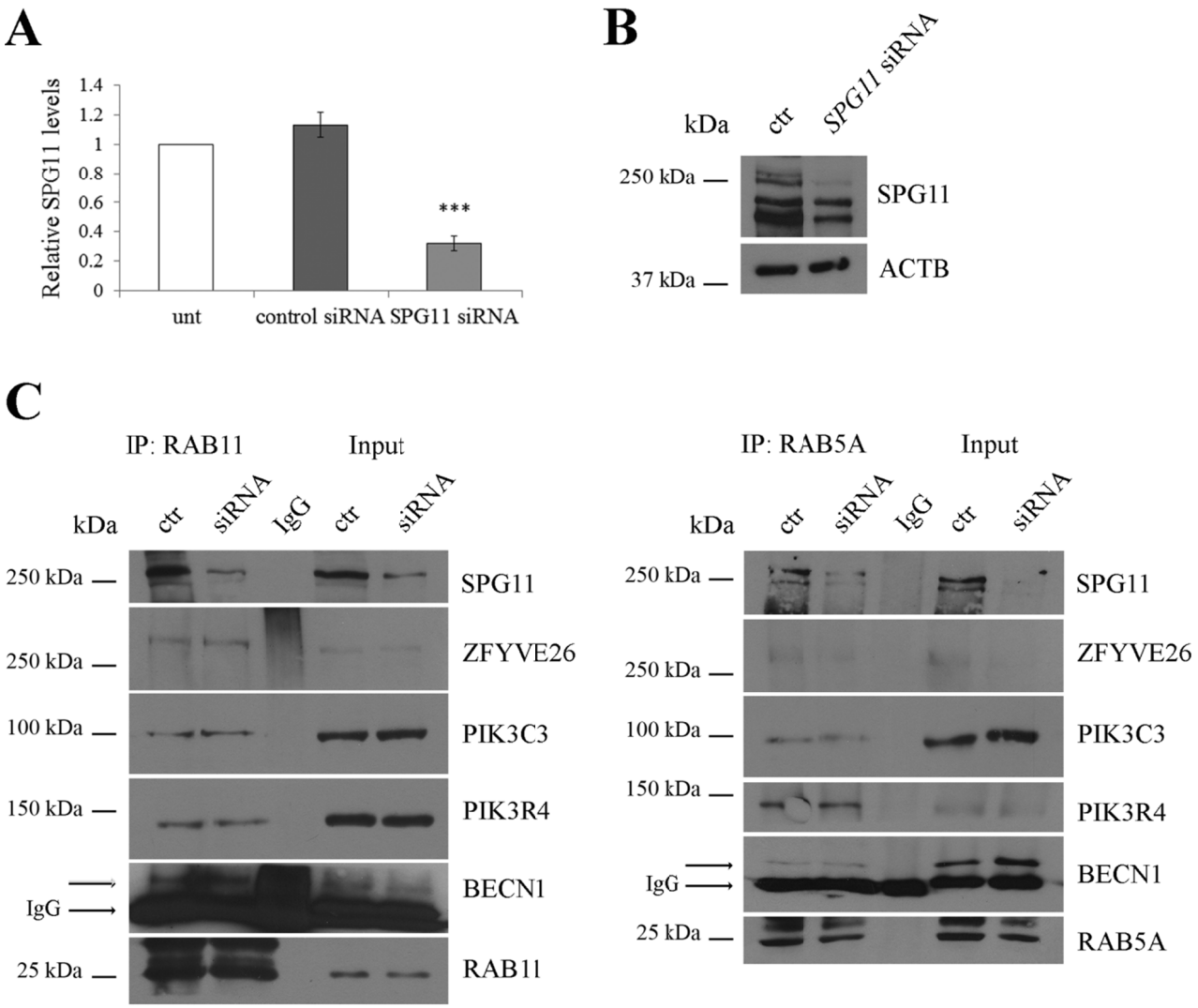

Figure S16. Effect of *SPG11* silencing on RAB5A and RAB11 interactions. (**A**) Analysis of *SPG11* siRNA silencing efficiency. HeLa cells were transiently transfected with *SPG11* siRNA or with a control siRNA and 48 h later RNA was extracted and retrotranscribed into cDNA. *SPG11* levels were analyzed by Real Time PCR. Untransfected cells were used as endogenous control (unt). The graph shows the residual *SPG11* expression in the transfected cells. Results are expressed as mean ± SEM of 3 independent experiments (*** $P<0.001$). (**B**). HeLa cells were transfected with *SPG11* siRNA or with the control siRNA (ctr) and 48 h later cells were lysed. 70 µg of total protein extracts were loaded on a 6% SDS- polyacrylamide gel and probed with anti-SPG11 Ab to show the residual SPG11 levels in *SPG11* siRNA-transfected cells. (**C**) Total protein extracts from *SPG11* siRNA-transfected cells were then subjected to immunoprecipitation (IP) with anti-RAB5A or -

RAB11A/B Abs. Proteins were loaded on 6% and 12% SDS-polyacrylamide gels. Silencing of *SPG11* has no effect on the interaction of RAB5A and RAB11 with ZFYVE26, PIK3C3, PIK3R4 and BECN1. Total protein extracts (5%) used for the IP were loaded as positive control (Input). Total protein extracts were immunoprecipitated with an Ab against rabbit IgG isotype as negative control (IgG). The 50-kDa rabbit IgG heavy chain is indicated (IgG heavy) where present.

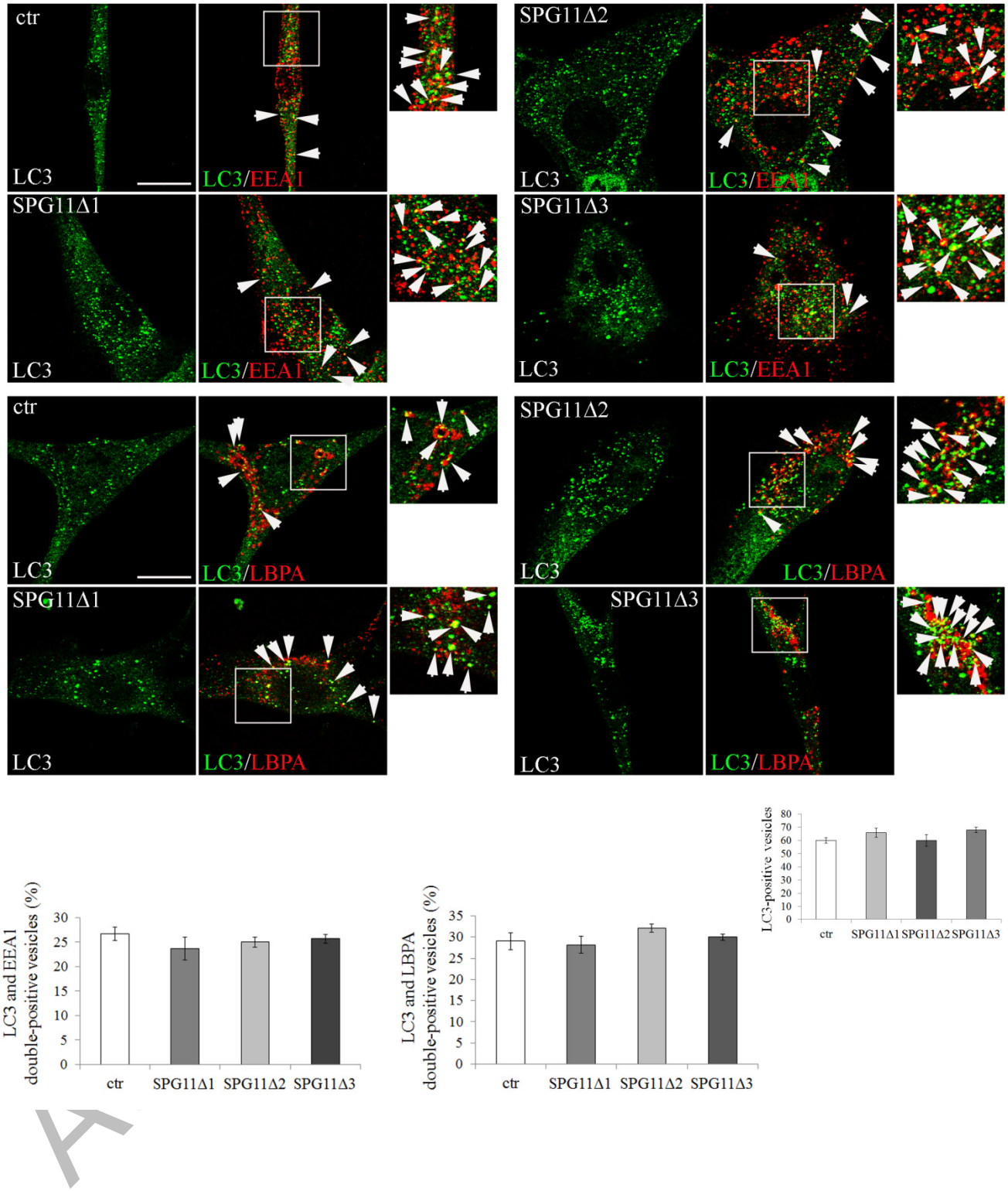

Figure S17. SPG11 does not alter autophagosome-endosome fusion. Controls and AR-SPG11 mutated cells were incubated with EBSS and 200 nM BafA for 30 min, fixed and stained with anti-LC3B (green) and anti-EEA1 or -LBPA (red) Abs. Colocalization of autophagosomes with early endosomes (EEA1) or MVB (LBPA) was analyzed. The small panels show a higher magnification of the area indicated in the squares. Arrows indicate colocalization (yellow). Scale bar: 10 mm. LC3

and EEA1 or LC3 and LBPA double-positive vesicles were counted, normalized to total LC3-positive vesicles and expressed as percentage of the total. Total LC3-positive vesicle number is shown on the right. The graphs show the mean ± SEM of 3 independent experiments for a total of at least 30 cells for each sample.

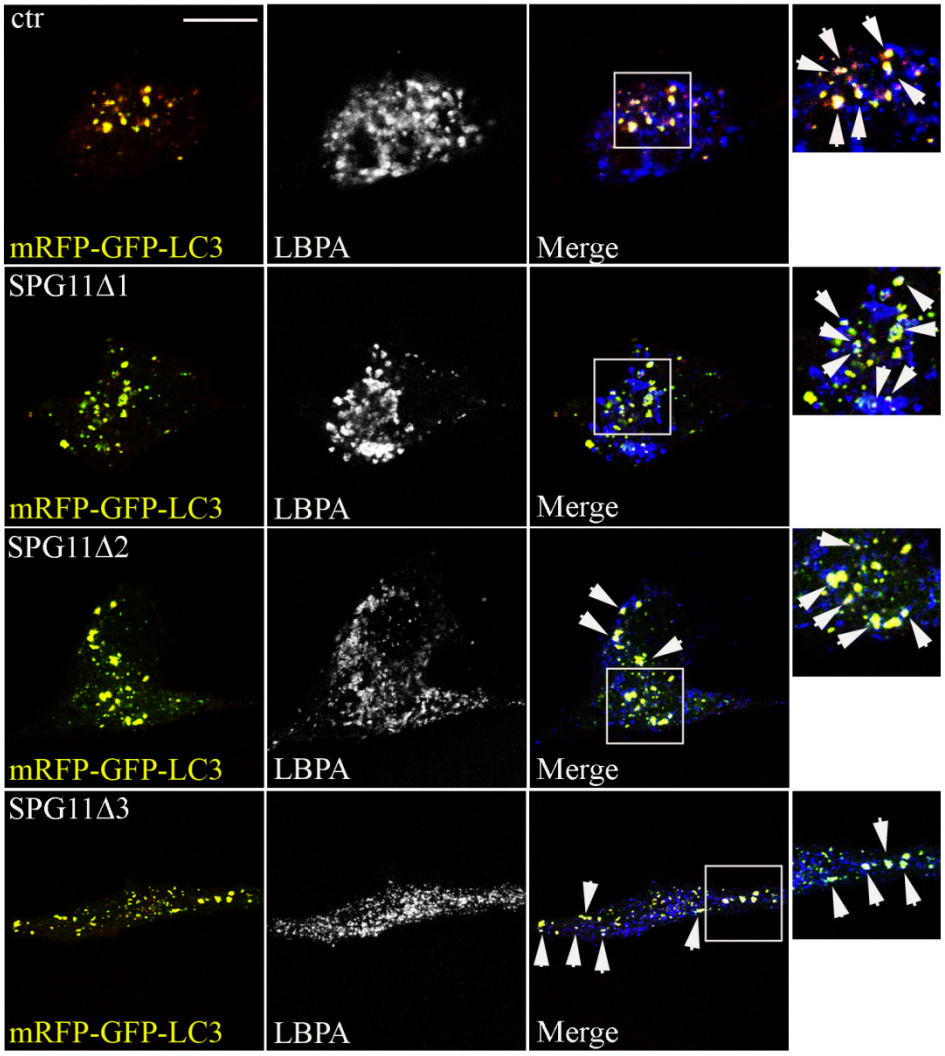
ctr
mRFP-GFP-LC3
LBPA
Merge
SPG11Δ1
mRFP-GFP-LC3
LBPA
Merge
SPG11Δ2
mRFP-GFP-LC3
LBPA
Merge
SPG11Δ3
mRFP-GFP-LC3
LBPA
Merge

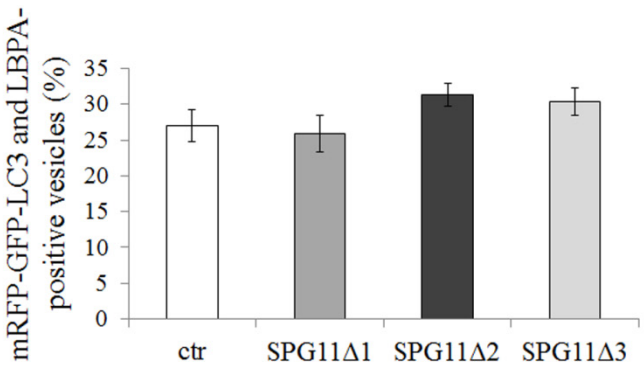
mRFP-GFP-LC3 and LBPA-positive vesicles (%)
35
30
25
20
15
10
5
0
ctr
SPG11Δ1
SPG11Δ2
SPG11Δ3

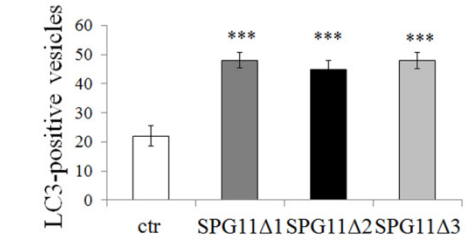
LC3-positive vesicles
60
50
40
30
20
10
0
***
***
***
ctr
SPG11Δ1
SPG11Δ2
SPG11Δ3

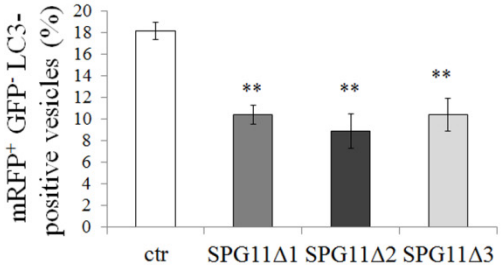
mRFP+ GFP- LC3-positive vesicles (%)
20
18
16
14
12
10
8
6
4
2
0
**
**
**
ctr
SPG11Δ1
SPG11Δ2
SPG11Δ3

Figure S18. SPG11 does not alter autophagosome-MVBs fusion. Controls and AR-SPG11 mutated cells were transfected with mRFP-GFP-LC3B (ptfLC3B) vector, incubated with EBSS for 30 min, fixed and stained with-anti LBPA (blue) Ab. Red and green channels were merged and mRFP-GFP-LC3-positive autophagosomes are showed in yellow. Colocalization of autophagosomes with MVBs was analyzed. The small panels on the right show a higher magnification of the area indicated in the square. Arrows indicates colocalization (white). Scale bar: 10 μm. $mRFP^+$ GFP^+ LC3-positive vesicles (yellow) positive for LBPA (mRFP-GFP-LC3 and LBPA, white) were counted, normalized to total LC3-positive vesicles and expressed as percentage of the total. Total LC3-positive vesicle number is shown in the graph on the right. $mRFP^+$ GFP^- LC3-positive vesicles (only red), corresponding to acidified autophagosomes, were also counted, normalized to total LC3-positive vesicles and expressed as percentage of the total. The graphs show the mean ± SEM of 3 independent experiments for a total of at least 30 cells for each sample (*** $P<0.001$; ** $P<0.01$).

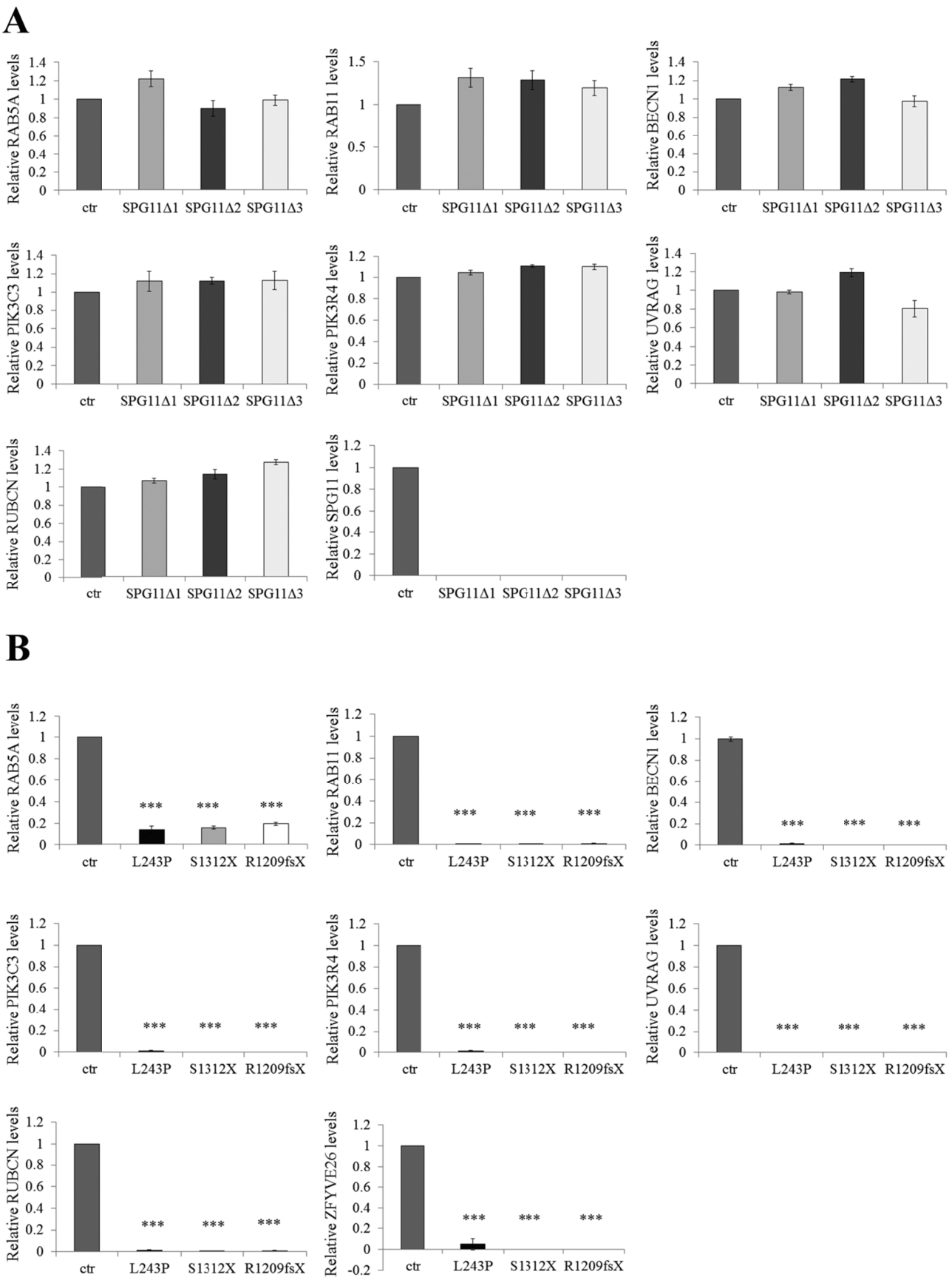
A
Relative RAB5A levels
Relative RAB11 levels
Relative BECN1 levels
Relative PIK3C3 levels
Relative PIK3R4 levels
Relative UVRAG levels
Relative RUBCN levels
Relative SPG11 levels
ctr
SPG11Δ1
SPG11Δ2
SPG11Δ3
B
Relative RAB5A levels
Relative RAB11 levels
Relative BECN1 levels
Relative PIK3C3 levels
Relative PIK3R4 levels
Relative UVRAG levels
Relative RUBCN levels
Relative ZFYVE26 levels
ctr
L243P
S1312X
R1209fsX
***

Figure S19. Quantification of coimmunoprecipitated proteins. (**A**) Proteins from Fig. 9B and from 2 replicates were quantified, normalized to total protein available for immunoprecipitation (input) and immunoprecipitated ZFYVE26 levels. (**B**) Proteins from Fig. 9C and from 2 replicates were quantified, normalized to total protein available for immunoprecipitation (input) and to immunoprecipitated SPG11 levels, and expressed as fold increase of control. RAB5A levels in SPG15 mutated cells were considered nonspecific, due to the absence of SPG11 protein in AR-SPG15 cells with the S1312X and R1209fsX mutations of ZFYVE26. The graphs show the mean ± SEM (*** $P<0.001$).

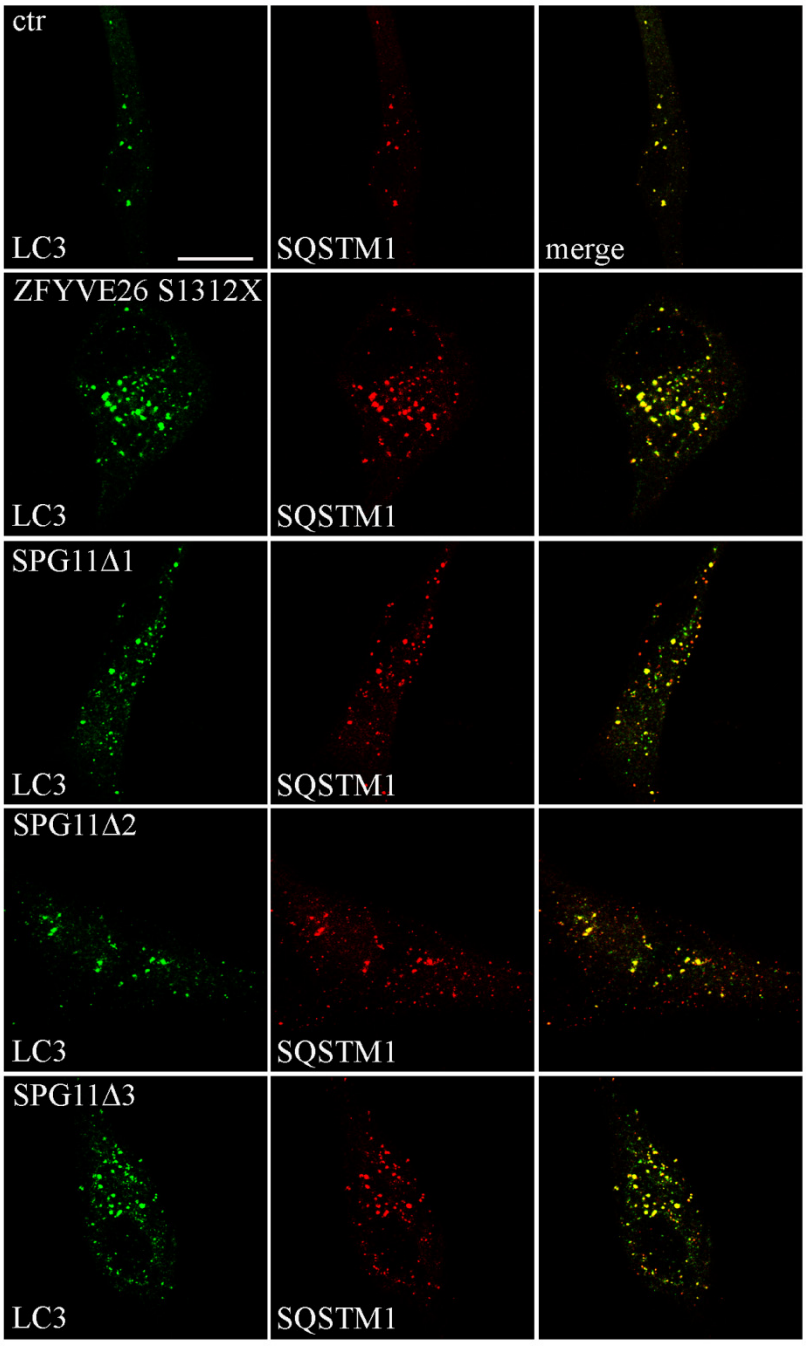
ctr
LC3
SQSTM1
merge
ZFYVE26 S1312X
LC3
SQSTM1
SPG11Δ1
LC3
SQSTM1
SPG11Δ2
LC3
SQSTM1
SPG11Δ3
LC3
SQSTM1

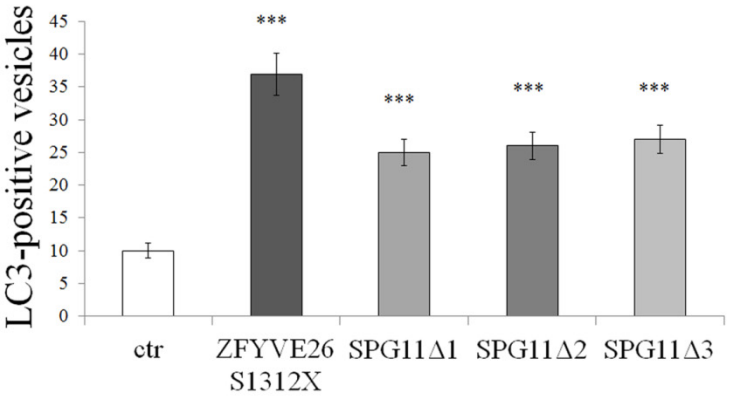
LC3-positive vesicles
45
40
35
30
25
20
15
10
5
0
***
***
***
***
ctr
ZFYVE26 S1312X
SPG11Δ1
SPG11Δ2
SPG11Δ3

Figure S20. SPG11 mutations induce reduced autophagosome accumulation compared with ZFYVE26 mutation. Controls (ctr), AR-SPG11 (SPG11Δ1, SPG11Δ2 and SPG11Δ3) and AR-SPG15 mutated cells with ZFYVE26 containing the S1312X mutation were fixed and immunostained with anti-LC3B (green) and anti-SQSTM1 (red) Ab. Yellow in the merge images indicates colocalization. Total LC3-positive vesicles were counted and are shown in the graph. The graphs show the mean ± SEM of 3 independent experiments for a total of at least 30 cells for each sample (*** $P<0.001$). Scale bar: 10 μm.

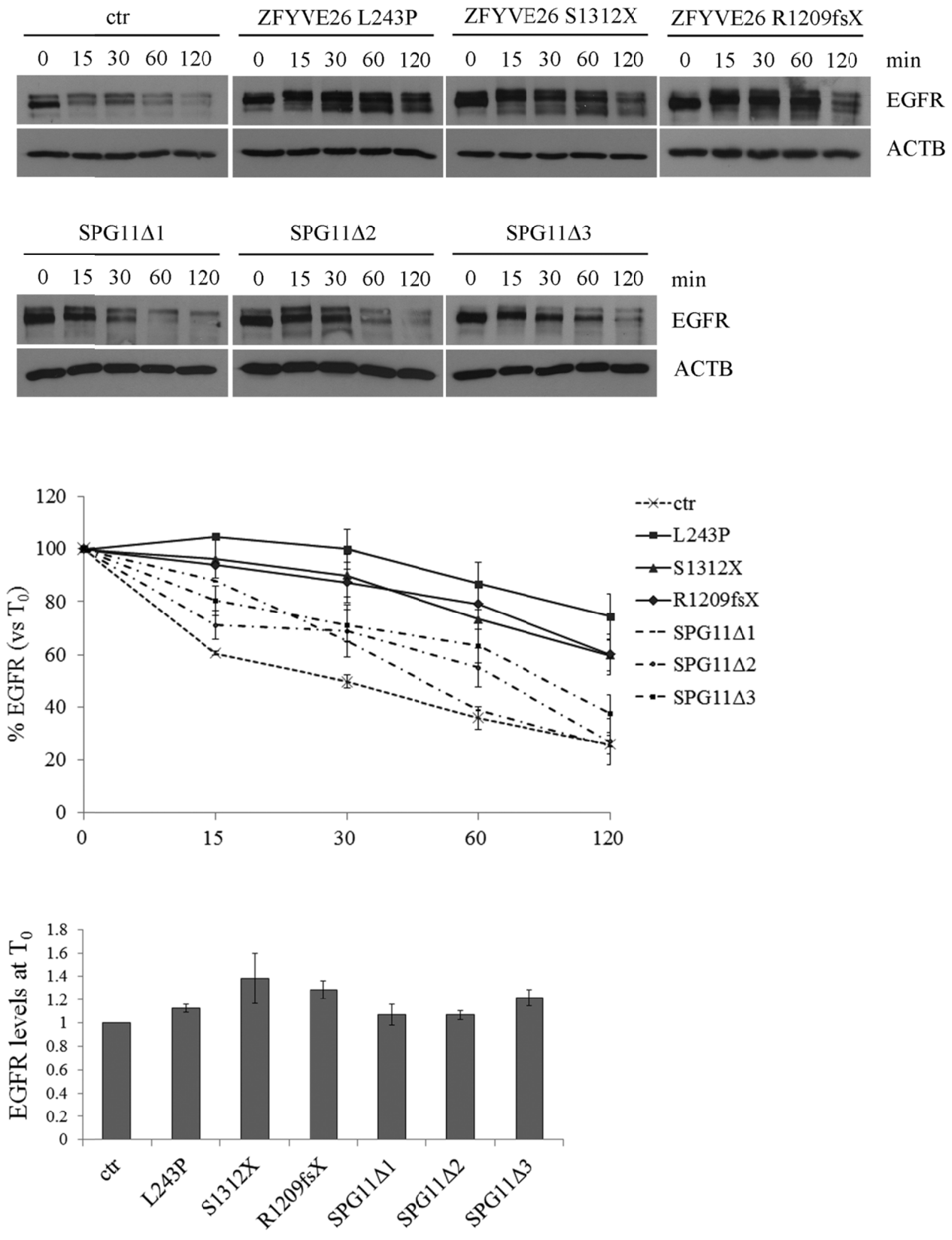

Figure S21. Analysis of EGFR degradation. Controls (ctr), AR-SPG11 cells (SPG11Δ1, SPG11Δ2 and SPG11Δ3 mutations) and AR-SPG15 mutated cells (with the L243P, R1209fsX and S1312X

mutations of ZFYVE26) were serum starved for 16 h and incubated with 200 ng/ml EGF for different times, from 0 to 120 min, to induce EGFR endocytosis and degradation. Cells were then lysed and subjected to SDS-PAGE and western blot using an anti EGFR antibody. Shown is a representative blot out of 3 replicates. EGFR levels were quantified, normalized to ACTB and expressed in the graph as percentage of the EGFR amount present at time zero (T_0=100%). EGFR levels at time zero are also shown.

Daniel J Klionsky
Life Sciences Institute University of Michigan;
Ann Arbor, MI 48109-2216, USA
Editor in Chief
Autophagy

Bosisio Parini, July 23rd 2018

Subject: Revision of Manuscript #2017AUTO0012R3

Dear Editor,

Please find enclosed the revised version of the manuscript "ZFYVE26/SPASTIZIN and SPG11/SPATACSIN mutations in hereditary spastic paraplegia types SPG15 and SPG11 have different effects on autophagy and endocytosis" by Vantaggiato C. et al. that had been submitted and accepted as an Article to this Journal.

We carefully red each comment and modified text and figures accordingly to the requests.

We changed the nomenclature in all figures (main and supplementary), accordingly with the text.

We used RAB5A(CA) and RAB5A(DN) for the constitutively active (CA) and the dominant-negative (DN) forms of RAB5. We checked and reported isoforms for antibodies and constructs; we checked the description of fusion constructs and confirm that MAP1LC3 was correctly reported as RFP-LC3; we confirm the correspondence between human HOOK1 and Drosophila Hook.

We added all missing information in the Material and Methods section.

AR-SPG15 and AR-SPG11 patients analysis and clinical data have been published in our previous works with one exception (patient carrying the SPG11Δ1 mutation) [8,14,38,39] . An overview of the clinical data is reported in supplementary Table S1. We reported this information in the text in Results section and in Material and Methods section together with the approval by the institutional Ethics Committee.

The information about untransfected cells (that are not mock-transfected cells) was also reported.

We reviewed the abbreviation list and the citation of references in the text, accordingly with Autophagy new reference citation style.

We accepted all your revisions (that are light blue coloured, as you did). All additional changes we made in the text and the required modifications are yellow coloured.

The co-authors of the manuscript have read it and agree to its submission for publication. All the Authors state that no conflict of interests and commercial relationships and/or supports from pharmaceutical or other companies are directly or indirectly involved or affected by the article.

Sincerely yours,

Maria Teresa Bassi Ph.D
"E. Medea" Scientific Institute,
Via d. Luigi Monza, 20,
23842 Bosisio Parini (Lecco), Italy.
Tel. 0039-031-877111; Fax. 0039-031-877499;
E-mail: mariateresa.bassi@lanostrafamiglia.it